# Contents

# List of Tables

# List of Figures

# Notation

**Acronyms**

| | |
|---|---|
| ALE | Arbitrary Lagrangian Eulerian |
| FEM | Finite Element Method |
| FSI | Fluid-Structure Interaction |
| GLS | Galerkin/Least-squares |
| SUPG | Streamline-Upwind-Petrov-Galerkin |
| XFEM | eXtended Finite Element Method |

**Alphabetical symbols**

| | |
|---|---|
| $C$ | Analytical solution parameter |
| $c_p$ | Specific heat $[\frac{J}{kg \cdot K}]$ |
| $D(\mathbf{v})$ | Rate of deformation tensor $[\frac{1}{s}]$ |
| $E$ | Error norm |
| $F(\mathbf{x}, t)$ | Normal level set convection speed $[\frac{m}{s}]$ |
| $\mathbf{f}_b$ | Buoyancy force in Navier-Stokes formulation $[\frac{N}{m^3}]$ |
| $G(T)$ | Enthalpy function $[\frac{J}{m^3}]$ |
| $\mathbf{g}$ | Gravity vector $[\frac{N}{kg}]$ |
| $g(\mathbf{x}, t)$ | Enrichment function |
| $H$ | Enthalpy variable $[\frac{J}{m^3}]$ |
| $H(\mathbf{x}, t)$ | Heaviside function |
| $\mathbf{I}$ | Identity matrix |
| $K_0$ | Permeability constant (Kozeny-Carman approximation) |
| $k$ | Thermal conductivity $[\frac{W}{m \cdot K}]$ |
| $k_{ij}$ | Stiffness coefficient for ALE methods |
| $L$ | Latent heat $[\frac{J}{kg}]$ |
| $m$ | Analytical solution parameter |
| $N_i(\mathbf{x})$ | Standard interpolation function |

| | |
|---|---|
| $N_j(\mathbf{x})$ | Enriched interpolation function |
| $\overline{N}$ | Lagrange multiplier interpolation function |
| $\mathbf{n}_\Gamma$ | Solid-liquid interface normal |
| $p$ | Pressure $[Pa]$ |
| $\mathbf{q}$ | Lagrange multiplier variable $[\frac{W}{m^2}]$ |
| $R(\mathbf{x})$ | Ramping function for weak enrichment |
| $T$ | Temperature variable $[K]$ |
| $T_m$ | Melting temperature $[K]$ |
| $T_{tol}$ | Tolerance value for void enrichment |
| $t$ | Time variable $[s]$ |
| $u(x,t)$ | Dummy variable |
| $\mathbf{v}$ | Velocity variable $[\frac{m}{s}]$ |
| $\mathbf{v}_\Gamma$ | Interface velocity $[\frac{m}{s}]$ |
| $\mathbf{v}_\phi$ | Level set convection velocity $[\frac{m}{s}]$ |
| $\mathbf{X}_i$ | ALE mesh movement constant |
| $\mathbf{x}$ | Space variable $[m]$ |
| $\mathbf{x}_\Gamma$ | Point on the interface $[m]$ |
| $x'$ | non-dimensionalized interface position in Stefan problem |
| $y'$ | non-dimensionalized interface position in Stefan problem |

**Greek symbols**

| | |
|---|---|
| $\alpha$ | Thermal diffusivity $[\frac{m^2}{s}]$ |
| $\beta$ | Penalization parameter |
| $\Gamma$ | Solid-liquid interface |
| $\Gamma_D$ | Dirichlet boundary condition |
| $\Gamma_N$ | Neumann boundary condition |
| $\Delta t$ | Time step $[s]$ |
| $\Delta\mathbf{x}$ | Interface thickness $[m]$ |
| $\Delta x$ | Mesh size $[m]$ |
| $x_\Gamma^a$ | Interface position in analytical solution of Stefan problem $[m]$ |
| $\delta T, \delta\mathbf{q}, \delta\mathbf{v}, \delta p, \delta\phi$ | Variable test functions |
| $\delta x$ | Distance for gradient based velocity calculation $[m]$ |
| $\eta$ | Thermal expansion coefficient $[\frac{1}{K}]$ |
| $\kappa_\Gamma$ | Curvature of $\phi(\mathbf{x},t)$ |
| $\Lambda$ | Scalar Lagrange multiplier |
| $\lambda$ | Analytical solution parameter |

| | |
|---|---|
| $\mu$ | Viscosity $[\frac{N \cdot s}{m^2}]$ |
| $\boldsymbol{\xi}$ | Space variable in element reference frame |
| $\rho$ | Density $[\frac{kg}{m^3}]$ |
| $\boldsymbol{\sigma}$ | Fluid stress tensor $[Pa]$ |
| $\tau^e$ | Stabilization parameter |
| $\Phi$ | Color function for diffused interfaces |
| $\phi(\mathbf{x}, t)$ | Level set variable $[m]$ |
| $\psi_j^{mod}$ | Modified enrichment function for weak discontinuities |
| $\psi_j(\mathbf{x}, t)$ | Shifted enrichment function |
| $\Omega$ | Problem domain |

**Superscripts, subscripts and modifiers**

| | |
|---|---|
| $a^*$ | Enriched degree of freedom |
| $a^+$ | Evaluated on $\phi(\mathbf{x}, t) > 0$ side of interface |
| $a^-$ | Evaluated on $\phi(\mathbf{x}, t) < 0$ side of interface |
| $a^{n+1}$ | $n + 1$ time step |
| $a^T$ | Vector transpose |
| $a_i$ | i$^{\text{th}}$ degree of freedom |
| $a_j$ | j$^{\text{th}}$ enriched degree of freedom |
| $a_l$ | Liquid phase |
| $a_s$ | Solid phase |
| $a_\Gamma$ | Solid-liquid interface |
| $\hat{a}$ | Boundary condition |
| $\langle a \rangle$ | Row vector |
| $\{a\}$ | Column vector |
| $[a]$ | Matrix |
| $[\![a]\!]$ | Value jump across $\Gamma$ |
| $\|\|a\|\|$ | Vector norm |

# Remerciements

J'aimerais, premièrement, remercier mon directeur de thèse, le Professeur Mario Fafard, qui a su m'intégrer dès mon arrivé dans son groupe de recherche et qui m'a guidé tout au long de mes travaux de doctorat. Nos nombreuses rencontres se sont passées dans une ambiance stimulante et positive et le temps qu'il m'a consacré a été grandement apprécié. Sa contribution à cette thèse, par ses conseils, ses encouragements et sa disponibilité, fut inestimable.

Je souhaite également remercier le Professeur Jean-Loup Robert qui a co-dirigé cette thèse. Il a régulièrement offert une perspective différente sur les défis à surmonter et ses conseils sur mon travail m'ont permis de progresser vers l'avant. Son interêt sincère et marqué pour mon travail m'a motivé à poursuivre mes efforts dans les moments plus difficiles.

Je suis aussi reconnaissant au Professeur Brian Helenbrook de Clarkson University qui m'a acceuilli dans son équipe pour un stage de six mois. Son implication dans mon cheminement et sa grande patience m'ont permis d'acquérir des connaissances cruciales à la réussite de mes travaux. Je suis fort reconnaissant à lui et toute son équipe pour leur acceuil chaleureux.

Le travail présenté dans cette thèse n'aurait jamais été complété sans l'apport des professionels de recherche Patrice Goulet et Hicham Chaouki. Leurs contributions au developpement des algorithmes sur lesquels sont basés mes travaux furent indispensables à l'avancement de ma thèse.

Je veux souligner la camaraderie et l'esprit d'équipe qui régnaient dans le local d'étudiants. J'aimerais remercier tout particulièrement Stéphane Thibodeau, Mathieu Fiset et Olivier Trempe qui m'ont aidé et encouragé tout au long de mon cheminement.

Merci aussi au Professeur François Mathieu-Potvin qui m'a permis d'utiliser ses li-

cences Comsol pour valider mes travaux.

Enfin, un grand merci à ma famille et mes amis ainsi que ma conjointe pour leur soutien.

La réalisation de ce projet a été rendu possible grâce au support financier du Conseil de recherches en sciences naturelles et en génie du Canada (CRSNG), de la compagnie Alcoa dans le cadre de la chaire de recherche industrielle CRSNG-Alcoa MACE3 et du Fonds de recherche du Québec-Nature et technologies (FRQNT) par l'intermédiaire du Centre de recherche sur l'aluminium – REGAL. Le FRQNT est tout particulièrement remercié pour le soutien financier pour mon stage chez le Pr Helenbrook.

# Avant-propos

Les trois premiers chapitres de cette thèse présentent la mise en context et les objectives de cette thèse, une revue de littérature sur la modélisation des problèmes de Stefan et de Stokes avec des discontinuités ainsi qu'une description de la méthode par éléments finis étendus (XFEM), utilsée dans les chapitres subséquents. La suite de l'avant-propos décrit brièvement les articles incluent dans la thèse, le rôle de l'auteur et des coauteurs et décrit les modifications apportées aux versions des articles qui se retrouvent dans la thèse.

## Article 1: A XFEM Lagrange Multiplier Technique for Stefan Problems

Le chapitre 4 présente l'article sur la résolution du problème de Stefan par multiplicateur de Lagrange soumis à la revue *Frontiers in Heat and Mass Transfer* le 2 mars 2016. Il est présentement sous évaluation. Certaines modifications ont été apportées au contenu afin d'éviter le dédoublement d'information dans la thèse. En particulier, la description de la méthode de fonction niveau (level set method), déjà présenté dans le chapitre 2 a été retirée. De plus, certains symboles ont été modifiés pour rester cohérant avec les autres chapitres de la thèse.

La présence de coauteurs met en évidence le travail d'équipe qui a été nécessaire au bon déroulement de ce projet. Mario Fafard et Jean-Loup Robert, directeur et codirecteur de cette thèse, ont encadré le développement du code présenté dans l'article et contribué à l'interpretation des résultats. Hicham Chaouki a contribué au développement des algorithmes associés à la méthode de fonction niveau ainsi qu'à la validation des équations de la formulation avec multiplicateur de Lagrange. Finalement, Donald Ziegler a représenté Alcoa, une source importante de financement, durant le développement du modèle.

L'article a été écrit par moi-même, en prenant en considération les conseils et commentaires de mes coauteurs, particulairement Hicham Chaouki. Je suis donc l'auteur principal.

## Article 2: A XFEM Phase Change Model with Convection

Le chapitre 5 présente l'article sur le système Stefan-Stokes couplé en éléments finis étendus soumis à la revue *International Journal of Heat and Fluid Flow* le 25 janvier 2016. Il est présentement sous évaluation. Certaines modifications ont été apportées au contenu afin d'éviter le dédoublement d'information dans la thèse et un problème de validation a été ajouté pour la formulation Stokes. Certains symboles ont été modifiés pour rester cohérants avec les autres chapitres de la thèse.

Mes directeurs de recherche, Mario Fafard et Jean-Loup Robert, ont encadré l'écriture du code présenté dans l'article et contribué à l'interprétation des résultats. Hicham Chaouki a développé la formulation Stokes (éléments finis standard) dans laquelle j'ai implementé les composantes nécessaires à la résolution par éléments finis étendus. Finalement, Donald Ziegler a représenté Alcoa, une source importante de financement, durant le développement du modèle.

L'article a été écrit par moi-même, en prenant en considération les conseils et commentaires de mes coauteurs, particulairement Hicham Chaouki.

## Article 3: Modelling of Phase Change with Non-Constant Density using XFEM and a Lagrange Multiplier

Le chapitre 6 présente l'article sur l'utilisation d'une densité distincte pour les phases solide et liquide qui sera soumis à une revue prochainement. Le contenu déjà présent dans les autres chapitres de cette thèse a été retiré. Certains symboles ont été modifiés pour rester cohérants avec les autres chapitres de la thèse.

Mes directeurs de recherche, Mario Fafard et Jean-Loup Robert, ont encadré l'écriture du code présenté dans l'article et contribué à l'interprétation des résultats. Hicham Chaouki a développé la formulation Stokes (éléments finis standard) qui a servi de point de départ pour la formulation avec densité variable. Donald Ziegler a représenté Alcoa, une source importante de financement, durant le développement du modèle et a fourni les propriétés de la cryolite utilisés pour le problème de validation présenté dans l'article.

L'article a été écrit par moi-même, en prenant en considération les conseils et commentaires de mes coauteurs, particulairement Hicham Chaouki.

# Chapter 1

# Introduction

## 1.1 Motivation

Today, aluminium is one of the most widely used metals worldwide. Its specific chemical and physical properties have allowed it to take an important role in a variety of areas. Lightweight and durable, it is gradually replacing steel in aerospace and automotive applications. In addition, it is infinitely recyclable, giving it an excellent prospect in the future as an environmentally responsible material. However, its production is still very energy intensive and releases a significant amount of greenhouse gases, especially $CO_2$. It is therefore essential to reduce the economical and environmental costs of producing aluminium so it can remain competitive on the world market as we gradually move towards greener industries.

The Hall-Héroult process [43] is the most common technology used to extract aluminium from alumina ($Al_2O_3$), a chemical compound that occurs naturally in bauxite. Alumina is dissolved in a cryolite bath at approximately 960 °C and exposed to an electric current of approximately 350 kA to induce the electrolysis reaction

$$2Al_2O_3 + 3C \rightarrow 4Al + 3CO_2 \tag{1.1}$$

and produce pure aluminium. The aluminium is recovered from the bottom of the electrolytic cell (see Figure 1.1) in liquid form. The heat generated by the Joule effect in the cell helps maintain the proper temperature within the liquid cryolite and an optimal reaction. In addition, the current produces a powerful magnetic field which circulates the fluid in the cell.

A major problem with the use of cryolite is its very corrosive nature, which will

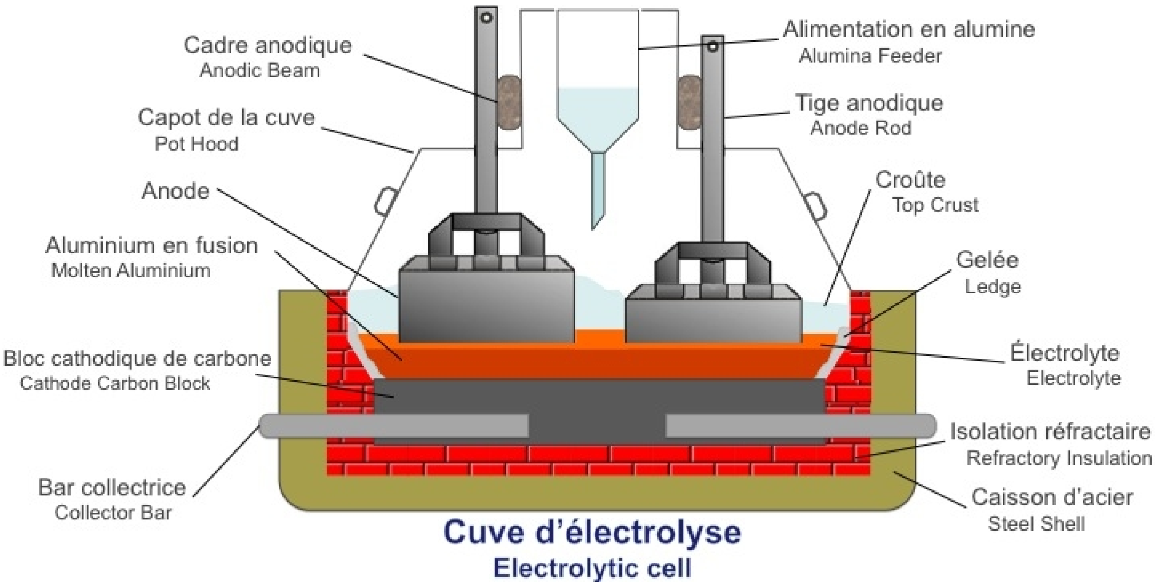

Figure 1.1 – Electrolytic Cell

eventually cause the cell walls to leak. To protect them, a nonreactive solid cryolite layer, called the ledge (figure 1.1), is maintained on the walls and can significantly increase the cell's life-span. However, the thickness of this solid layer changes the electrical and thermal efficiency of the reaction and thus the operating costs of the aluminium plant. This layer also modifies the motion of the liquid cryolite within the electrolytic cell, which affects the transport of heat and must be taken into account. Another important source of disturbance in the cell is the regular replacement of the anodes. When inserted into the cell, the anode is at room temperature (35°C). As a result, a layer of ledge quickly forms on the anode's surface which will then melt as the anode reaches the cell's operation temperature. This recurring perturbation affects the dynamics of the entire cell but is still poorly understood. Consequently, knowledge of the ledge thickness and fluid flow inside the cell are key elements to optimizing the entire process and reducing production costs for aluminum smelters.

The harsh environment prevailing inside the cell makes the acquisition of experimental data very difficult and in some cases impossible. To gain a better understanding of the electrolytic cell's behavior and thus optimize the process, aluminium smelters have turned to numerical models to reproduce the physics involved in the Hall-Héroult process. In this context, the three-dimensional and multiphysical nature of such a model poses a challenge. Specifically, a variety of phenomena occur simultaneously in the cell and the three distinct phases (liquid cryolite, solid cryolite

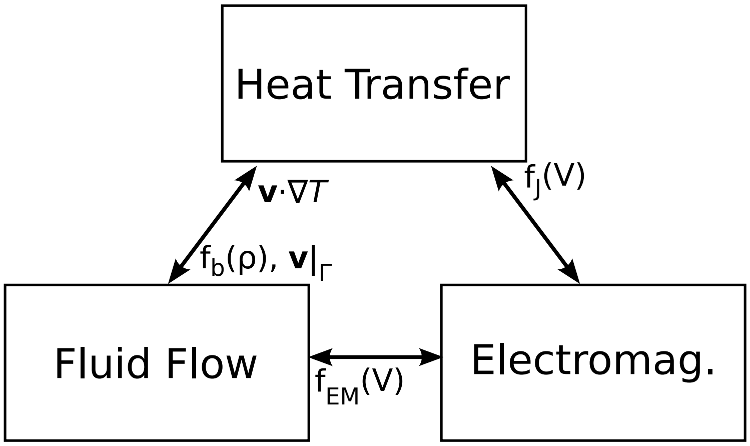

Figure 1.2 – Coupling of physical phenomena

and liquid aluminium) form separate three-dimensional domains that fluctuate over time with complex interactions at the material interfaces.

The main phenomena in the cell are heat transfer, fluid flow and electromagnetism. The electric current required for the electrolysis reaction (1.1) generates heat by the Joule effect, which acts as a volumetric heat source term. The presence of liquid phases inside the cell adds a convective term to the heat transfer problem. The current also influences the motion of the fluid through the magnetic force applied to the cryolite. Finally, the material properties (electrical and thermal conductivity, density) are temperature and phase dependent, creating buoyancy effects in the fluid and mass flow at the solid-fluid interface. A detailed model of the cell must include all these interactions in order to represent the behavior properly.

A complete analysis of an electrolysis cell must also take into account the discontinuities due to changes in physical properties between material domains. At the solid-fluid cryolite interface, the enthalpy undergoes a near discontinuous change due to the absorption or release of energy during the phase change. At the same interface, the fluid velocity jumps from zero in the solid phase to non-zero in the liquid phase in a discontinuous manner. At the cryolite-aluminum interface, the discontinuous change in material properties creates a jump in the velocity gradient and pressure. As these interfaces move over time, their positions must be recalculated in order to correctly evaluate the material properties in each phase and apply the associated boundary conditions on the interfaces.

The multiphysical nature of the problem considerably complicates the choice of the appropriate numerical method to solve the system of equations. The various mechanisms have unique numerical challenges and their interdependence adds a new layer of difficulty to obtaining a converged solution. The selected numerical strategy must be relatively easy to apply to different physics. It must also be able to handle the complex, and *a priori* unknown, geometries that may emerge over time due to interface movement. In addition to the complexity of the phenomena, the necessity of a three-dimensional model with so many degrees of freedoms can be very costly in computation time. The development of a particularly fast algorithm for solving the problem will be essential in order to exploit the model effectively in an industrial context.

## 1.2 Thesis Contribution and Novelty

A complete three dimensional model including all the phenomena mentioned previously and their interactions is beyond the scope of a single thesis. However, the choices made in this work regarding numerical techniques and physical assumptions should be inline with the long term goal of constructing such a model. This project concentrates on developing the numerical framework required to model the behavior of the cryolite bath. The liquid aluminium underneath and open air above are therefore completely removed and no fluid-fluid interfaces are considered. The model only includes liquid and solid phases within a fixed domain. Moreover, the electrical problem will be completely ignored, meaning that no Joule effect or magneto-hydraulic forces (Lorentz) will be considered. These contributions being additional source terms, they can easily be added to the formulations developed in this work.

The changes in material properties (thermal conductivity, density and heat capacity) at the phase change will be taken into account but the properties will be assumed constant within each phase. The material will be assumed to have an isothermal phase change. The problem will be solved in two dimensions but careful consideration for the extension to three dimensions will be taken into account throughout this work. Considering these assumptions, a numerical model with two coupled systems of equations will be required. The first is the heat transfer problem involving phase change (commonly called Stefan problem) and the second is the Navier-Stokes equations for incompressible flow in the liquid phase.

The main objective of this work is to develop an efficient way to handle the time-dependent discontinuities in the temperature, velocity and pressure fields caused by the phase change process. Even though this project focuses on the phase change process, other projects are currently underway to tackle the various other discontinuities present in the overall aluminium smelting process and will be implemented in the same computer program. The code developed for the phase change problem must therefore be applicable to other physics with as little modifications as possible. To fulfill all of these requirements, the extended finite element method [13] was selected and will be discussed in depth in chapter 3.

The model was coded in FESh++, a multi-physics C++ object-oriented solver. This solver is already used as part of the research in thermal-electro-mechanical problems for the REGAL [27, 35]. It is on this platform that were added the necessary components for the simulation of the cryolite. These components were numerous, as FESh++ did not offer the proper tools for the management of time-dependent discontinuities.

This project has several innovative elements. First, a variation on the method of Lagrange multipliers, based on [34], was developed to apply the fusion temperature on the interface. Furthermore, the solid-liquid interface velocity is determined by the jump in heat flux at the interface. The extended finite element solidification models found in the literature calculate this value using the gradient of the temperature field. In the model proposed in this thesis, the novel Lagrange multiplier solution is used to evaluate the jump in heat flux. Its performance is then compared to the temperature gradient based evaluation.

Second, few extended finite element solidification models which include convective effects are listed in the literature. Thereof, none consider the discontinuous nature of the interface directly in the resolution of the fluid flow problem. Instead, they use classical finite element techniques to approximate the interface using continuous interpolations. This aspect was corrected in this model by developing a coupled heat transfer/fluid flow model using the extended finite element method to include the discontinuities in both physics.

Thirdly, a large majority of work done in phase change problems, and all extended finite element models found in the literature, assume a constant and unique material density for both phases. In most situations, the difference in density between solid and liquid phases is relatively small and the assumption has a small impact on the solution. However, cryolite does not fall in this category and the density may change considerably ($\approx 25\%$) between phases. In order to include this change in density and conserve the overall mass of the system, a non-zero boundary condition is applied on the velocity at the phase-change interface for the resolution of the Navier-Stokes equations. The specific value is dependent on the change in density and the velocity of the interface, increasing the non-linearity of the coupled system. The use of the extended finite element method for the resolution of the Navier-Stokes equations allows this particular boundary condition to be applied directly on the interface in a similar fashion to the melting temperature.

## 1.3 Thesis Organization

The thesis is divided as follows. In chapter 1, the motivations for developing the model are discussed as well as the main contributions of this thesis to the advancement of extended finite element modelling. In chapter 2, a review of the literature on modelling discontinuities, the Stefan problem and Navier-Stokes equations in particular, is presented. Chapter 3 gives an in-depth description of the extended finite element method and related numerical tools, including the level set method. Chapter 4 presents the article on the development of the Lagrange multiplier formulation used in the thesis. Chapter 5 presents the coupled Stefan and Stokes formulation using the extended finite element method. The density is considered constant. Chapter 6 presents the complete model, including the density difference between the solid and liquid phases.

# Chapter 2

# Literature Review

## 2.1 Introduction

Several methods are found in the literature to numerically model physical phenomena. The particular physics studied in this project (heat transfer and fluid dynamics) and the continuous nature of the material encourages the use of the finite element method (FEM) [66] as a modelling tool [10, 27, 35, 45]. This chapter explores the main approaches used in the finite element method to model phase change problems and handle discontinuous interfaces in general. Section 2.2 gives a general description of these techniques, their advantages and their drawbacks. In sections 2.3 and 2.4, a review of their application to the Stefan and Navier-Stokes problems, respectively, are given as well as advantages and drawbacks associated to the specific problem.

## 2.2 Interface Handling Techniques

The finite element method has been proven to be robust for a variety of problems, is geometrically flexible and is well understood in the literature. However, particular situations can still cause problems. The finite element method uses a polynomial interpolation within individual elements. Consequently, it can only reproduce a function with discontinuities in the variable (strong discontinuity) or its derivative (weak discontinuity) by separating the domain into submeshes, treated separately. This means that the discontinuity's location must be known *a priori* in order to properly adapt the mesh to this additional geometrical constraint.

The situation is further complicated when these discontinuities can move in time.

In this case, the interface moves within the mesh and its management becomes very complex and often very difficult from a practical point of view. To handle such situations, three adaptations of the finite element algorithm have been developed in the literature.

In the first, the interface is modelled in a diffused manner, which converts the discontinuity into a steep (but finite) gradient [9, 10, 79]. Secondly, the interface can be defined by a set of nodes on the mesh. Mesh control techniques allow the set of nodes to move within the mesh, based on the desired interface velocity, and reorganize the surrounding nodes to maintain an acceptable mesh distortion. This approach is called the arbitrary Lagrangian-Euleurian method (ALE) [37, 39, 51]. Lastly, a technique called the extended finite element method (XFEM) provides the ability to have discontinuous solutions within elements [13, 21, 22, 56]. To do so, the Lagrange polynomial interpolation is enriched with a carefully selected function to introduce a discontinuous behavior in the solution at an arbitrary location, independent of the mesh.

### 2.2.1 Diffused Interface

The simplest technique to represent a discontinuity in the finite element context is to approximate it by a rapid change in the solution over a finite distance $\Delta\mathbf{x}$ [9, 60]. This approach allows the use of a standard polynomial interpolation in the finite element formulation and uses a state variable such as the temperature or a level set function $\phi(\mathbf{x}, t)$ to define the color function $\Phi$ which describes the "amount", between 0 and 100%, of a particular phase at a given point in the domain. A smooth function is then used to describe the mixed region where the phase transition occurs. A general example is

$$\Phi = \begin{cases} 1 & \text{if } \phi(\mathbf{x}, t) > \frac{\Delta\mathbf{x}}{2} \\ 0 & \text{if } \phi(\mathbf{x}, t) < -\frac{\Delta\mathbf{x}}{2} \\ f(\phi) & \text{if } \phi(\mathbf{x}, t) \in \left[-\frac{\Delta\mathbf{x}}{2}, \frac{\Delta\mathbf{x}}{2}\right] \end{cases} \tag{2.1}$$

where $f(\phi)$ is an interpolation function used in the range $\left[-\frac{\Delta\mathbf{x}}{2}, \frac{\Delta\mathbf{x}}{2}\right]$ to transition from one side of the discontinuity to the other.

An important step in this approach is the selection of a transition distance $\Delta\mathbf{x}$. The larger the transition region, the lower the solution gradient and the easier the system will be to converge, at the cost of accuracy. For smaller transition regions, the rapid change in the solution will require a more refined mesh to properly capture the solution's behavior near the interface.

This technique is commonly used to implement simple models requiring less computing power because the accuracy of the solution can be easily increased by refining the mesh. The large amount of degrees of freedom required to model a complete electrolysis cell inhibits the use of refined meshes. Furthermore, the absence of a properly defined interface complicates the application of boundary conditions. Most applications require a modification of the governing equations to apply the boundary condition implicitly, which shall be discussed in sections 2.3 and 2.4. This step in the development of a physical model is not always intuitive. In sum, the diffused interface technique is simple to handle and implement numerically but does not offer the desired accuracy or general applicability required for this model and its planned evolution.

### 2.2.2 Arbitrary Lagrangian-Eulerian Method

The arbitrary Lagrangian-Eulerian (or ALE) method [15, 37, 38, 44] offers an interesting alternative to diffused interfaces because it stores the interface on mesh nodes. This results in an exact representation of the discontinuity because the finite element method can include discontinuities in the solution that occur at element boundaries. The main idea behind this method is to combine the advantages of a Lagrangian reference frame, which allows the mesh nodes to move, with those of an Eulerian reference frame with a fixed mesh (better suited for problems involving convection, such as the Navier-Stokes equations). The result is a system of equations in an Eulerian reference which takes into account the movement of the nodes.

The interface is related to a set of nodes that move in the mesh and the solution can capture the discontinuities. Furthermore, interface boundary conditions on these nodes are applied quite easily. The movement of the nodes adds an additional convection term to the governing equations, described by

$$\frac{\partial u}{\partial t} + \nabla \cdot \left( \left( \mathbf{v} - \frac{\partial \mathbf{x}}{\partial t} \right) u \right) = f(u) \tag{2.2}$$

for a pure transport problem where $\mathbf{v}$ is the physical convection velocity and $f(u)$ a source term.

The governing equations of the problem must be modified to account for the convection term, which is independent of the particular physical problem and will be identical for all applications. Note that in the case where $\frac{\partial \mathbf{x}}{\partial t} = \mathbf{v}$, the formulation reduces to a purely Lagrangian reference frame and if $\frac{\partial \mathbf{x}}{\partial t} = 0$, we obtain a purely Eulerian description of the flow.

The displacement of the interface nodes is determined by the interface velocity specified by the particular problem at hand and is given as

$$\mathbf{x}^{n+1} = \mathbf{x}^{n} + \Delta t \mathbf{v}^{n} \tag{2.3}$$

where $\mathbf{x}^{n+1}$ is the updated node position, $\mathbf{x}^{n}$ the old node position and $\mathbf{v}^{n}$ the interface velocity at the specified node.

The movement of the mesh adds a significant level of complexity to the geometry of the problem. Although only the movement of the nodes on the interface has any physical meaning, the entire domain must be mobile in order to maintain an acceptable mesh distortion. A typical mesh movement equation for nodes not on the interface is of the form [37]

$$\sum_{j} k_{ij} \left( \mathbf{x}_j - \mathbf{x}_i \right) = \mathbf{X}_i \qquad k_{ij} = \frac{1}{\|\mathbf{x}_j - \mathbf{x}_i\|^2} \tag{2.4}$$

where the nodes are represented as the ends of springs with a non-linear stiffness coefficient $k_{ij}$ and $\mathbf{X}_i$ is a constant associated with node i of the initial mesh.

It is the constant $\mathbf{X}_i$ that constricts the mesh to a structure similar to the original mesh. The sum over j is done on all nodes directly linked to node i. Without this redistribution of the mesh, highly distorted elements or negative volumes may occur. Moreover, the basic properties of the element, such as the Jacobian matrix, must be recalculated at each time step (or iteration).

The position of each node becomes two or three additional degree of freedom, depending on the number of dimensions, and are added to the total number of unknowns, increasing the computation cost of the model. Also, developing a fairly robust algorithm to handle complex interface movements is difficult, especially in three dimensions. In cases with large displacements, a remeshing is often required to maintain the accuracy of the solution. The remeshing process can also be complex and introduces an error in the interpolation of the solution from one mesh to the other. Even though the ALE method can accurately account for the discontinuities, the increase in computational effort and code complexity caused by the movement of the nodes considerably reduces its appeal for this project.

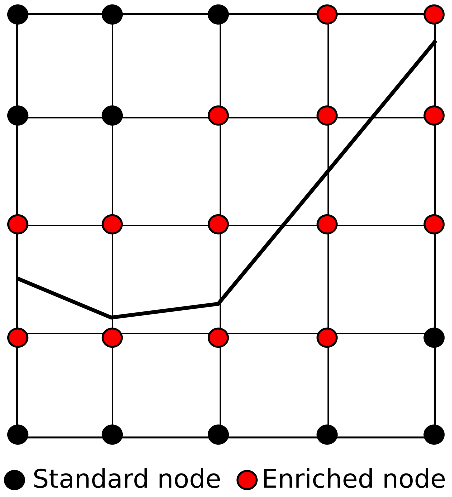

Figure 2.1 – Standard and enriched nodes in a mesh involving a discontinuity

### 2.2.3 Extended Finite Element Method

The extended finite element method (XFEM) [13, 30] is different from the mesh manipulation associated with the ALE techniques. The extended finite element method includes additional degrees of freedom and modifies the interpolation functions of the element in order to accurately represent functions with strong or weak discontinuities in the solution. These changes are based on the concept of partition of unity [5] already used to define the standard interpolation functions. In the context of XFEM, the interpolation space is increased using specially chosen functions of the form

$$u(x,t) = \sum_{i\in I} N_i(\mathbf{x}) u_i(t) + \sum_{j\in J} N_j(\mathbf{x}) \psi_j(\mathbf{x},t) u_i^*(t) \tag{2.5}$$

in order to accurately represent the discontinuous behavior of the solution, known *a priori*.

The sets I and J in (2.5) represent the sets of standard and enriched nodes, respectively, as seen in figure 2.1. The main advantage of the extended finite element method is the use of an additional function $\psi_j(\mathbf{x},t)$ in the interpolation that can reproduce a discontinuity within an element. The discontinuity may therefore move independently of the nodes and eliminates the need to change the mesh during the simulation.

The extended finite element method modifies the underlying interpolation functions that approximate the solution. This means that the governing equations of the physical problem are not modified. In addition, the enrichment generates degrees of free-

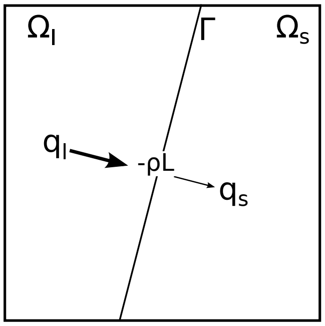

Figure 2.2 – Schematic representation of energy conservation at interfaces

dom that are local to the interface, reducing their impact on the calculation time. Finally, the interface location is stored using the level set method, which will be described in detail in section 3.5, and is more efficient and robust than moving the nodes themselves as in the ALE method.

## 2.3 Stefan Problem

Following the solidification (or melting) front of a phase change problem is expressed by the Stefan problem [64]

$$(\rho c_p)_i \left( \frac{\partial T}{\partial t} + \mathbf{v}_i \cdot \nabla T \right) = \nabla \cdot (k_i \nabla T) \quad \mathbf{x} \in \Omega_i \; i = l, s \tag{2.6a}$$

$$[\![ -k_i \nabla T ]\!] = \rho_s L \mathbf{v}_\Gamma \qquad \mathbf{x} \in \Gamma \tag{2.6b}$$

$$T_s = T_l = T_m \qquad \mathbf{x} \in \Gamma \tag{2.6c}$$

where $\rho$ is the density, $c_p$ the heat capacity and $k$ the thermal conductivity. The subscripts $l$ and $s$ indicate the liquid and solid phases, respectively. In the presence of melt convection, an additional convective term with velocity $\mathbf{v}$ is added to equation (2.6a), in the fluid domain only. The second equation (2.6b) expresses the relationship between the jump in heat flux at the interface (left-hand side of the equation) and the latent heat $L$ released or absorbed as the interface moves with velocity $\mathbf{v}_\Gamma$ [64] and is illustrated in figure 2.2. Finally, an additional boundary condition, equation (2.6c), must be applied in order to maintain the interface at the melting temperature $T_m$

It is possible to eliminate the explicit tracking of the interface by rewriting (2.6a) using the enthalpy as the conserved property in the material derivative, known as the enthalpy formulation or method [10, 74, 79]. Equation (2.6a) then takes the form

$$\frac{\partial H}{\partial t} + \mathbf{v} \cdot \nabla H = \nabla \cdot (k_i \nabla T) \qquad \mathbf{x} \in \Omega_i i = l, s \tag{2.7a}$$

$$H - G(T) = 0 \qquad \mathbf{x} \in \Omega_i i = l, s \tag{2.7b}$$

where $H$ is the enthalpy and $G(T)$ is a known function, given below.

The advantage of this formulation is that the enthalpy includes the total energy of the material. As a consequence, the enthalpy will take into account the latent heat absorbed or released at the interface during the phase change. The interface location and movement is then implicitly determined by the evolution of the enthalpy solution during the simulation. Note that (2.7) is non-linear and will require an iterative solver.

The addition of a second unknown to the problem requires an additional equation to relate the temperature to the corresponding enthalpy value. This is obtained by expressing the enthalpy as a known function

$$G(T) = \begin{cases} \left(\rho c_p\right)_s T & \text{if } T < T_m - \varepsilon \\ f(T) & \text{if } T_m - \varepsilon \leq T \leq T_m + \varepsilon \\ \left(\rho c_p\right)_s T_m + (\rho c_p)_l (T - T_m) + \rho_l L & \text{if } T > T_m + \varepsilon \end{cases} \tag{2.8}$$

whose behavior during the phase change, $f(T)$, depends on the particular material used in the model.

A large number of materials have an isothermal phase change. In these cases, a physically accurate function $G(T)$ is discontinuous at the melting temperature. A finite element (or finite volume) algorithm will be unable to reproduce this behavior. To obtain a solvable system, $G(T)$ must be smoothed out near the interface by using some interpolation function $f(T)$, as shown in figure 2.3. For non-isothermal problems, the enthalpy varies continuously across the phase change temperature range and the smoothing function may not be required, depending on the particular material.

Replacing the discontinuous relationship between the temperature and enthalpy at the phase-change by a smooth function $f(T)$ introduces a physical approximation into the model. Furthermore, $f(T)$ may still have an important gradient, which will increase the number of iterations required to obtain a converged solution [10] and the mesh density required to obtain an acceptable solution near the interface. The

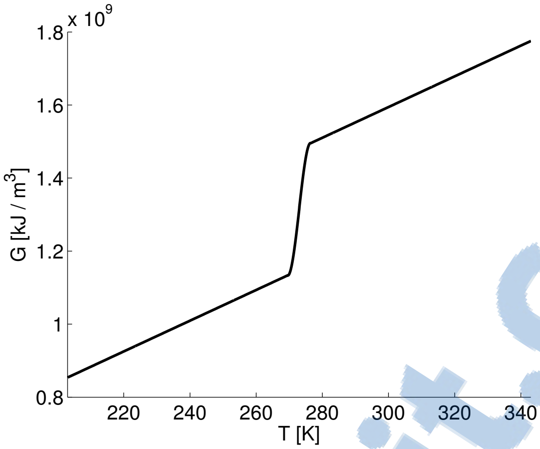

Figure 2.3 – Enthalpy function G as a function of temperature

appropriate choice of temperature range $\varepsilon$ will determine the balance between the accuracy of the model and its computational cost.

Whereas the enthalpy formulation diffuses the phase change over a certain temperature range, an alternative approach for isothermal phase change problems is to diffuse the interface over the spatial domain [19, 75]. These models use a level set function $\phi(\mathbf{x}, t)$ to monitor the interface and rewrite the conservation equation (2.6a) in a form which is applicable throughout the domain using continuous interpolation functions [75]:

$$\left(\rho c_p\right) \frac{\partial T}{\partial t} + \left(\rho c_p\right)_l \mathbf{v} \cdot \nabla T = \nabla \cdot (k \nabla T) - \rho_s \left(L + \left(c_s - c_l\right)\left(T - T_m\right)\right) \frac{\partial \Phi}{\partial t} \tag{2.9a}$$

$$\left(\rho c_p\right) = \left(\rho c_p\right)_l \Phi + \left(\rho c_p\right)_s (1 - \Phi) \tag{2.9b}$$

$$k = k_l \Phi + k_s (1 - \Phi) \tag{2.9c}$$

An example of a color function is given as [75]:

$$\Phi = \begin{cases} 1 & \text{if } \phi(\mathbf{x}, t) > \varepsilon \\ 0 & \text{if } \phi(\mathbf{x}, t) < \varepsilon \\ \frac{\phi}{2\varepsilon} + 0.5 & \text{if } \phi(\mathbf{x}, t) \in [-\varepsilon, \varepsilon] \end{cases} \tag{2.10}$$

The impact of using (2.9) on the precision of the model is similar to using the enthalpy formulation (2.7). We introduce an error (approximation) in the model and the larger the diffused interface thickness, the larger the error.

The resolution of (2.6) with the arbitrary Lagrangian-Eulerian method [39]

$$\left(\rho c_p\right)_i \frac{\partial T}{\partial t} + \nabla \cdot \left( \left( \mathbf{v} - \frac{\partial \mathbf{x}}{\partial t} \right) \left(\rho c_p\right)_i T - k_i \nabla T \right) = f(u) \tag{2.11}$$

is simple to implement from a physical point of view. Since the interface is defined by a set of nodes, the application of boundary conditions (melting temperature), the evaluation of the thermal properties and the evaluation of the interface velocity are done in the same manner as the finite element method. The challenge is to properly move the nodes within the mesh to follow the phase change and all the disadvantages mentioned in section 2.2 reduce the usefulness of this approach in three dimensional problems.

A direct resolution of (2.6) requires the explicit monitoring of the interface to calculate the interface velocity, based on the heat flux, and impose the melting temperature. The extended finite element method offers a numerical framework to solve this problem. Indeed, several models have been done on solidification problems with XFEM [14, 22, 46, 54, 83]. These models enrich the temperature variable's interpolation to allow a discontinuous jump in the temperature gradient. Typically, this function is the absolute value of the level function, as will be discussed in chapter 3. The result is a model that accurately follows the interface discontinuity on a fixed mesh without modifying the governing equations

It is important to mention that all the models presented in this section assume an identical density for both phases of the material. This assumption is valid for most solid-liquid phase changes because the variation in density between the phases is usually small; the density variation for water is $\approx$ 9%. The cryolite bath however, is known to have an important variation in density ($\approx$ 25%) during the phase change. In this case, the mass balance at the interface [64], equation (2.12), implies that the velocity $\mathbf{v}_l$ of the liquid phase at the interface is not zero and the no-slip condition is no longer valid. The velocity boundary condition becomes [64]:

$$\mathbf{v}_l = \frac{\rho_l - \rho_s}{\rho_l} \mathbf{v}_\Gamma \tag{2.12}$$

Consequently, the coupling of this problem with the fluid flow must absolutely include the density variation to conserve mass and obtain a physically admissible flow.

In sum, several models are available for modelling phase change phenomena. However, the most common techniques, diffused interfaces and ALE models, have a significant trade-off between accuracy and computation time and require important changes to the governing equations. This is why the extended finite element, which follows the interface using the efficient level set method and include the discontinuity directly in the interpolation scheme, was used in this work.

## 2.4 Navier-Stokes Equations

To determine the fluid velocity the Navier-Stokes equations [45] must be solved. In this work, we consider an incompressible Newtonian fluid, resulting in the simplified system

$$\frac{\partial\left(\rho\mathbf{v}\right)}{\partial t}+\nabla\cdot\left(\rho\mathbf{v}\mathbf{v}\right)=\mu\nabla^{2}\mathbf{v}-\nabla p+\rho\mathbf{g} \tag{2.13a}$$

$$\nabla\cdot\mathbf{v}=0 \tag{2.13b}$$

where $\rho$ is the fluid density, $\mu$ the dynamic viscosity, $\mathbf{v}$ the velocity, p the hydrostatic pressure and $\mathbf{g}$ the gravitational force vector. System (2.13) is only valid in the fluid domain. In diffused interface models, the Navier-Stokes equations are modified with a color function (2.1) to be applicable on the entire domain, including a "mushy" transition zone from the liquid to solid phase where the velocity is zero. System (2.13) then takes the form [75]

$$\begin{aligned}\frac{\partial\left(\rho\mathbf{v}\right)}{\partial t}+\nabla\cdot\left(\frac{\rho^{2}}{\rho_{l}}\frac{\mathbf{v}\mathbf{v}}{\Phi}\right)=\mu\nabla^{2}\left(\frac{\rho}{\rho_{l}}\mathbf{v}\right)-\nabla p+\frac{p}{\Phi}\nabla\Phi\\ -\mu\frac{\left(1-\Phi\right)^{2}}{\Phi^{2}}\frac{\rho}{\rho_{l}}\frac{\mathbf{v}}{K_{0}}+\Phi\rho\mathbf{g}\end{aligned} \tag{2.14a}$$

$$\nabla\cdot\mathbf{v}=0 \tag{2.14b}$$

where $\Phi$ is the liquid fraction, $\rho\equiv\rho_{l}\Phi+\rho_{s}\left(1-\Phi\right)$, the mixed density and $\mathbf{v}=\Phi\mathbf{v}_{l}$ the volume-averaged velocity. $K_0$ is the permeability constant of the Kozeny-Carman approximation used to impose the zero velocity condition in the solid phase.

Since the phase domains are defined by the heat transfer problem, the solid fraction $\Phi$ can be directly defined from the enthalpy [16] or a level set function [75] describing the interface position. When $\Phi=1$ the domain is pure liquid and (2.14) reduces to (2.13). In contrast, when $\Phi=0$, the domain is completely solid and the velocity will drop to 0. Also note that the no-slip condition at the solid-liquid interface is constructed into the governing equations (2.14). This makes the application of a non-zero velocity interface boundary condition non-trivial with this approach .

Navier-Stokes models based on the ALE method are used in a wide range of physical models, including fluid-structure interactions [48], two fluid flow [15, 38] and phase change problems [11]. Since elements are entirely in the solid or liquid domain, no mushy region is required to allow the resolution of the Navier-Stokes equations in regions with mixed phases. System (2.13) is solved in the liquid phase, with proper boundary conditions applied to the appropriate nodes.

A smaller number of applications have been found in the literature using the extended finite element method. A particular problem which has received much attention is fluid-structure interactions. In this problem, a flexible structure is submerged in a fluid exerting a force (pressure) upon it. The solid (structure) and fluid domains vary over time, as the structure interacts with the fluid. To solve the Navier-Stokes equations in the fluid domain only [33] used a "void" enrichment scheme for the velocity and pressure fields. This enrichment effectively removes the structure from the computational domain and allows the application of appropriate velocity boundary conditions on the interface. The interface movement is then calculated from the structure's movement, determined from solid mechanics.

The fluid problem defined in fluid-structure interactions is quite similar to the case of solidification. In both problems, the domain is split into a region where the Navier-Stokes equations must be solved and another where they are not applicable. Another key commonality is the application of velocity boundary conditions at the interface. In the case of fluid-structure interactions, the structure (interface) and fluid velocities at the interface must match and may be non-zero. In fluid-structure interactions, the fluid velocity may point in an arbitrary direction but must remain normal to the interface in phase change problems. In non-constant density phase change problems, the fluid velocity is proportional to the interface velocity and may be non-zero at the interface. This is an important distinction from other applications, such as constant density phase change, where a no-slip condition (zero velocity) is applied on the interface.

The main distinction is the calculation of the interface velocity, which is based on energy conservation at the interface for phase change problems. To our knowledge, no extended finite element model for phase-change problems and complete fluid model can be found in the literature. For completeness, we mention other extended finite element models for the Navier-Stokes equations using different enrichment schemes for two-fluid flow [21, 29] and the handling of boundary layers and shocks in fluid flow [1].

The Navier-Stokes equations and the convective-diffusion heat transfer equation include a hyperbolic term, requiring a stabilization term to remove the non-physical oscillations that may appear when the convective transport dominates the problem [31, 42, 67]. Two techniques are particularly common; Streamline-Upwind -Petrov-Galerkin (SUPG) [18]

$$\sum_e \int_{\Omega^e} (\mathbf{v} \cdot \nabla \delta \mathbf{v})\, \tau^e \mathbf{r}_{\mathbf{v}}\, \mathrm{d}\Omega \tag{2.15}$$

and Galerkin/Least-squares (GLS) [41]

$$\sum_e \int_{\Omega^e} \left( \mathbf{v} \cdot \nabla \delta \mathbf{v} - \mu \nabla^2 \delta \mathbf{v} - \nabla \delta p \right) \tau^e \mathbf{r}_{\mathbf{v}}\, \mathrm{d}\Omega \tag{2.16}$$

where $\mathbf{r}_{\mathbf{v}}$ is the residual of (2.13a) and $\tau^e$ is an element dependent numerical parameter with dimensions of time. Both techniques are very similar in their application to the Navier-Stokes equations and add an additional term to the residual of (2.13a).

As was explained for the Stefan problem, several approaches have been used to model discontinuous jumps in the velocity and pressure solutions. The most common techniques being the diffused interface and ALE models, the same difficulties discussed for the Stefan problem are present. Futhermore, the flexibility required to apply a non-zero velocity condition on the interface can be difficult to obtain in diffused models, where the boundary condition is often implicitly included in the problem formulation (Kozeny-Carman approximation). The ALE method allows such velocity boundary conditions but considerably increases the computational cost of the model. This is why the extended finite element was also selected to model the fluid flow during the phase change.

# Chapter 3

# The Extended Finite Element Method

## 3.1 Introduction

The objective of this chapter is to present the extended finite element method. Section 3.1 gives an overview of the method. Section 3.2 describes the different enrichment schemes used in the work to reproduce the various physical discontinuities of the Stefan problem and Navier-Stokes equations. Section 3.3 explains the penalty and Lagrange multiplier methods which are used to apply the Dirichlet boundary conditions on the interface. Section 3.4 details the integration of the finite element formulation in cut elements, particularly the time derivatives. Section 3.5 gives an overview of the level set method which is used to store and move the interface position.

The extended finite element method [12, 13, 24] is based on the partition of unity method [5, 24, 53] which allows the selection of local test and trial functions in the finite element formulation that correctly reproduces the desired behavior of the solution. The standard interpolation, related to the set of degrees of freedom $I$ (black nodes in figure 2.1), is improved upon by adding a second set $J$ of degrees of freedom (red nodes in figure 2.1), using carefully selected enrichment functions $g(\mathbf{x}, t)$ as given in:

$$u(\mathbf{x}, t) = \sum_{i \in I} N_i(\mathbf{x}) u_i + \sum_{j \in J} N_j(\mathbf{x}) g(\mathbf{x}, t) u_j^* \tag{3.1}$$

These added degrees of freedom will "enrich" the interpolation and allow the solution to reproduce the behavior of $g(\mathbf{x}, t)$ within the element.

The particular type of behavior is determined by the enrichment function $g(\mathbf{x}, t)$, known *a priori*. The main strength of this method is that the interpolation scheme can reproduce discontinuities inside the element, independently of the mesh. This means that the position of the discontinuity can move in time without changing the underlying mesh. Furthermore, the set of nodes J with enriched degrees of freedom does not need to cover the entire calculation domain. Only those nodes who's support is intersected by the interface and have a modified behavior must be enriched, making the additional computational costs local.

An important aspect of the finite element method is the Kronecker-$\delta$ property of the overall approximation which requires that the approximation for $u(\mathbf{x}, t)$ at node i be equal to the nodal value $u_i$. Evaluating (3.1) at node i clearly shows the loss of the Kronecker-$\delta$ property :

$$\begin{aligned} u(\mathbf{x}_i, t) &= N_i(\mathbf{x}_i)u_i + N_i(\mathbf{x}_i)g(\mathbf{x}, t)u_i^* \\ &= u_i + g(\mathbf{x}, t)u_i^* \end{aligned} \tag{3.2}$$

To correct this problem, the enrichment function $g(\mathbf{x}, t)$ is "shifted" with respect to its value at the particular degree of freedom's supporting node

$$\psi_j(\mathbf{x}, t) = g(\mathbf{x}, t) - g(\mathbf{x}_j, t) \tag{3.3}$$

and the Kronecker-$\delta$ property is recovered:

$$\begin{aligned} u(\mathbf{x}_i, t) &= N_i(\mathbf{x}_i)u_i + N_i(\mathbf{x}_i)\psi_i(\mathbf{x}_i, t)u_i^* \\ &= u_i \end{aligned} \tag{3.4}$$

The interface geometry is stored and transported in a computationally efficient manner, most commonly using the level set method [62]. The method uses a scalar variable to store the position of the interface, where the discontinuous behavior of the solution is desired. This makes the definition of the enrichment functions straight forward, as they can be defined with respect to the level set function $\phi(\mathbf{x}, t)$.

## 3.2 Enrichment Strategies

### 3.2.1 Strong enrichment

Certain situations may require a jump in the solution value at the interface, called a strong discontinuity. Problems in solid mechanics involving cracks [50, 56, 71] and

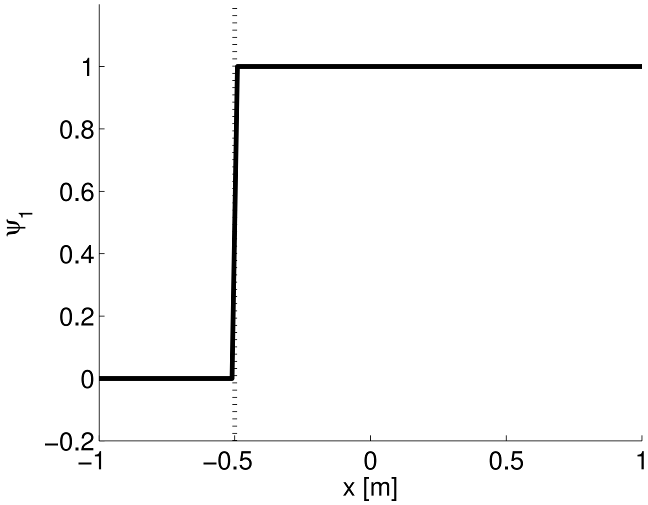

Figure 3.1 – Strong discontinuity enrichment function for left node of 1D element.

the use of Lagrangian multipliers as described later in this thesis are examples of problems with instantaneous jumps of the solution across the interface. In this case, a modified Heaviside function

$$\psi_j(\mathbf{x},t) = H(\mathbf{x},t) - H(\mathbf{x}_j,t) \tag{3.5a}$$

$$H(\mathbf{x},t) = \begin{cases} 1 & \text{if } \phi(\mathbf{x},t) > 0 \\ 0 & \text{if } \phi(\mathbf{x},t) < 0 \end{cases} \tag{3.5b}$$

is used to reproduce the behavior as seen in figure 3.1.

The amplitude of the jump in the solution is evaluated as:

$$\begin{aligned} [\![u(\mathbf{x},t)]\!] &= u(\mathbf{x}^+,t) - u(\mathbf{x}^-,t) \\ &= \sum_{i\in I} N_i(\mathbf{x}^+)u_i + \sum_{j\in J} N_j(\mathbf{x}^+)\psi_j(\mathbf{x}^+,t)u_j^* \\ &\quad - \sum_{i\in I} N_i(\mathbf{x}^-)u_i - \sum_{j\in J} N_j(\mathbf{x}^-)\psi_j(\mathbf{x}^-,t)u_j^* \end{aligned} \tag{3.6}$$

Since the interpolation functions $N_i(\mathbf{x})$ and $N_j(\mathbf{x})$ are continuous at the interface, equation (3.6) can be simplified to:

$$\begin{aligned} [\![u(\mathbf{x},t)]\!] &= \sum_{j\in J} N_j(\mathbf{x}) \left( (\psi_j(\mathbf{x}^+,t) - \psi_j(\mathbf{x}^-,t) \right) u_j^* \\ &= 2\sum_{j\in J} N_j(\mathbf{x})u_j^* \end{aligned} \tag{3.7}$$

The gradient is evaluated as:

$$\nabla u(\mathbf{x}, t) = \sum_{i \in I} \nabla N_i(\mathbf{x}) u_i(t) + \sum_{j \in J} \left( \nabla N_j(\mathbf{x}) \psi(\mathbf{x}, t) + N_j(\mathbf{x}) \nabla \psi_j(\mathbf{x}, t) \right) u_i^*(t) \tag{3.8}$$

Note that the gradient may also involve a jump at the interface due to the presence of the $\nabla N_j(\mathbf{x}) \psi_j(\mathbf{x}, t)$ term:

$$\begin{aligned} [\![ \nabla u(\mathbf{x}, t) ]\!] &= \sum_{j \in J} \nabla N_j(\mathbf{x}) \left( \left( \psi_j(\mathbf{x}^+, t) - \psi_j(\mathbf{x}^-, t) \right) u_j^* \right. \\ &= 2 \sum_{j \in J} \nabla N_j(\mathbf{x}) u_j^* \end{aligned} \tag{3.9}$$

### 3.2.2 Weak enrichment

When problems involve different materials, the solution may be continuous across the material interface but involve a jump in the gradient, called a weak discontinuity. This type of situation appears in phase change problems [14, 22, 83], immiscible two fluid flows [21] and solid mechanics [72]. To properly solves these problems, a continuous function with a discontinuous derivative at the interface is required for the enriched degrees of freedom. A possible choice to reproduce this behavior is the absolute value of the level set field:

$$\psi_j(\mathbf{x}, t) = |\phi(\mathbf{x}, t)| - |\phi(\mathbf{x}_j, t)| \tag{3.10}$$

As seen in figure 3.2, the resulting enrichment function is continuous, with a jump in the gradient (from -1 to +1 in the case of a signed distance function) at the interface. The jump in the gradient of $\psi_j(\mathbf{x}, t)$ will be present in the gradient of the overall approximation:

$$[\![ \nabla u(\mathbf{x}, t) ]\!] = \sum_{j \in J} N_j(\mathbf{x}) \left( \nabla \psi_j(\mathbf{x}^+, t) - \nabla \psi_j(\mathbf{x}^-, t) \right) u_j^*(t) \tag{3.11}$$

When using equation (3.10) special attention must be given to elements containing enriched nodes without being intersected by the interface, called blending elements [28]. This is because the enriched nodes will not form a partition of unity ($\sum N_j(\mathbf{x}) \neq 1$) within the blending element and spurious terms will remain. The result is a significant drop in the convergence rate of the entire solution. The cause is illustrated with a simple one-dimensional example.

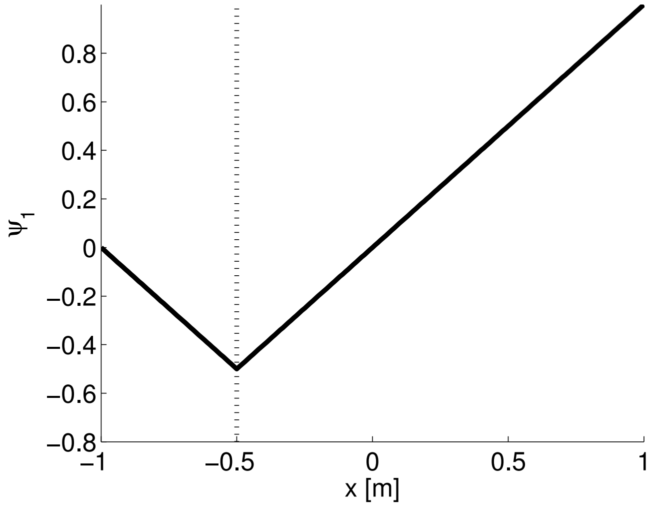

Figure 3.2 – Weak discontinuity enrichment function for left node of 1D element.

Consider a 1D problem with a linear solution, such as the steady state diffusion equation, using two linear elements for the solution variable $u(\mathbf{x}, t)$. The right element contains a (weak) discontinuity in the solution and both nodes are enriched. The solution inside this element (the "enriched" element in figure 3.3) is of the form:

$$u^e(\mathbf{x}, t) = \sum_1^2 N_i(\mathbf{x})u_i + \sum_1^2 N_j(\mathbf{x})\psi_j(\mathbf{x}, t)u_j^* = N_2u_2 + N_3u_3 + N_2\psi_2u_2^* + N_3\psi_3u_3^* \tag{3.12}$$

where the enriched degrees of freedom $u_2^*$ and $u_3^*$ define the jump in the solution gradient (see equation 3.11). Although quadratic terms are present in $N_2\psi_2$ and $N_3\psi_3$, the interpolation functions $N_2$ and $N_3$ represent a partition of unity and the quadratic terms can cancel each other out (if, for example $u_2^* = u_3^*$) while maintaining a discontinuous change in slope. The resulting solution in the enriched element is a piecewise linear function, as required by the steady state diffusion equation.

Let us now consider the left "blending" element (see figure 3.3) with a standard node 1 and an enriched node 2 as shown in figure 3.3. The approximation for $u(\mathbf{x}, t)$ in this element is given by:

$$u(\mathbf{x}, t) = \sum_1^2 N_i(\mathbf{x})u_i + \sum_1^1 N_j(\mathbf{x})\psi_j(\mathbf{x}, t)u_j^* = N_1u_1 + N_2u_2 + N_2\psi_2u_2^* \tag{3.13}$$

The standard part of the approximation forms a linear partition of unity and can properly reproduce the analytical (linear) solution. However, the enrichment part introduces a quadratic term ($N_2\psi_2$) into the approximation which cannot be can-

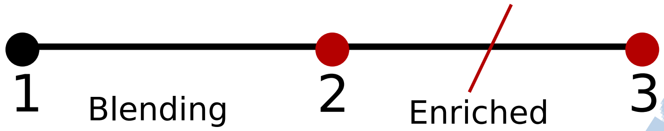

Figure 3.3 – 1D Example of impact of blending elements. Red nodes are "true" enrichment nodes

celled by the standard (and linear) degrees of freedom or another quadratic enrichment term (only one enriched degree of freedom is present), resulting in a loss in convergence of the entire solution.

A modified enrichment scheme, which adds an extra layer of enriched nodes to complete the partition of unity inside blending elements, must be used to maintain an optimal convergence rate as described in [28, 69]. The enrichment function inside blending elements is modified with a ramp function

$$\psi_j^{mod}(\mathbf{x}, t) = N_j(\mathbf{x}) R(\mathbf{x}) \tag{3.14a}$$

$$R(\mathbf{x}) = \sum_{j \in J^*} N_j(\mathbf{x}) \tag{3.14b}$$

where the set $J^*$ is the set of "true" enriched nodes in the element.

As $\mathbf{x}$ tends to a node outside of the set $J^*$, the ramp function tends to zero and the contribution of the enriched degree of freedom disappears. This technique has also been applied to higher-order formulations with curved geometries [20]. Another modified interpolation scheme can be found in [25, 59].

As shown in [54], the handling of blending elements can be avoided by using a Heaviside enrichment as described in the previous section on strong discontinuities. This is possible because the Heaviside enrichment also includes a discontinuity in the gradient, as shown in equation (3.9), and even though the enrichment function is discontinuous, the resulting approximation need not be. In this case, an additional constraint (boundary condition) is applied to enforce the continuity of the solution at the interface. This constraint is not required when using the absolute value function because it is continuous by construction. Finally, a more complex $C^1$ continuous enrichment strategy for weak discontinuities has been developed in [46].

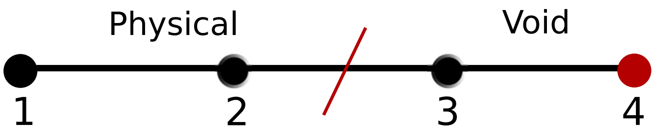

Figure 3.4 – 1D Example of void enrichment. The red node is removed from the system

### 3.2.3 Void enrichment

Certain physical problems can involve sub-domains where the solution is non-physical and must be ignored. Such problems include geometries involving voids in mechanics [72], imperfectly bonded interfaces in elasticity problems [36] and thin structures in fluid-structure interactions [33]. In these cases, we wish to prevent the empty space or undesired structure from contributing to the overall solution. The internal boundary between physical and non-physical domains can then be properly taken into account, improving accuracy. We may also wish to define a larger structured mesh and then solve the problem for only a particular geometry inside the mesh, ignoring the non-physical domain.

Voids do not add a particular non-linear behavior to the solution. Instead, they are used to reduce certain degrees of freedom's domain of influence. This means that no new information, thus no new degrees of freedom, are required. Instead, we modify the interpolation scheme of the standard degrees of freedom in intersected elements to eliminate their contribution in the non-physical domain. The resulting approximation is

$$u(\mathbf{x},t) = \sum_{i\in I} N_i(\mathbf{x})\psi_i(\mathbf{x},t)u_i \tag{3.15a}$$

$$\psi(\mathbf{x},t) = \begin{cases} 1 & \text{if } \phi(\mathbf{x},t) \geq 0 \\ 0 & \text{if } \phi(\mathbf{x},t) < 0 \end{cases} \tag{3.15b}$$

where the Heaviside function (3.15b) is used to set the interpolation to zero inside the non-physical domain, excluding the interface. For elements completely inside the non-physical domain, the degrees of freedom carry no information and are removed from the system as shown in figure 3.4. This approach results in a global system matrix which is identical to a standard finite element approach that does not integrate the non-physical domain.

## 3.3 Dirichlet Boundary Conditions

The imposition of Dirichlet boundary conditions in the extended finite element method can be quite a challenge because the interface does not cross the nodes of the mesh. This means that we cannot apply the boundary condition directly on the nodal degrees of freedom as is usually done in finite elements [66]. In this situation, the two most widely used numerical techniques to apply Dirichlet boundary conditions are the penalty method [14, 22] and Lagrange multipliers [4, 34, 55].

The penalty method applies the interface boundary condition $\overline{u}$ by multiplying the residual form of the constraint with a large penalization parameter $\beta$

$$f_{pen} = \int_{\Gamma} \delta u \beta \left( u - \overline{u} \right) \, \mathrm{d}\Gamma \tag{3.16}$$

and including it in the weak form of the finite element formulation.

This technique has the advantage of being simple to implement. However, it uses a free numerical parameter to be determined by trial and error. In addition, the accuracy of flux evaluations near and at the interface depend on the technique used to calculate them and the parameter $\beta$ [47].

A Lagrange multiplier [4, 34] can also be used to impose the boundary conditions. In this case, a second variable $\Lambda$ is introduced into the system with the interface constraint. For the steady state diffusion equation [55] the system is of the form:

$$\int_{\Omega} \nabla \delta u \nabla u \, \mathrm{d}\Omega - \int_{\Gamma} \delta u \Lambda \, \mathrm{d}\Gamma = 0 \tag{3.17a}$$

$$\int_{\Gamma} \delta \Lambda \left( u - \overline{u} \right) \, \mathrm{d}\Gamma = 0 \tag{3.17b}$$

This technique requires more computational effort but uses no arbitrary parameter. Furthermore, the jump in heat flux at the interface is given directly by $\Lambda$. In problems where the heat flux determines the interface velocity, this asset is non-negligible.

The main challenge in using Lagrange multipliers is the determination of the appropriate Lagrange multiplier space to satisfy the LLB condition [3, 17]. The use of the wrong multiplier space can lead to oscillations in the flux values and a degeneration of the solution [26, 47]. The selection of a correct function space is non-trivial and numerous strategies are found in the literature [6, 8, 55].

A modified Lagrange multiplier formulation was developed in [32] to obtain a stable Lagrange multiplier on the same function space as the solution. To do so, the scalar

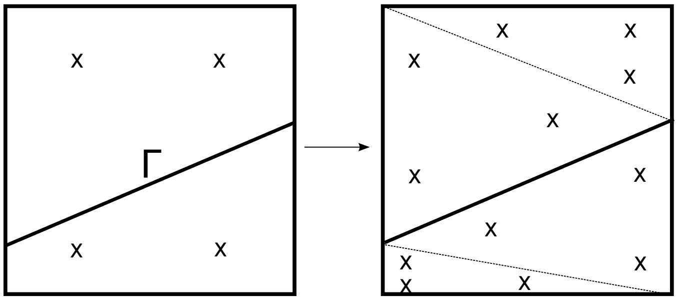

Figure 3.5 – Decomposition of element into triangles for element integration

Lagrange multiplier Λ, which represents the flux at the interface, is redefined as the projection of a flux vector **q** on the interface. The flux is weakly coupled with the solution u in the domain, resulting in :

$$\int_\Omega \nabla \delta u \ \nabla u \ \mathrm{d}\Omega - \int_\Gamma \delta u \mathbf{q} \cdot \mathbf{n}_\Gamma \ \mathrm{d}\Gamma = 0 \tag{3.18a}$$

$$\int_\Omega \delta \mathbf{q} \cdot (\mathbf{q} + \nabla u) \ \mathrm{d}\Omega - \int_\Gamma \delta \mathbf{q} \cdot \mathbf{n}_\Gamma (u - \overline{u}) \ \mathrm{d}\Gamma = 0 \tag{3.18b}$$

## 3.4 Numerical Integration

The introduction of discontinuous approximations inside elements greatly reduces the precision of standard Gaussian quadrature and may lead to rank deficient matrices [22]. An accurate but geometrically complex solution is to subdivide elements involving discontinuities into continuous subelements [22, 34, 56] as shown in figure 3.5. Each element is subdivided into a number of subelements (lines, triangles or tetrahedra) to properly fit the contour of the interface (point, line or surface) and element boundaries. The integral over the entire element $I_e$ is then the sum of the integration of each subelement $I_s$ using standard Hammer quadrature.

Quadrature rules are only readily available on reference elements, meaning that the subelement's quadrature points in its reference frame $\boldsymbol{\xi}'$ must be transformed back into the cut element's reference frame $\boldsymbol{\xi}$ given as

$$\begin{aligned} I_e &= \int_{\Omega^e} f(\mathbf{x})\,\mathrm{d}\mathbf{x} = \int_{\Omega^e} f(\boldsymbol{\xi})|J_x|\,\mathrm{d}\boldsymbol{\xi} && (3.19a)\\ &= \sum_s \left( \int_{\Omega^s} f(\boldsymbol{\xi})\,\mathrm{d}\boldsymbol{\xi} \right) |J_x| \\ &= \sum_s \left( \sum_q f(\boldsymbol{\xi'}_q) w_q |J_\xi| \right) |J_x| \\ J_x &= \frac{\partial \mathbf{x}}{\partial \boldsymbol{\xi}},\ J_\xi = \frac{\partial \boldsymbol{\xi}}{\partial \boldsymbol{\xi}'} && (3.19b) \end{aligned}$$

where $\Omega^e$ is the element domain, s the set of subelements and q the quadrature points.

Since a linear interpolation is used for the geometry and interface, the Jacobians are constant per element. It is important to note that subelements carry no degrees of freedom or interpolation functions. They are only required as a geometric tool to construct the element integrals. As a result, derivatives are defined purely in the reference element $\boldsymbol{\xi}$ and are evaluated as usual.

The main difficulty in determining the proper quadrature points is the geometrical subdivision of the element. In transient problems, the interface can intersect the element in a wide variety of ways, requiring the use of very robust algorithms. This is particularly difficult in 3D. Furthermore, the location of quadrature points must change as the interface moves in time, requiring that every cut element be subdivided at each time step. The subdivision is applied only to a small number of elements, reducing the overall increase in computational effort required. Since a Delaunay triangulation library [68] was readily available and involved minimal modifications to the currently used integration algorithm, the subdivision technique is used in this thesis.

Other techniques for generating accurate quadrature points without element subdivisions have been developed in the literature [57, 58, 77, 78], based on increasing the number of standard quadrature points locally, modifying the integral domain or modifying the interpolation functions.

An important aspect of moving interface problems is the integration of time derivatives. Consider a simple Backward-Euler time stepping scheme:

$$\int_\Omega \delta u \frac{\partial u}{\partial t}\,\mathrm{d}\Omega = \int_\Omega \delta u^{n+1} \frac{u^{n+1} - u^n}{\Delta t}\,\mathrm{d}\Omega \tag{3.20}$$

In the case of enriched elements, the interpolation functions at time steps $n$ and $n+1$ are different for both the test function $\delta u$ and trial function $u$. Consequently, a choice must be made in the evaluation of $u^n$. If the interpolation at time $n$ is used

$$u^n(\mathbf{x}) = \sum_{i \in I} N_i(\mathbf{x}) u_i^n + \sum_{j \in J} N_j^n(\mathbf{x}) \psi_j^n(\mathbf{x}) u_j^{*n} \tag{3.21}$$

two discontinuities, representing the interface at times $n$ and $n+1$ are present in (3.20).

In this case, the integration scheme must take both interfaces into account when generating the integration subelements to obtain optimal convergence [30]. This can be a difficult task and can increase the number of subelements required to fit the geometry, even when the total number of quadrature points required to evaluate the integral exactly is reached. A second option is to use (3.21) and only consider the current interface position when generating the subelements. This approach leads to a numerically stable solution, albeit a slightly less accurate one [30], and has been successfully used in various applications [21, 22] where a weak discontinuity is present. This option was used in the current work.

Finally, a third option is to use the current time step interpolation functions to evaluate the solution at the previous time step using:

$$u^n(\mathbf{x}) = \sum_{i \in I} N_i(\mathbf{x}) u_i^n + \sum_{j \in J} N_j^{n+1}(\mathbf{x}) \psi_j^{n+1}(\mathbf{x}) u_j^{*n} \tag{3.22}$$

In this case, only the current interface discontinuity is present in the integral, simplifying the subdivision process. As the interface moves, certain elements become enriched while others "lose" their enrichment. In other words, the enriched node set J varies at each time step. Consequently, the set of enriched interpolation functions $N_j^{n+1}(\mathbf{x})\psi_j^{n+1}$ may cover nodes with no enriched degrees of freedom. To solve this problem, an estimate, based on surrounding nodes, of previous values is used for previously non-existent nodes [32]. Work done in FSI applications [32] has suggested that this approach may be better suited for problems involving the void enrichment scheme discussed in section 3.2 when a precise pressure solution is desired.

## 3.5 The Level Set Method

Tracking moving interfaces in engineering problems is a complex task, particularly in three dimensions. It is often best to follow these interfaces explicitly to apply physical conditions or extract information from the solution. To do this, the most common technique found in the literature is the level set method [61, 63]. The principle behind this method is to introduce a variable $\phi(\mathbf{x}, t)$ to represent the interface location. The interface is then defined as the position where $\phi(\mathbf{x}, t) = 0$. This function must therefore have the following properties

$$\phi(\mathbf{x}, t) > 0 \text{ for } \mathbf{x} \in \Omega_1 \tag{3.23a}$$

$$\phi(\mathbf{x}, t) < 0 \text{ for } \mathbf{x} \in \Omega_2 \tag{3.23b}$$

$$\phi(\mathbf{x}, t) = 0 \text{ for } \mathbf{x} \in \Gamma \tag{3.23c}$$

$$\Gamma(t) = \{\mathbf{x} \in \Omega_1 \cup \Omega_2 : \phi(\mathbf{x}, t) = 0\} \tag{3.23d}$$

where $\Omega_1 \cap \Omega_2 = \emptyset$ and $\Gamma$ is the common interface to both domains, described in equation (3.23d).

A standard definition for $\phi(\mathbf{x}, t)$ is the signed distance (positive on one side of the interface and negative on the other) between the point $\mathbf{x}$ and the interface $\Gamma$ [61]:

$$\phi(\mathbf{x}, t) = \min_{\mathbf{x}_\Gamma \in \Gamma} |\mathbf{x} - \mathbf{x}_\Gamma(t)| \operatorname{sign}\left(\mathbf{n}_\Gamma \cdot (\mathbf{x} - \mathbf{x}_\Gamma(t))\right) \tag{3.24}$$

If the interface moves in time, the level set variable $\phi(\mathbf{x}, t)$ is updated at each time step using the transport equation

$$\frac{\partial \phi}{\partial t} + F\|\nabla \phi\| = 0 \qquad \mathbf{x} \in \Omega \tag{3.25a}$$

$$F(\mathbf{x}, t) = \frac{\nabla \phi}{\|\nabla \phi\|} \cdot \mathbf{v}_\phi \tag{3.25b}$$

where F is the speed normal to the interface. The weak form is implemented in the finite element model:

$$\int_\Omega \delta\phi \frac{\partial \phi}{\partial t} \, \mathrm{d}\Omega + \int_\Omega \delta\phi F \|\nabla \phi\| \, \mathrm{d}\Omega = 0 \tag{3.26}$$

As it is a first order wave equation, equation (3.26) must be stabilized to prevent convergence problems associated with hyperbolic equations [22, 62]. The Galerkin/Least Square method (GLS) [22, 41] is used in this work and the term

$$\sum_e \int_{\Omega^e} \left( \frac{F}{\|\nabla \phi\|} \nabla \delta\phi \cdot \nabla \phi \right) \tau^e \left( \frac{\partial \phi}{\partial t} + F\|\nabla \phi\| \right) \, \mathrm{d}\Omega \tag{3.27}$$

is added to the residual (3.26) where $\tau^e$ is a element dependent numerical parameter.

Only the velocity at the interface has any physical meaning. It is arbitrary in the rest of the domain and has no impact on the location of the interface. Nonetheless, the transport equation (3.25) requires a properly defined convection velocity on the entire resolution domain. As such, the resolution of the level set problem must include a velocity spreading problem, where the physically defined interface velocity is extended to the entire level set resolution domain by solving equation:

$$\operatorname{sign}(\phi)\nabla F \cdot \nabla\phi = 0 \qquad \mathbf{x} \in \Omega \tag{3.28a}$$

$$F = \frac{\nabla\phi}{\|\nabla\phi\|} \cdot \mathbf{v}_\Gamma \qquad \mathbf{x} \in \Gamma \tag{3.28b}$$

Generally, the level set function will deviate from a signed distance function over time due to the variation of $F(\mathbf{x}, t)$ on the domain [62]. This distortion does not change the position of the interface but modifies the gradient of $\phi(\mathbf{x}, t)$ near the interface ($\|\nabla\phi\| \neq 1$) and introduces errors in the solution of the physical problem solved using the level set solution. Therefore, it is necessary to reset $\phi(\mathbf{x}, t)$ regularly to maintain an acceptable behavior of its gradient near the interface.

The level set method makes the interface easy to locate and track over time without adding significant numerical difficulties [22, 73]. Compared to other interface handling techniques such as the volume of fluid method [40], the level set method is very robust and properly represents curves or complex surfaces, even in three dimensions. It can also handle interface merging and splitting naturally. The calculation of geometric characteristics such as the interface's curvature and normal are easily obtained using [61]:

$$\mathbf{n}_\Gamma = \frac{\nabla\phi}{\|\nabla\phi\|} \tag{3.29}$$

$$\kappa_\Gamma = -\nabla \cdot \mathbf{n}_\Gamma \tag{3.30}$$

The level set formulation is also simple to add to an already existing finite element program as an additional variable of the problem, with its own differential equation to solve. In addition, it offers the advantage of only being required near the interface and does not need to be solved on the entire computational domain of the physical problem. Finally, its main asset is its accuracy and flexibility even in three dimensional cases. Although the work presented in this thesis is in two dimensions, the algorithms that were developed will be extended to three dimensions in future work and a robust three dimensional interface management tool will be needed. This is why the level set method was selected for this project.

# Chapter 4

# A XFEM Lagrange Multiplier Technique for Stefan Problems: Article 1

## 4.1 Resumé

Le problème de changement de phase en deux dimensions a été résolu en utilisant la méthode des éléments finis étendus avec une nouvelle formulation Lagrange pour appliquer la température de fusion à l'interface. L'espace du multiplicateur de Lagrange est identique à celui de la solution et la formulation ne nécessite pas de stabilisation. La vitesse de l' interface solide-liquide est déterminée par le saut dans le flux de chaleur à travers l'interface. Deux méthodes pour calculer le saut sont utilisées et comparées. La première est basée sur un gradient de température moyenne près de l'interface. La seconde utilise la solution du multiplicateur de Lagrange pour évaluer le saut. Les résultats démontrent que la stratégie du multiplicateur de Lagrange est plus robuste et plus précise.

## 4.2 Abstract

The two dimensional phase change problem was solved using the extended finite element method with a novel Lagrange formulation to apply the interface boundary condition. The Lagrange multiplier space is identical to the solution space and does not require stabilization. The solid-liquid interface velocity is determined by the jump in heat flux across the interface. Two methods to calculate the jump are

used and compared. The first is based on an averaged temperature gradient near the interface. The second uses the Lagrange multiplier solution to evaluate the jump. The Lagrange multiplier based approach was shown to be more robust and precise.

## 4.3 Introduction

The finite element method [66] has been extensively studied and successfully used in a wide variety of scenarios involving continuous media but particular situations are still problematic. The finite element method uses polynomial interpolations within individual elements to approximate the solution. Consequently, it can only be applied to problems with discontinuities by splitting the domain into submeshes. This makes the finite element method ill suited to solve problems involving discontinuities that are part of the solution or move in time. The Stefan problem [9, 39, 60, 64] for the isothermal solidification or melting of a material is one such situation.

The extended finite element method [12, 13, 24] is based on the partition of unity method [5, 24, 53]. Using carefully selected functions $\psi_j(\mathbf{x}, t)$, the technique adds additional degrees of freedom that will “enrich" the interpolation and allow the solution to adopt a discontinuous behavior. The particular type of behavior is determined by the enrichment function $\psi_j(\mathbf{x}, t)$, known *a priori*. Only those nodes who’s support is cut by the interface and have a modified behavior must be enriched (see figure 2.1), making the additional computational costs local to the interface. The interface geometry is stored and transported in a computationally efficient manner, most commonly using the level set method [61, 63].

An important challenge in the extended finite element method is the imposition of Dirichlet boundary conditions on the interface. The absence of nodes on the interface means that we cannot apply specified values directly and an additional constraint must be added in the finite element formulation to apply the appropriate boundary condition on the interface. The two main numerical techniques used are the penalty method [14, 22, 83] and Lagrange multiplier method [4, 47, 55]. The penalty method requires the definition of a free numerical parameter to be determined by trial and error. The Lagrange multiplier requires no such numerical parameter but is more computational expensive and may present oscillations in the solution near the interface if an improper interpolation space is used for the multiplier [47, 55].

A recent effort has been done by Gerstenberger and Wall [34] to eliminate this obstacle and facilitate the use of Lagrange multipliers. They have developed a Lagrange multiplier formulation for the solution of problems involving voids in the geometry. The main advantage of their approach is the use of identical interpolation spaces for the solution and Lagrange fields. Although no mathematical proof of its stability was given, numerical applications with the stationary diffusion equation [32] and Navier-Stokes equations in fluid-structure interactions [34] were shown to be stable.

In the work presented here, this novel Lagrange multiplier technique is applied to the classical two dimensional Stefan phase-change problem. The physical nature of the problem being quite different to the FSI problem [33], a different type of enrichment scheme is required. Specifically, a weakly discontinuous temperature field and strongly discontinuous Lagrange multiplier field at the liquid/solid interface. The jump in the Lagrange multiplier value at the interface is then used to determine the interface velocity and compared with a temperature gradient based heat flux calculation.

The paper is divided as follows. The governing equations for the Stefan problem are described in section 4.4 . The finite element formulation, level set problem and details concerning the interface movement and extended finite element method are described in section 4.5. Benchmark examples are then solved in section 4.6 to validate the new Lagrange multiplier approach and compare its performance with the penalization technique commonly found in the literature. Finally, the paper ends with some concluding remarks in section 4.7.

## 4.4 Governing Equations

### 4.4.1 Problem Formulation

Consider a domain $\Omega$ with an initial temperature $T(x, t_0)$ and interface $\Gamma$ separating solid ($\Omega_s$) and liquid ($\Omega_l$) phases with different thermal properties. We suppose that the density is identical in both phases and that the material has an isothermal phase change at some melting temperature $T_m$. Applying the conservation of energy in $\Omega$

results in equation

$$\left(\rho c_p\right)_i \frac{\partial T}{\partial t} - \nabla \cdot (k_i \nabla T) = 0 \qquad \mathbf{x} \in \Omega_i \; i = l,s \tag{4.1a}$$

$$T - T_m = 0 \qquad \mathbf{x} \in \Gamma \tag{4.1b}$$

$$T = \hat{T} \qquad \mathbf{x} \in \Gamma_D \tag{4.1c}$$

$$-k\nabla T \cdot \mathbf{n} = \hat{q} \qquad \mathbf{x} \in \Gamma_N \tag{4.1d}$$

where $(c_p)_i, i = l,s$ is the specific heat, $k_i, i = l,s$ the thermal conductivity and $\rho$ the density. Additionally, the melting temperature must be applied on the solid-liquid interface (4.1b). Dirichlet and Neumann type boundaries away from the interface are applied on $\partial\Omega = \Gamma_N \cup \Gamma_D$ as usual (4.1c,4.1d).

Conservation of energy at the interface requires that the jump in heat flux normal to the interface (caused by the imposition of the melting temperature) be related to the rate of solidification or melting of the material

$$[\![-k_i \nabla T]\!] \cdot \mathbf{n}_\Gamma = (k_l \nabla T_l - k_s \nabla T_s) \cdot \mathbf{n}_\Gamma = \rho L v_\Gamma \qquad \mathbf{x} \in \Gamma \tag{4.2}$$

where $L$ is the latent heat and $v_\Gamma$ the normal interface velocity [64]. The normal vector $\mathbf{n}_\Gamma$ points from the liquid to solid phase, meaning that the interface velocity is positive for melting and negative for solidification.

Tracking the moving interface is done using the level set method [61, 63]. The principle behind this method is to introduce a new variable $\phi(\mathbf{x}, t)$ defined as the signed distance function to the interface (3.24). The interface is then easily identified as the set of points where $\phi(\mathbf{x}, t) = 0$. For more details concerning the level set method, see section 3.5.

### 4.4.2 Enriched Interpolation Scheme

To account for the jump in heat flux at the interface, the temperature field must be continuous with a jump in the gradient. This behavior is captured by using the approximation [22]

$$T(\mathbf{x}, t) = \sum_{i \in I} N_i^T(\mathbf{x}) T_i(t) + \sum_{j \in J} N_j^T(\mathbf{x}) \psi_j^T(\mathbf{x}, t) T_j^*(t) \tag{4.3a}$$

$$\psi_j^T(\mathbf{x}, t) = |\phi(\mathbf{x}, t)| - |\phi(\mathbf{x}_j, t)| \tag{4.3b}$$

for the temperature field where $N_i^T(\mathbf{x})$ and $N_j^T(\mathbf{x})$ are the standard interpolation functions, $T_i$ and $T_j^*$ the standard and enriched degrees of freedom, respectively and $\psi_j^T(\mathbf{x}, t)$ the enrichment function, based on the absolute value of the level set field.

When using (4.3) special attention must be given to elements containing enriched nodes that are not cut by the interface, called blending elements. A modified interpolation scheme must be used in these elements to maintain an optimal convergence rate, as described in [28, 69]. A more compact way to write (4.3) is by using the more standard matrix form:

$$T(\mathbf{x},t) = \langle N_T \rangle \{T\} \tag{4.4a}$$

$$\langle N_T \rangle = \langle N_1^T,\ ...,\ N_{n_I}^T,\ N_1^T \psi_1,\ ...,\ N_{n_J}^T \psi_{n_J} \rangle \tag{4.4b}$$

$$\{T\} = \langle T_1,\ ...,\ T_{n_I},\ T_1^*,\ ...,\ T_{n_J}^* \rangle^T \tag{4.4c}$$

where $n_I$ and $n_J$ are the number of nodes in sets $I$ and $J$.

The Lagrange multiplier $\mathbf{q}$ must reproduce the behavior of the heat flux, which will have a jump at the interface. This behavior is captured by using the approximation:

$$\mathbf{q}(\mathbf{x},t) = \sum_{i \in I} N_i^q(\mathbf{x})\ \mathbf{q}_i(t) + \sum_{j \in J} N_j^q(\mathbf{x}) \psi_j^q(\mathbf{x},t)\ \mathbf{q}_j^*(t) \tag{4.5a}$$

$$\psi_j^q(\mathbf{x},t) = H(\phi(\mathbf{x},t)) - H(\phi(\mathbf{x}_j,t)) \tag{4.5b}$$

$$H(\mathbf{x},t) = \begin{cases} 1 & \text{if } \phi(\mathbf{x},t) < 0 \\ 0 & \text{if } \phi(\mathbf{x},t) > 0 \end{cases} \tag{4.5c}$$

Following expression (4.4), the Lagrange multiplier may be written as:

$$\mathbf{q}(\mathbf{x},t) = [N_q]\{\mathbf{q}\} \tag{4.6a}$$

$$[N_q] = \begin{bmatrix} N_1^q & ... & N_{n_I}^q & N_1^q \psi_1^q & ... & N_{n_J}^q \psi_{n_J}^q & 0 & ... & 0 & 0 & ... & 0 \\ 0 & ... & 0 & 0 & ... & 0 & N_1^q & ... & N_{n_I}^q & N_1^q \psi_1^q & ... & N_{n_J}^q \psi_{n_J}^q \end{bmatrix} \tag{4.6b}$$

$$\{\mathbf{q}\} = \langle q_1^x, \ldots, q_{n_I}^x,\ q_1^{x*},\ ...,\ q_{n_J}^{x*},\ q_1^y,\ \ldots, q_{n_I}^y,\ q_1^{y*}, ..., q_{n_J}^{y*} \rangle^T \tag{4.6c}$$

where $[N_q]$ is the matrix of interpolation functions.

## 4.5 Numerical Implementation

### 4.5.1 Finite Element Formulation

The weak form of the energy conservation equation (4.1a) is

$$\int_{\Omega} \delta T \rho c_p \frac{\partial T}{\partial t} \, \mathrm{d}\Omega + \int_{\Omega} \nabla \delta T \; k \nabla T \, \mathrm{d}\Omega + \int_{\Gamma_N} \delta T \hat{q} \, \mathrm{d}\Gamma = 0 \tag{4.7}$$

where $\delta T$ is the test function. Using a backward Euler scheme for the time derivative of T in (4.7) gives [30]:

$$\int_{\Omega} \delta T \rho \frac{\left(c_p T\right)^{n+1} - \left(c_p T\right)^{n}}{\Delta t} \, \mathrm{d}\Omega + \int_{\Omega} \nabla \delta T^{n+1} \; k^{n+1} \nabla T^{n+1} \, \mathrm{d}\Omega + \int_{\Gamma_N} \delta T \hat{q} \, \mathrm{d}\Gamma = 0 \tag{4.8}$$

Substituting the approximation for the temperature field into (4.8) leads to the finite element system of equations:

$$\frac{1}{\Delta t}[M]\{T\}^{n+1} + [K]\{T\}^{n+1} = \frac{1}{\Delta t}[M]^{*}\{T\}^{n} - \{f\}_q^{n+1} \tag{4.9a}$$

$$[M] = \sum_e \int_{\Omega^e} \{N_T\}^{n+1} \rho c_p^{n+1} \langle N_T \rangle^{n+1} \, \mathrm{d}\Omega \tag{4.9b}$$

$$[M]^{*} = \sum_e \int_{\Omega^e} \{N_T\}^{n+1} \rho c_p^{n} \langle N_T \rangle^{n} \, \mathrm{d}\Omega \tag{4.9c}$$

$$[K] = \sum_e \int_{\Omega^e} ([B_T]^T)^{n+1} k^{n+1} [B_T]^{n+1} \, \mathrm{d}\Omega \tag{4.9d}$$

$$\{f\}_q^{n+1} = \sum_e \int_{\Gamma^e} \{N_T\}^{n+1} \hat{q} \, \mathrm{d}\Gamma \tag{4.9e}$$

$$B_{ij} = \frac{\partial N_i}{\partial x_j}$$

In elements which are intersected by the interface, an additional constraint must be applied to the formulation to take into account the interface boundary condition (4.1b). In this work, two methods are used. The first is the penalization method [14, 22, 83], which applies the melting temperature on the interface by multiplying (4.1b) by a very large penalization parameter $\beta$

$$f_{pen} = \int_{\Gamma} \delta T \beta (T - T_m) \, \mathrm{d}\Gamma \tag{4.10}$$

and including it in the weak form (4.7) for intersected elements only.

The complete system of equations for intersected element then becomes:

$$\left(\frac{1}{\Delta t}[M] + [K] + [P]\right)\{T\}^{n+1} = \frac{1}{\Delta t}[M]^{*}\{T\}^{n} - \{f\}_{q}^{n+1} + \{f\}_{pen}^{n+1} \tag{4.11a}$$

$$[P] = \sum_{e}\int_{\Gamma^e}\{N_T\}^{n+1}\beta\langle N_T\rangle^{n+1}\,\mathrm{d}\Gamma \tag{4.11b}$$

$$\{f\}_{pen}^{n+1} = \sum_{e}\int_{\Gamma^e}\{N_T\}^{n+1}\beta\;T_m\,\mathrm{d}\Gamma \tag{4.11c}$$

This method is simple to implement and adds very little computational effort. However, the choice of $\beta$ can be an important factor in the solution's precision. If $\beta$ is too small, the constraint will not be properly taken into account. If $\beta$ is too large, oscillations can appear along the interface [47]. Moreover, the optimal value is problem dependent and must be found by trial and error.

The second method used in this work to impose the proper boundary condition on the interface is the Lagrange multiplier [47]. This method adds a secondary variable to the formulation. Physically, this secondary variable corresponds to the heat flux generated on the interface from the additional constraint on the problem. Normally, this secondary flux variable is defined purely on the interface and requires the primary (temperature) and secondary (heat flux) variables to respect the inf-sup condition [3, 17]. Otherwise, oscillations may appear in the solution near the interface [8, 47, 55].

To overcome this difficulty, a new adaptation of this method was developed in [6, 34], based on the Lagrange multiplier technique found in [84]. Here, the Lagrange multiplier is defined as a vectorial flux and interpolated on the same mesh as the temperature field. The projection of this secondary variable on the interface is then used as a scalar Lagrange multiplier to impose the melting temperature. Note that since the secondary variable is now a vector field, two additional unknowns have been added. To obtain a properly defined problem, the secondary variable is weakly coupled with the flux calculated from the temperature gradient in the domain and a complete system of equations is obtained [32]:

$$\int_{\Omega}\delta T\rho c_p\frac{\partial T}{\partial t}\,\mathrm{d}\Omega + \int_{\Omega}\nabla\delta T\;k\nabla T\,\mathrm{d}\Omega + \int_{\Gamma_N}\delta T\hat{q}\,\mathrm{d}\Gamma_N - \int_{\Gamma}\delta T\mathbf{q}\cdot\mathbf{n}_{\Gamma}\,\mathrm{d}\Gamma = 0 \tag{4.12a}$$

$$\int_{\Omega}\delta\mathbf{q}\cdot\left(\frac{1}{k}\mathbf{q} + \nabla T\right)\,\mathrm{d}\Omega - \int_{\Gamma}\delta\mathbf{q}\cdot\mathbf{n}_{\Gamma}\left(T - T_m\right)\,\mathrm{d}\Gamma = 0 \tag{4.12b}$$

After applying the backward Euler scheme [30] to the time derivative and replacing $T$ and $\mathbf{q}$ with their interpolation schemes (4.4) and (4.6), we obtain the following system of equations for intersected elements:

$$\begin{bmatrix} \frac{1}{\Delta t}[M]+[K] & -[L] \\ [Q]-[L]^T & [M_q] \end{bmatrix} \begin{Bmatrix} \{T\}^{n+1} \\ \{\mathbf{q}\}^{n+1} \end{Bmatrix} = \begin{bmatrix} \frac{1}{\Delta t}[M]^* & 0 \\ 0 & 0 \end{bmatrix} \begin{Bmatrix} \{T\}^{n} \\ \{\mathbf{q}\}^{n} \end{Bmatrix} - \begin{Bmatrix} \{f\}_q^{n+1} \\ \{f\}_{lag} \end{Bmatrix} \tag{4.13a}$$

$$[M_q] = \sum_e \int_{\Omega^e} \frac{1}{k^{n+1}} \left([N_q]^T\right)^{n+1} [N_q]^{n+1} \, \mathrm{d}\Omega \tag{4.13b}$$

$$[Q] = \sum_e \int_{\Omega^e} \left([N_q]^T\right)^{n+1} [B_T]^{n+1} \, \mathrm{d}\Omega \tag{4.13c}$$

$$[L] = \sum_e \int_{\Gamma^e} \{N_T\}^{n+1} [N_q]^{n+1} \mathbf{n}_\Gamma \, \mathrm{d}\Gamma \tag{4.13d}$$

$$\{\mathbf{f}\}_{lag} = \sum_e \int_{\Gamma^e} ([N_q]^T)^{n+1} \cdot \mathbf{n}_\Gamma \, T_m \, \mathrm{d}\Gamma \tag{4.13e}$$

In elements which are not cut by the interface, the boundary condition is removed and the system reduces to:

$$\begin{bmatrix} \frac{1}{\Delta t}[M]+[K] & 0 \\ [Q] & [M_q] \end{bmatrix} \begin{Bmatrix} \{T\}^{n+1} \\ \{\mathbf{q}\}^{n+1} \end{Bmatrix} = \begin{bmatrix} \frac{1}{\Delta t}[M]^* & 0 \\ 0 & 0 \end{bmatrix} \begin{Bmatrix} \{T\}^{n} \\ \{\mathbf{q}\}^{n} \end{Bmatrix} - \begin{Bmatrix} \{f\}_q^{n+1} \\ 0 \end{Bmatrix} \tag{4.14}$$

As described in [34], the interpolation used for the Lagrange multiplier can be $\mathrm{C}^{-1}$ discontinuous at inter-element boundaries, allowing the condensation of equation (4.13) on the element level. The resulting contribution of $\mathbf{q}$ is added to the global matrix for elements intersected by the interface. Only the temperature field is solved, reducing the size of the global system of equations. The secondary flux variables may then be calculated from the temperature values [34].

### 4.5.2 Level Set Formulation

Once an initial value $\phi(\mathbf{x}, t_0)$ is defined using (3.24), the interface movement is governed by its transport equation (3.26). In this work, an explicit time scheme is used to solve (3.26).

The main disadvantage of the the level set method is its tendency to deviate from a signed distance function over time [61]. This error accumulates with additional time steps and degrades the quality of the solution, particularly the level set gradient near the interface. This distortion can be a source of error in the numerical solution

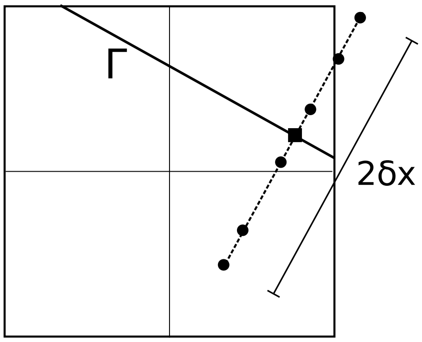

Figure 4.1 – Gradient based velocity calculation. Circles show T evaluation points, square shows $v_\Gamma$ evaluation point

of the level set formulation and the physical problem on which it is based. Therefore, it is necessary to reinitialize $\phi(\mathbf{x}, t)$ regularly to maintain an acceptable solution ($\|\nabla\phi\| \approx 1$). Another limitation to the level set method is the use of an explicit time scheme, which limits the size of the time step. The explicit time step is required in order to determine the nodes to enrich. In other words, the interface position must be determined before equations (4.11) or (4.13) can be solved.

### 4.5.3 Interface velocity calculation

The proper evaluation of fluxes on either side of the interface in equation (4.2) is crucial in obtaining a precise and robust model. The simplest way to evaluate the jump in heat flux across the discontinuity is to evaluate the gradient at points in the solid and liquid phases at some small distance perpendicular to the interface [22, 83]. However, this approach may be the least accurate option [47]. A more involved but robust technique is to evaluate the temperature at multiple points at specific distances from the interface to obtained an averaged value [14]. This approach is used in this work and of the form

$$\begin{aligned} v_\Gamma = \frac{1}{\rho L}\frac{2}{5}\Bigg[ & k_s \frac{2\,T(x_\Gamma) + T(x_s^{\delta x/4}) - T(x_s^{3\delta x/4}) - 2\,T(x_s^{\delta x})}{\delta x} \\ & -k_l \frac{2\,T(x_l^{\delta x}) + T(x_l^{3\delta x/4}) - T(x_l^{\delta x/4}) - 2\,T(x_\Gamma)}{\delta x}\Bigg] \end{aligned} \tag{4.15}$$

where $\delta x$ is some fraction of the average element size (figure 4.1).

When applying the Lagrange multiplier technique another option becomes available. As previously mentioned, the Lagrange multiplier corresponds to the heat flux within the element. We can evaluate the jump in heat flux across the interface directly from the Lagrange field, given by:

$$v_\Gamma = \frac{[\![\mathbf{q}]\!] \cdot \mathbf{n}_\Gamma}{\rho L} = \frac{(\mathbf{q}_l - \mathbf{q}_s) \cdot \mathbf{n}_\Gamma}{\rho L} \tag{4.16}$$

This is done by evaluating the Lagrange field on the interface, approaching from either side. A similar strategy was used by [54], using an iterative procedure based on the LATIN method to impose the interface temperature. To our knowledge, no Lagrange multiplier based algorithm for the Stefan problem has been developed using this strategy for the interface velocity.

The final algorithm can be described as follows. Assuming a given time $t^n$, temperature solution $T^n$ and level set solution $\phi^n$, the strategy to solve for $\phi^{n_1}$ and $T^{n+1}$ consists in the following steps:

1. Compute the interface velocity $\mathbf{v}_\Gamma^n$ using (4.15) or (4.16)
2. Construct F on the level set domain by solving problem (3.28)
3. Solve for $\phi^{n+1}$ using (3.26)
4. Solve for $T^{n+1}$ using (4.11) or (4.13)
5. Set $t^{n+1} = t^n$ and go to step 1

## 4.6 Results

To validate the new Lagrange formulation and compare its performance with the penalty method, two benchmark problems were solved with both approaches. To evaluate the precision of the imposed Dirichlet boundary condition on the interface, the penalty (4.11) and Lagrange formulations (4.13) were compared using the same gradient based interface velocity algorithm (4.15), referred to as case I. A third solution to the problem was also obtained by using the Lagrange multiplier jump value to evaluated the interface velocity (4.16), referred to as case II .

To evaluate the impact of the Lagrange field's polynomial degree on the solution, two implementations of the Lagrange formulation were used. In the first, the Lagrange field is linear and continuous at inter-element boundaries (C$^0$ continuous). In the second, the Lagrange field is constant per element and condensed on the element level (C$^{-1}$ continuous) [34]. Both linear and constant interpolation schemes were tested with both gradient (4.15) and Lagrange (4.16) based velocity values, for

| Properties | Solid | Liquid | Interface |
|---|---|---|---|
| $\rho c_p$ [J/m$^3$ K] | $2.05 \times 10^6$ | $2.59 \times 10^6$ | - |
| $k$ [W/m K] | 4.02 | 2.89 | - |
| $\rho L$ [J/m$^3$] | - | - | $8.03 \times 10^7$ |
| $T_m$ [K] | - | - | 273.0 |

Table 4.1 – Material properties for 2 phase 1D problem

a total of 4 distinct solving algorithms based on the Lagrange multiplier technique and one using penalization. The temperature field interpolation is linear in all cases.

### 4.6.1 2 Phase 1D problem

The first benchmark problem is the one dimensional two phase analytical solution of the Stefan problem in a semi-infinite domain ($x > 0$), taken from [54]. The thermal properties are phase dependent and given in table 4.1. The domain is initially liquid, as shown in figure 4.2, with the solid-liquid interface 2 mm away from the left domain boundary. The computation is done on a rectangle 0.1 m long and 0.025 m wide (figure 4.2). The initial temperature is 277 K. The top and bottom edges are insulated. At $t = 0$, the temperature on the left edge is lowered to 263 K and the right edge is maintained at 277 K. Temperature evaluation points for the gradient based velocity calculations are taken at a maximum distance of 10% of the mean element size, $\beta = 10^8$ where applicable and the convergence criteria for the Newton-Raphson algorithm is $10^{-6}$.

The interface position, as a function of time for both interface boundary condition techniques, is shown in figure 4.3. Three different mesh sizes were used to verify the convergence of the various techniques, and are shown in figure 4.4. The error norms are calculated using (4.17a) where $x_\Gamma^a$ is the analytical interface position for a semi-infinite medium and $\lambda = 0.3073$ [54]. The time step was chosen as $\Delta t = \Delta x^2 \left(\frac{\rho c_p}{k}\right)_s$ [54].

$$E = \int_0^t \sqrt{(x_\Gamma - x_\Gamma^a)^2} \mathrm{dt} \tag{4.17a}$$

$$x_\Gamma^a = 2\lambda \sqrt{\frac{k}{\left(\rho c_p\right)_s} t} \tag{4.17b}$$

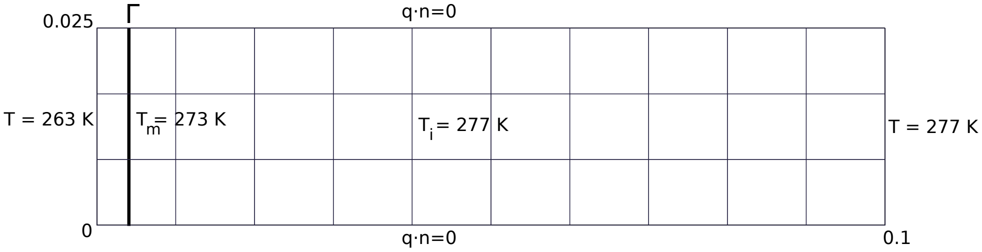

Figure 4.2 – 1D problem definition. Largest mesh size shown (30 elements)

As shown in figure 4.3, the numerical solutions follows the analytical solution up to approximately 3000 seconds. Beyond this point, the effects of the finite computation domain become apparent. The same behavior was observed by [54]. Consequently, the error norms shown in figure 4.4 are calculated over the time interval [0, 3000]. The convergence curves show that all techniques converge to the analytical value. However, differences in performance for the different algorithms are apparent. It is clear that using the Lagrange multiplier to evaluate the interface velocity (case II) improves the solution compared to the gradient based evaluation (case I). This behavior is explained by the approximative nature of the gradient based calculation, which uses multiple values further away from the interface to determine a locally averaged gradient. To obtain a precise value, the flux jump must be calculated directly on the interface. The use of the Lagrange multiplier gives us an easy and precise way of doing so.

The use of different interpolation schemes has a much smaller impact on performance. A small increase in precision is obtained by using a linear interpolation for the Lagrange multiplier field, no matter the interface velocity used. In fact, the use of a constant per element Lagrange field leads to a slightly less precise solution than the penalization technique when the gradient based interface velocity is used. This difference may be caused by the use of bi-linear quadrilateral elements for the temperature field. When using bi-linear interpolation functions, the gradient varies linearly inside the element. Consequently, the constant per element Lagrange field cannot reproduced the behavior of the temperature gradient within the element exactly. An identical performance is observed between the linear Lagrange field and penalization algorithms using the gradient based interface velocity, indicating that both approaches enforce the melting temperature equivalently.

From a more practical point of view, the gradient based calculation has certain drawbacks. First of all, it requires the determination of 6 evaluation points normal to the

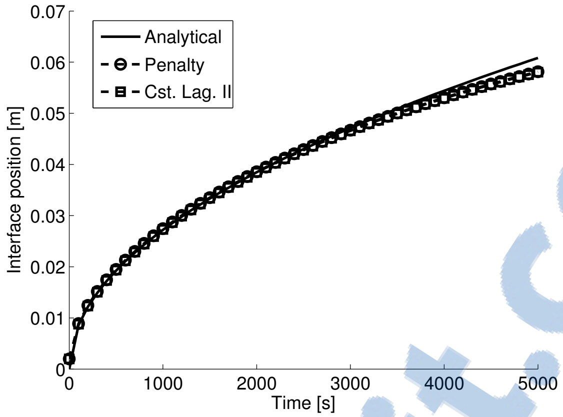

Figure 4.3 – Interface position for 1D problem. Penalization and Cst. Lag. II algorithms shown

interface, which will vary with changing interface geometries and must be determined at every time step. Secondly, some of theses points may be outside of the calculation domain depending on the interface position (see figure 4.1) and must be treated by some approximation, depending on the situation. These extra tasks increase the computational effort and code complexity. By contrast, the Lagrange based velocity is evaluated directly on the interface and avoids these extra steps and approximations. Ultimately, the extra computational effort required for the gradient based interface velocity is traded for the effort required to solve the more involved condensed Lagrange formulation. Depending on the exact implementation, either approach may be slightly faster. In our case, the condensed Lagrange formulation was slightly quicker. The uncondensed Lagrange formulation lead to a much larger tangent matrix and was the slowest due to the longer global system resolution time.

Time steps significantly smaller than $\Delta x^2 \left(\frac{\rho c_p}{k}\right)_s$ would lead to erroneous interface temperatures at early times with the Lagrange formulation as shown in figure 4.5. The effect of time step size on the solution of transient heat transfer problems using the finite element method has been previously investigated in [76]. However, it is important to note that the penalty formulation was unaffected at the tested time step of $\frac{\Delta x^2}{100}\left(\frac{\rho c_p}{k}\right)_s$(figure 4.5), suggesting that the Lagrange multiplier is more sensitive to this phenomenon.

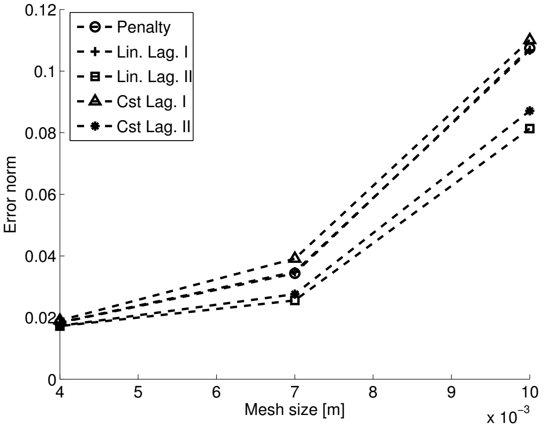

Figure 4.4 – Interface position error norm for 1D problem for different mesh sizes

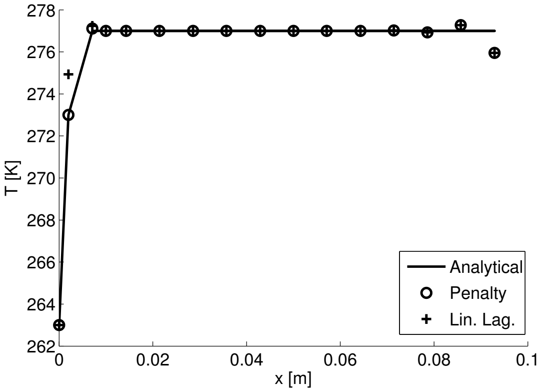

Figure 4.5 – Temperature profile at $1^{st}$ time step using $\Delta t = \frac{\Delta x^2}{100}\left(\frac{\rho c_p}{k}\right)_s$

### 4.6.2 2 Phase 2D problem

The second benchmark problem is the two phase analytical solution of the Stefan problem in two dimensions, taken from [2]. The thermal properties are constant and given in table 4.2. The domain is a 2 m by 2 m square with the interface initally at 0.035 m from the boundary as shown in figure 4.6. The domain is initially liquid with initial temperature 273.3 K. The top and right edges are insulated. At $t = 0$, the temperature on the left and lower edges are lowered to 272 K. The analytical solution of this problem was first developed in [65]. The non-dimensionalized interface position $y'(x')$ is determined using equation (4.18c) where $C = 0.159$, $m = 5.02$ and $\lambda = 0.70766$ for the given material properties and boundary conditions, $\alpha$ is the

| Property | Solid | Liquid | Interface |
|---|---|---|---|
| $\rho c_p$ [J/m$^3$ K] | 1.0 | 1.0 | - |
| $k$ [W/m K] | 1.0 | 1.0 | - |
| $L$ [J/kg] | - | - | 0.25 |
| $T_m$ [K] | - | - | 273.0 |

Table 4.2 – Material properties for 2D problem

thermal diffusivity and $x'$ the non-dimensionalized x axis.

$$y'(x') = \left(\lambda^m + \frac{C}{(x')^m - \lambda^m}\right)^{\frac{1}{m}} \tag{4.18a}$$

$$x' = \frac{x_\Gamma}{\sqrt{4\alpha t}} \tag{4.18b}$$

$$y' = \frac{y_\Gamma}{\sqrt{4\alpha t}} \tag{4.18c}$$

Temperature evaluation points for the gradient based velocity calculations are taken at a maximum distance of 35% of the mean element size, $\beta = 10^9$ where applicable and the convergence criteria for the Newton-Raphson algorithm is $10^{-4}$. The level set formulation used in this work does not have a reinitialization procedure. To validate the present Lagrange formulation and compare the various algorithms, the problem was simulated using $\Delta t$ =$5 \times 10^{-5}$ s. The small time step was used to properly capture the rapid interface movement in the first few time steps, caused by the important temperature gradient between the boundary and initial interface. The final interface position at $t = 0.025\ s$ is shown for the different algorithms and the analytical solution in figure 4.7. The error norms for the final interface position are given in table 4.3. The error norms were calculated using equation (4.19) where $(x_n^{num}, y_n^{num})$ is the position on the interface of the numerical solution, $(x'_{min}, y'_{min})$ the position on the analytical interface (4.18a) closest to $(x_n^{num}, y_n^{num})$ and n the total number of points taken on the interface.

$$E = \frac{1}{n}\sum_{1}^{n}\sqrt{(x'_{min} - x_n^{num})^2 + (y'_{min} - y_n^{num})^2} \tag{4.19}$$

As shown in figure 4.7, the numerical solution is in agreement with the analytical solution for all algorithms, indicating that both approaches enforce the melting temperature appropriately in 2D as well. No improvement in the solution is obtain by using the linear or constant Lagrange formulation compared to the penalty formulation when using the gradient based interface velocity. Using the linear Lagrange

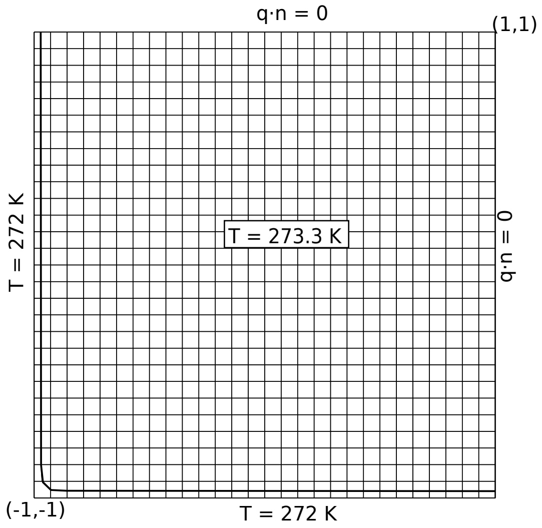

Figure 4.6 – 2D problem definition (784 elements)

field interface velocity significantly improved the solution. The use of the constant Lagrange field interface velocity also increased the accuracy but to a smaller extent. This is probably due to the inability of the constant Lagrange field to reproduce the linear gradient of the bi-linear quadrangle interpolation used for the temperature. As a result, a linear Lagrange formulation, using a Lagrange based interface velocity, would lead to an optimal algorithm in terms of accuracy. To reduce the resolution time, a C$^{-1}$ continuous linear interpolation could be used and condensed on the element level [34].

It is well known in the literature that the level set field must be regularly reinitialized to maintain accurate results [22, 62]. The one dimensional problem does not require this step because the interface velocity is constant on the entire domain. The two dimensional problem involves varying interface velocities in space and distortions in the level set field may appear. The absence of a reinitialization step in this work did not have a significant impact on the stability of the simulation. However, a detailed convergence study for different time steps and mesh sizes would be influenced by the accumulated error in the level set field and has not been done.

Another practical aspect that was observed in the 2D case was the importance of numerical parameter selection. For the penalty formulation, two user-based numerical parameters are required: the penalty term $\beta$ and the maximum element distance $\delta x$ to evaluate the interface velocity. An inappropriate selection of either of these parameters could lead to a significant reduction in precision of the interface position,

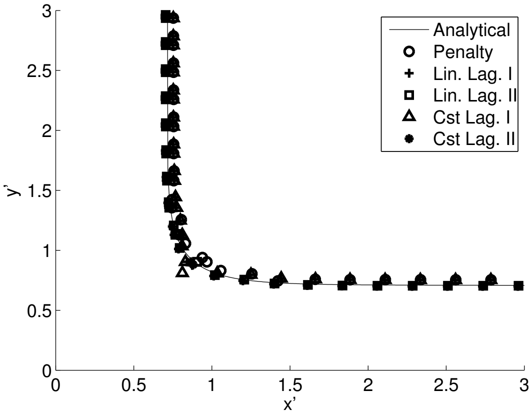

Figure 4.7 – Final non-dimensionalized interface position for 2D problem

| Algorithm | Error norm |
|---|---|
| Penalty | 0.043 |
| Lin. Lag. I | 0.041 |
| Lin. Lag. II | 0.005 |
| Cst. Lag. I | 0.044 |
| Cst. Lag. II | 0.010 |

Table 4.3 – Error norms for 2D benchmark final interface position

with the distance $\delta x$ having a much more significant impact than $\beta$. As an example, the benchmark problem using the penalty formulation was solved using $\delta x = 20\%$. The interface position at $t = 6.25 \times 10^{-3}$s, at which point the program fails, is shown in figure 4.8. The failure is caused by the important variation in the calculated heat flux near the interface, greatly distorting the interface.

## 4.7 Conclusion

In this work, the Lagrange multiplier scheme developed by [34] was applied to the classical Stefan problem in one and two dimensions using a weakly discontinuous temperature field and strongly discontinuous flux-based Lagrange field. We have shown that it allows the application of Dirichlet boundary conditions with comparable precision to the penalty technique [22] using constant and linear interpolation schemes for the Lagrange field. Furthermore, a gain in accuracy was obtained by calculating the interface velocity using the Lagrange field instead of the more widely used temperature gradient and reduced the discrepancy in computational cost be-

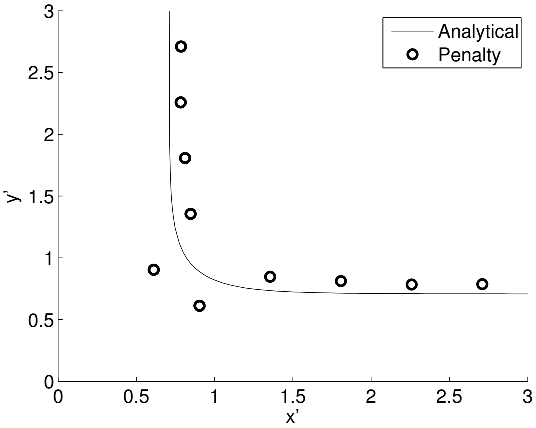

Figure 4.8 – Interface position at $t$ =6.25 $\times$ $10^{-3}$ using $\delta x = 20\%$

tween the two techniques. The Lagrange based formulation requires no user defined numerical parameters, improving the model's robustness. Further work will be realized to account for convection in the liquid phase and mass flux at the interface in problems involving different densities in the solid and liquid phases.

# Chapter 5

# A XFEM Phase Change Model with Convection: Article 2

## 5.1 Resumé

Un modèle à deux phases pour les problèmes de solidification bidimensionnelles avec convection a été développé en couplant le problème de Stefan avec le problème de Stokes. La méthode des éléments finis étendus (XFEM) a été utilisée pour capturer la forte discontinuité dans la vitesse et la pression ainsi que le saut dans le flux de chaleur à l'interface du changement de phase. La température de fusion et la vitesse nulle à l'interface ont été imposées en utilisant un multiplicateur de Lagrange et la méthode de pénalisation, respectivement. Les formulations résultantes ont ensuite été couplées en utilisant un algorithme d'itération par point fixe. Le modèle a été capable de reproduire les simulations de référence tout en conservant une interface nette de changement de phase.

## 5.2 Abstract

A model for two dimensional solidification problems including convection was developed by coupling the Stefan problem with the Stokes problem. The extended finite element method (XFEM) was used to capture the strong discontinuity in velocity and pressure as well as the jump in heat flux at the phase change interface. The melting temperature and no-slip condition were imposed on the interface us-

ing a Lagrange multiplier and the penalization method, respectively. The resulting formulations were then coupled using a fixed point iteration algorithm. The model was able to reproduce the benchmark simulations while maintaining a sharp phase change interface.

## 5.3 Introduction

Numerous extended finite element models for the solution of the classical (diffusive) Stefan problem are found in the literature [14, 22, 46, 54]. However, most real-life scenarios involve heat and mass transfer by convection in the liquid phase [16, 80, 83]. The impact of this additional contribution on the behavior of the phase change interface has been explored for dendritic solidification in [83] using an extended finite element formulation for the Stefan problem and a phase-field formulation for the Navier-Stokes equations. To our knowledge, no coupled extended finite element formulation for both Stefan and Stokes equations exists in the literature. Such an approach reduces the algorithm's complexity, as a single numerical method is used to model the discontinuities in both problems. Furthermore, the extended finite element method allows for accurate results with larger mesh sizes compared to diffused techniques.

A Navier-Stokes formulation using XFEM to track an explicit solid-liquid interface has been developed in [32] and applied to fluid-structure interaction (FSI) problems. In this formulation, the Navier-Stokes equations are only solved in the liquid phase and appropriate boundary conditions are applied to allow the fluid pressure to interact with the solid structure.

For the Stefan problem, a Lagrange multiplier formulation using XFEM was recently developed [52] based on the work done in [34] on fluid structure interactions. In [52], the Lagrange multiplier formulation was shown to be stable and more precise than the penalty method commonly used [22] but did not include convective heat transfer, required for problems involving fluids.

For more complex problems, the use of different densities in the solid and liquid phases for the phase-change problem leads to a mass flux boundary in the Navier-Stokes equations which may be difficult to implement using a diffused solid-liquid boundary. The explicit interface used in this work provides a solid framework for developing such models.

In the work presented here, a coupled formulation using the extended finite element method for both the Stefan problem and Stokes equations is developed. The convective term present in the energy equation is obtained from the solution of the Stokes equations and the Boussinesq approximation is used to generate the natural convection within the liquid. A fixed point iteration scheme is then used to obtain a converged solution for a given time step. The Lagrange multiplier and penalty methods are used to apply the temperature and velocity Dirichlet boundary conditions on the interface, respectively.

The paper is divided as follows. The governing equations for the Stefan and Stokes problems are described in section 5.4. The finite element formulation, level set problem and details concerning the interface movement and extended finite element method are described in section 5.5. A benchmark example is then solved in section 5.6 to validate the algorithm. To this end, the commercial finite element simulation software Comsol was used. Finally, the paper ends with some concluding remarks.

## 5.4 Governing Equations

### 5.4.1 Stefan Formulation

Consider a domain $\Omega$ with an initial temperature $T(x, t_0)$ and interface $\Gamma$ separating solid ($\Omega_s$) and liquid ($\Omega_l$) phases with different thermal properties. We suppose that the density is identical in both phases and that the material has an isothermal phase change at some melting temperature $T_m$. Applying the conservation of energy in $\Omega$ results in equations

$$\left(\rho c_p\right)_s \frac{\partial T}{\partial t} - \nabla \cdot (k_s \nabla T) = 0 \qquad \mathbf{x} \in \Omega_s \tag{5.1a}$$

$$\left(\rho c_p\right)_l \left(\frac{\partial T}{\partial t} + \mathbf{v} \cdot \nabla T\right) - \nabla \cdot (k_l \nabla T) = 0 \qquad \mathbf{x} \in \Omega_l \tag{5.1b}$$

$$T - T_m = 0 \qquad \mathbf{x} \in \Gamma \tag{5.1c}$$

$$T = \hat{T} \qquad \mathbf{x} \in \Gamma_D \tag{5.1d}$$

$$-k \nabla T \cdot \mathbf{n} = \hat{q} \qquad \mathbf{x} \in \Gamma_N \tag{5.1e}$$

where $c_p$ is the specific heat, $k$ the thermal conductivity, $\rho$ the density and $\mathbf{v}$ the liquid phase velocity. Additionally, the melting temperature must be applied on the solid-liquid interface (5.1c). Dirichlet and Neumann type boundaries away from the interface are applied on $\partial\Omega = \Gamma_N \cup \Gamma_D$ as usual (5.1d,5.1e).

Conservation of energy at the interface requires that the jump in heat flux normal to the interface (caused by the imposition of the melting temperature) be related to the rate of solidification or melting of the material as described by

$$[\![-k\nabla T]\!] \cdot \mathbf{n}_\Gamma = (k_l \nabla T_l - k_s \nabla T_s) \cdot \mathbf{n}_\Gamma = \rho L v_\Gamma \qquad \mathbf{x} \in \Gamma \tag{5.2}$$

where $L$ is the latent heat and $v_\Gamma$ the normal interface velocity [64]. The normal vector $\mathbf{n}_\Gamma$ points from the liquid to solid phase, meaning that the interface velocity is positive for melting and negative for solidification.

Tracking the moving interface is done using the level set method [61, 63]. The principle behind this method is to introduce a new variable $\phi(\mathbf{x}, t)$ defined as the signed distance function to the interface (3.24). The interface is then easily identified as the set of points where $\phi(\mathbf{x}, t) = 0$. In this work, the level set field is constructed so that the liquid phase is on the positive side of the interface (i.e. $\mathbf{x} \in \Omega_l$ if $\phi(\mathbf{x}, t) > 0$).

### 5.4.2 Stokes formulation

In the present study, the liquid phase velocity $\mathbf{v}$ is governed by the Stokes problem for viscous incompressible fluids:

$$\rho \frac{\partial \mathbf{v}}{\partial t} = \nabla \cdot \sigma + \mathbf{f}_b \qquad \mathbf{x} \in \Omega_l \tag{5.3a}$$

$$\nabla \cdot \mathbf{v} = 0 \qquad \mathbf{x} \in \Omega_l \tag{5.3b}$$

$$\mathbf{v} = 0 \qquad \mathbf{x} \in \Gamma \tag{5.3c}$$

$$\mathbf{v} = \hat{\mathbf{v}} \qquad \mathbf{x} \in \Gamma_D \tag{5.3d}$$

$$\sigma \cdot \mathbf{n} = \hat{\sigma} \qquad \mathbf{x} \in \Gamma_N \tag{5.3e}$$

$$\mathbf{f}_b = \rho \eta (T - T_m) \mathbf{g} \tag{5.3f}$$

$$\sigma = -p\mathbf{I} + 2\mu D(\mathbf{v}) \tag{5.3g}$$

$$D(\mathbf{v}) = \frac{1}{2} \left( \nabla \mathbf{v} + \nabla \mathbf{v}^T \right) \tag{5.3h}$$

where $p$ is the pressure, $\mu$ the viscosity, $\mathbf{f}_b$ the buoyancy source term, $\eta$ the thermal expansion coefficient and $D(\mathbf{v})$ the rate of deformation tensor. The convection term required to solve the complete Navier-Stokes equations requires a stabilization term to obtained converged (and accurate) solutions at higher Reynold numbers and will be implemented in the future.

The buoyancy force $\mathbf{f}_b$ term will create natural convection currents caused by variations in temperature. The density is assumed constant and identical for both phases

(Boussinesq approximation) so no mass flux is present at the interface and a no-slip condition is applied (5.3c). The other physical properties are assumed constant. The initial velocity field $\mathbf{v}(\mathbf{x}, t_0)$ is assumed divergence-free with a given initial pressure field $p(\mathbf{x}, t_0)$. Dirichlet and Neumann type boundaries away from the interface are applied on $\partial\Omega = \Gamma_N \cup \Gamma_D$ as usual (5.3d, 5.3e).

### 5.4.3 Enriched Interpolation Scheme

To account for the jump in heat flux at the interface, the temperature gradient must be discontinuous. Furthermore, the application of the interface boundary condition (5.1c), implies that the temperature is continuous at the interface. This behavior is captured by using approximation (4.3) [22].

When using (4.3) special attention must be given to elements containing enriched nodes that are not cut by the interface, called blending elements. A modified interpolation scheme must be used in these elements to maintain an optimal convergence rate, as described in [28, 69].

In order to capture the jump in the heat flux at the interface, a Lagrange multiplier **q** is used [32]. The interpolation scheme for the Lagrange multiplier is given by (4.5) and in matrix form (4.6).

The Stokes equations are valid (and solved) in the liquid phase only. For this purpose, the fluid-structure interaction approach, proposed in [33], is used. The velocity and pressure fields are interpolated using the following scheme:

$$\mathbf{v}(\mathbf{x}, t) = \sum_{i \in I} N_i^v(\mathbf{x}) \psi^v(\mathbf{x}, t)\ \mathbf{v}_i(t) \tag{5.4a}$$

$$p(\mathbf{x}, t) = \sum_{i \in I} N_i^p(\mathbf{x}) \psi^v(\mathbf{x}, t)\ p_i(t) \tag{5.4b}$$

$$\psi^v(\mathbf{x}, t) = \begin{cases} 1 & \text{if } \phi(\mathbf{x}, t) > 0 \\ 0 & \text{if } \phi(\mathbf{x}, t) < 0 \end{cases} \tag{5.4c}$$

Following (4.4) and (4.6), the velocity and pressure fields may be rewritten as:

$$\mathbf{v}(\mathbf{x}, t) = [N_v]\{\mathbf{v}\} \tag{5.5a}$$

$$p(\mathbf{x}, t) = \langle N_p \rangle \{\, p\} \tag{5.5b}$$

$$[N_v] = \begin{bmatrix} N_1^v \psi_1^v & ... & N_{n_I}^v \psi_{n_I}^v & 0 & ... & 0 \\ 0 & ... & 0 & N_1^v \psi_1^v & ... & N_{n_I}^v \psi_{n_I}^v \end{bmatrix} \tag{5.5c}$$

$$\{\mathbf{v}\} = \langle v_1^x, ... \,, \; v_{n_I}^x, v_1^y, ... \,, \; v_{n_I}^y \rangle^T \tag{5.5d}$$

$$\langle N_p \rangle = \langle N_1^p \psi_1^v, ..., \; N_{n_I}^p \psi_{n_I}^v \rangle \tag{5.5e}$$

$$\{p\} = \langle p_1, \; ..., \; p_{n_I} \rangle^T \tag{5.5f}$$

When using this interpolation scheme, the solid part of the domain is ignored. Also, enriched degrees of freedom are not required because no new information (behavior) is introduced. All velocity and pressure degrees of freedom whose support is completely inside the solid domain are removed from the system of equations.

## 5.5 Numerical Implementation

### 5.5.1 Stefan Problem

The weak form of the energy conservation equations (5.1a,5.1b) is

$$\int_{\Omega} \delta T \rho c_p \frac{\partial T}{\partial t} \, \mathrm{d}\Omega + \int_{\Omega_l} \delta T \rho c_p \mathbf{v} \cdot \nabla T \, \mathrm{d}\Omega + \int_{\Omega} \nabla \delta T \, k \nabla T \, \mathrm{d}\Omega - \int_{\Gamma} \delta T \mathbf{q} \cdot \mathbf{n}_\Gamma \, \mathrm{d}\Gamma = 0 \tag{5.6a}$$

$$\int_{\Omega} \delta \mathbf{q} \cdot \left( \frac{1}{k} \mathbf{q} + \nabla T \right) \, \mathrm{d}\Omega - \int_{\Gamma} \delta \mathbf{q} \cdot \mathbf{n}_\Gamma \, (T - T_m) \, \mathrm{d}\Gamma = 0 \tag{5.6b}$$

where $\delta T$ and $\delta \mathbf{q}$ are the test functions for the temperature and Lagrange multiplier fields, respectively. The Neumann boundary condition has been omitted for the sake of clarity. The method used in this work to impose the melting temperature on the interface is the stable Lagrange multiplier used in [52] and originally developed in [6, 34]. The Lagrange multiplier is defined as a vectorial flux and interpolated on the same mesh as the temperature field. The projection of this secondary variable on the interface is then used as a scalar Lagrange multiplier to impose the melting temperature.

Using a backward Euler scheme for the time derivative of T [30] in (5.6) gives:

$$\begin{aligned}\int_{\Omega} \delta T^{n+1} \rho \frac{(c_p T)^{n+1} - (c_p T)^{n}}{\Delta t} \,\mathrm{d}\Omega + \int_{\Omega_l} \delta T^{n+1} \rho c_p^{n+1} \mathbf{v}^{n+1} \cdot \nabla T^{n+1} \,\mathrm{d}\Omega \\ + \int_{\Omega} \nabla \delta T^{n+1} k^{n+1} \nabla T^{n+1} \,\mathrm{d}\Omega - \int_{\Gamma} \delta T^{n+1} \mathbf{q}^{n+1} \cdot \mathbf{n}_{\Gamma} \,\mathrm{d}\Gamma = 0\end{aligned} \tag{5.7a}$$

$$\int_{\Omega} \delta \mathbf{q}^{n+1} \cdot \left( \frac{1}{k^{n+1}} \mathbf{q}^{n+1} + \nabla T^{n+1} \right) \,\mathrm{d}\Omega - \int_{\Gamma} \delta \mathbf{q}^{n+1} \cdot \mathbf{n}_{\Gamma} \left( T^{n+1} - T_m \right) \,\mathrm{d}\Gamma = 0 \tag{5.7b}$$

where $n$ indicates the previous time step.

After replacing $T$ and $\mathbf{q}$ with their approximations we obtain the system of equations

$$\begin{bmatrix} \frac{1}{\Delta t}[M] + [C] + [K] & -[L] \\ [Q] - [L]^T & [M_q] \end{bmatrix} \begin{Bmatrix} \{T\}^{n+1} \\ \{\mathbf{q}\}^{n+1} \end{Bmatrix} = \begin{bmatrix} \frac{1}{\Delta t}[M]^* & 0 \\ 0 & 0 \end{bmatrix} \begin{Bmatrix} \{T\}^{n} \\ \{\mathbf{q}\}^{n} \end{Bmatrix} - \begin{Bmatrix} 0 \\ \{\mathbf{f}_l\} \end{Bmatrix} \tag{5.8a}$$

$$[M] = \sum_e \int_{\Omega^e} \{N_T\}^{n+1} \rho c_p^{n+1} \langle N_T \rangle^{n+1} \,\mathrm{d}\Omega \tag{5.8b}$$

$$[M]^* = \sum_e \int_{\Omega^e} \{N_T\}^{n+1} \rho c_p^{n} \langle N_T \rangle^{n} \,\mathrm{d}\Omega \tag{5.8c}$$

$$[C] = \sum_e \int_{\Omega_l^e} \{N_T\}^{n+1} \rho c_p^{n+1} \mathbf{v}^{n+1} [B_T]^{n+1} \,\mathrm{d}\Omega \tag{5.8d}$$

$$[K] = \sum_e \int_{\Omega^e} ([B_T]^T)^{n+1} k^{n+1} [B_T]^{n+1} \,\mathrm{d}\Omega \tag{5.8e}$$

$$[M_q] = \sum_e \int_{\Omega^e} \frac{1}{k^{n+1}} ([N_q]^T)^{n+1} [N_q]^{n+1} \,\mathrm{d}\Omega \tag{5.8f}$$

$$[Q] = \sum_e \int_{\Omega^e} ([N_q]^T)^{n+1} [B_T]^{n+1} \,\mathrm{d}\Omega \tag{5.8g}$$

$$[L] = \sum_e \int_{\Gamma^e} \{N_T\}^{n+1} [N_q]^{n+1} \mathbf{n}_{\Gamma} \,\mathrm{d}\Gamma \tag{5.8h}$$

$$\{\mathbf{f}_l\} = \sum_e \int_{\Gamma^e} ([N_q]^T)^{n+1} \mathbf{n}_{\Gamma} \, T_m \,\mathrm{d}\Gamma \tag{5.8i}$$

where $B_{ij} = \frac{\partial N_j}{\partial x_i}$ is the gradient matrix. The interpolation for the temperature field is linear and constant per element for the Lagrange multiplier.

In elements that are not cut by the interface, no constraint is present. Consequently, the interface integrals are removed from the formulation and the system reduces to:

$$\begin{bmatrix} \frac{1}{\Delta t}[M] + [C] + [K] & 0 \\ [Q] & [M_q] \end{bmatrix} \begin{Bmatrix} \{T\}^{n+1} \\ \{\mathbf{q}\}^{n+1} \end{Bmatrix} = \begin{bmatrix} \frac{1}{\Delta t}[M]^* & 0 \\ 0 & 0 \end{bmatrix} \begin{Bmatrix} \{T\}^{n} \\ \{\mathbf{q}\}^{n} \end{Bmatrix} \tag{5.9}$$

### 5.5.2 Stokes Problem

The weak form of the Stokes problem (5.3) is given as follows

$$\begin{aligned}
&\int_{\Omega_l} \delta\mathbf{v} \cdot \rho \frac{\partial \mathbf{v}}{\partial t} \, \mathrm{d}\Omega + \int_{\Omega_l} 2\mu \; D(\delta\mathbf{v}) : D(\mathbf{v}) \, \mathrm{d}\Omega - \int_{\Omega_l} (\nabla \cdot \delta\mathbf{v}) p \, \mathrm{d}\Omega \\
&+ \int_{\Omega_l} \delta\mathbf{v} \cdot \mathbf{f}_b \, \mathrm{d}\Omega = 0 \qquad (5.10a)
\end{aligned}$$

$$\int_{\Omega_l} \delta p \; \nabla \cdot \mathbf{v} \, \mathrm{d}\Omega = 0 \qquad (5.10b)$$

where $\delta\mathbf{v}$ and $\delta p$ are the test functions for the velocity and pressure, respectively. The Neumann boundary condition has been omitted for the sake of clarity. Using a backward Euler scheme for the time derivative of $\mathbf{v}$ [30] in (5.10) gives the system of equations:

$$\begin{aligned}
&\int_{\Omega_l} \delta\mathbf{v}^{n+1} \cdot \frac{(\rho\mathbf{v})^{n+1} - (\rho\mathbf{v})^{n}}{\Delta t} \, \mathrm{d}\Omega + \int_{\Omega_l} 2\mu D(\delta\mathbf{v}^{n+1}) : D(\mathbf{v}^{n+1}) \, \mathrm{d}\Omega \\
&- \int_{\Omega_l} \nabla \cdot \delta\mathbf{v}^{n+1} p^{n+1} \, \mathrm{d}\Omega + \int_{\Omega_l} \delta\mathbf{v}^{n+1} \cdot \mathbf{f}_b^{n+1} \, \mathrm{d}\Omega = 0 \qquad (5.11a)
\end{aligned}$$

$$\int_{\Omega_l} \delta p^{n+1} \; \nabla \cdot \mathbf{v}^{n+1} \, \mathrm{d}\Omega = 0 \qquad (5.11b)$$

Substituting the approximation for the velocity and pressure fields into (5.11) leads to the finite element system of equations

$$\begin{bmatrix} [K] & -[D] \\ [D]^T & 0 \end{bmatrix} \begin{Bmatrix} \{\mathbf{v}\}^{n+1} \\ \{p\}^{n+1} \end{Bmatrix} = \begin{bmatrix} [M]^* & 0 \\ 0 & 0 \end{bmatrix} \begin{Bmatrix} \{\mathbf{v}\}^{n} \\ \{p\}^{n} \end{Bmatrix} - \begin{Bmatrix} \{\mathbf{f}_b\} \\ 0 \end{Bmatrix} \tag{5.12a}$$

$$[K] = [M] + \begin{bmatrix} [A_{11}] & [A_{12}] \\ [A_{12}]^T & [A_{22}] \end{bmatrix} \tag{5.12b}$$

$$[M] = \frac{1}{\Delta t} \sum_e \int_{\Omega^e} ([N_v]^T)^{n+1} \rho [N_v]^{n+1} \, \mathrm{d}\Omega \tag{5.12c}$$

$$[M]^* = \frac{1}{\Delta t} \sum_e \int_{\Omega^e} ([N_v]^T)^{n+1} \rho [N_v]^{n} \, \mathrm{d}\Omega \tag{5.12d}$$

$$[A_{11}] = \sum_e \int_{\Omega^e} 2\mu \left( \{B_x\}^{n+1} \langle B_x \rangle^{n+1} + \frac{1}{2} \{B_y\}^{n+1} \langle B_y \rangle^{n+1} \right) \mathrm{d}\Omega \tag{5.12e}$$

$$[A_{22}] = \sum_e \int_{\Omega^e} 2\mu \left( \frac{1}{2} \{B_x\}^{n+1} \langle B_x \rangle^{n+1} + \{B_y\}^{n+1} \langle B_y \rangle^{n+1} \right) \mathrm{d}\Omega \tag{5.12f}$$

$$[A_{12}] = \sum_e \int_{\Omega^e} 2\mu \left( \frac{1}{2} \{B_y\}^{n+1} \langle B_x \rangle^{n+1} \right) \mathrm{d}\Omega \tag{5.12g}$$

$$[D] = \sum_e \int_{\Omega^e} \langle \langle B_x \rangle^{n+1} \langle B_y \rangle^{n+1} \rangle^T \langle N_p \rangle^{n+1} \, \mathrm{d}\Omega \tag{5.12h}$$

$$\{\mathbf{f}_b\} = \sum_e \int_{\Omega_l^e} [N_v]^{n+1} \rho \eta (T^{n+1} - T_m) \mathbf{g} \, \mathrm{d}\Omega \tag{5.12i}$$

$$\langle B_x \rangle = \frac{\partial \langle N \rangle}{\partial x} \quad \langle B_y \rangle = \frac{\partial \langle N \rangle}{\partial y} \tag{5.12j}$$

The no-slip interface boundary condition is imposed using the penalty method [14, 22]. This technique multiplies the residual form of equation (5.3c) by a very large penalization parameter $\lambda$ and introduces it in the finite element formulation of the momentum equation. This method is simple to implement and has proven to be robust for a variety of problems. The formulation for elements intersected by the interface becomes:

$$\begin{bmatrix} [K'] & -[D] \\ [D]^T & 0 \end{bmatrix} \begin{Bmatrix} \{\mathbf{v}\}^{n+1} \\ \{p\}^{n+1} \end{Bmatrix} = \begin{bmatrix} [M]^* & 0 \\ 0 & 0 \end{bmatrix} \begin{Bmatrix} \{\mathbf{v}\}^{n} \\ \{p\}^{n} \end{Bmatrix} - \begin{Bmatrix} \{\mathbf{f}_b\} \\ 0 \end{Bmatrix} \tag{5.13a}$$

$$[K'] = [K] + [P] \tag{5.13b}$$

$$[P] = \sum_e \int_{\Gamma^e} ([N_v]^T)^{n+1} \lambda [N_v]^{n+1} \, \mathrm{d}\Gamma \tag{5.13c}$$

To solve (5.12) and (5.13) the interpolation functions for the velocity and pressure fields must satisfy the (inf-sup) condition. In this work, a pair of stable $Q_2$-$Q_1$ quadrilateral elements was used for the velocity and pressure fields, respectively.

An appropriate element size was used to maintain a low enough Peclet number to avoid oscillations in the Stefan problem. The validation problems presented in the results section are compared with the solution obtained using the commercial finite element code Comsol using a Stokes formulation in which a moving mesh algorithm is used to capture the interface movement.

The interpolation scheme (5.4) is known to cause problems when the physical domain (liquid phase) covers a very small area of the node's support [49]. The small contribution of the concerned degree of freedom causes a significant increase in the condition number of the global system [49], leading to divergent solutions. An efficient solution was developed in [49]. When a degree of freedom's contribution to the system is too small, it is removed from the system. The criteria for removing a degree of freedom is [49]

$$\left( \max_{e \in E_i} \frac{\int_{\Omega_l^e} N_i(\mathbf{x})\, \mathrm{d}\Omega}{\int_{\Omega^e} N_i(\mathbf{x})\, \mathrm{d}\Omega} \right)^{-\frac{1}{2}} > T_{tol} \tag{5.14}$$

where $E_i$ is the set of elements connected to node i, $\Omega_l^e$ the liquid domain area in the element, $\Omega^e$ the element area, $N_i(\mathbf{x})$ the interpolation function and $T_{tol}$ a user defined tolerance value. The greater the value for $T_{tol}$, the smaller the contribution of the degree of freedom can be before it is removed.

The stopping criteria (5.14) is used on a stabilized $Q_1$-$Q_1$ in [49], meaning that the velocity and pressure interpolation functions are identical, bi-linear and positive-semidefinite. The quadratic interpolation used for velocity in this work however, is not positive-semidefinite. This means that certain interface positions can lead to near zero integrals in (5.14) even when the liquid area is large, because the negative-valued areas of the interpolation would cancel out the positive-valued areas. To maintain the original objective of evaluating the relative contribution of the degree of freedom to the complete element, a modified criteria was used, given by equation

$$\left( \max_{e \in E_i} \frac{\int_{\Omega_l^e} |N_i(\mathbf{x})|\, \mathrm{d}\Omega}{\int_{\Omega^e} |N_i(\mathbf{x})|\, \mathrm{d}\Omega} \right)^{-\frac{1}{2}} > T_{tol} \tag{5.15}$$

where the absolute value of the interpolation function is used.

Furthermore, in [49] a preconditioner is applied to the global system before solving, allowing the use of a higher value of $T_{tol}$ while maintaining an optimal condition number and accurate solution. Considering the relatively heuristic modifications made to the removal of degrees of freedom caused by the use of a $Q_2$-$Q_1$ formulation and to simplify the implementation of our model, the preconditioner was not applied in this work.

The systems of equations (5.8) and (5.12) are coupled through the convection and buoyancy terms, respectively. To obtain a converged solution for both systems, a fixed point iteration scheme is used. The basic approach is to alternate between the two problems, using the updated solution of each problem when solving the other. Once the residuals of both problems, using the most recent solution, are below a certain stopping criteria, the global problem is considered converged and the algorithm proceeds to the next time step.

### 5.5.3 Interface velocity calculation

The proper evaluation of the interface velocity is crucial in obtaining a precise and robust model. For this particular problem, the interface velocity is determined by the jump in heat flux at the interface, described in (5.2). The use of a Lagrange multiplier to impose the melting temperature allows the evaluation of the jump in heat flux directly from the Lagrange field $\mathbf{q}$.

The final algorithm can be described as follows. Assuming a given time $t^n$, temperature solution $T^n$, velocity solution $\mathbf{v}^n$, pressure solution $p^n$ and level set solution $\phi^n$, the strategy to solve for $T^{n+1}$, $\mathbf{v}^{n+1}$ and $p^{n+1}$ consists in the following steps:

1. Compute the interface velocity $\mathbf{v}_\Gamma^n$ using (4.16)
2. Construct F on the level set domain by solving (3.28)
3. Solve for $\phi^{n+1}$ using (3.26)
4. Solve the coupled Stefan-Stokes problem:
   4.1. Solve for $T_{i+1}^{n+1}$ using (5.8) and $\mathbf{v}_i^{n+1}$
   4.2. Solve for $\mathbf{v}_{i+1}^{n+1}$ and $p_{i+1}^{n+1}$ using (5.12) and $T_{i+1}^{n+1}$
5. Evaluate (5.8) and (5.12). If both residuals are below the tolerance criteria, go to step 6. If not, $i = i + 1$ and go to step 4
6. Set $t^{n+1} = t^n$ and go to step 1.

## 5.6 Results

### 5.6.1 Flow over a cylinder

To validate the Stokes formulation, the flow over a cylinder was modelled. The domain is 1 m long and 0.5 m wide and the cylinder is centered at (0.4,0.25) m with a radius of 0.05 m. The material properties used are given in table 5.1. Two different boundary conditions were tested. In the first, referred to as case I (see figure 5.1), the top, bottom and right boundaries all have velocity boundary conditions, $\mathbf{v}_1 = (-0.1,\ 0)$ m/s (Re =10). The left boundary is an open boundary ($p_0 = 0$ Pa). In the second set of boundary conditions, referred to as case II (see figure 5.2), the top and bottom boundaries are walls ($\mathbf{v}_0 = (0,\ 0)$ m/s), the left boundary has a pressure condition $p_1 = -5$ Pa and the right wall is an open boundary ($p_0 = 0$ Pa). The no-slip condition was applied using $\beta = 10^8$ and the convergence criteria for the Newton-Raphson algorithm is $10^{-6}$.

The results obtained with the XFEM algorthim using a void enrichment scheme were compared to the results obtained with a conforming mesh, solved in the commercial software Comsol. Comparisons of the velocity profile in the domain, at the center of the cylinder and the pressure profile on the cylinder's circumference for case I are given in figures 5.3 and 5.4, respectively. The same profiles obtained using the case II boundary conditions are given in figures 5.5 and 5.6, respectively.

| Property | Value |
|---|---|
| $\rho$ [kg/m$^3$] | $1 \times 10^3$ |
| $\mu$ [N$\cdot$ s/m$^2$] | 10 |

Table 5.1 – Material properties for flow over a cylinder

As can be seen in the figures, the XFEM formulation is in excellent agreement with the solutions obtained with Comsol. The void enrichment scheme allows the XFEM formulation to remove the interior of the cylinder from the solution domain, even though the mesh does not conform to the cylinder's geometry. Furthermore, the no-slip condition applied on the cylinder contour is correctly applied using the penalty technique.

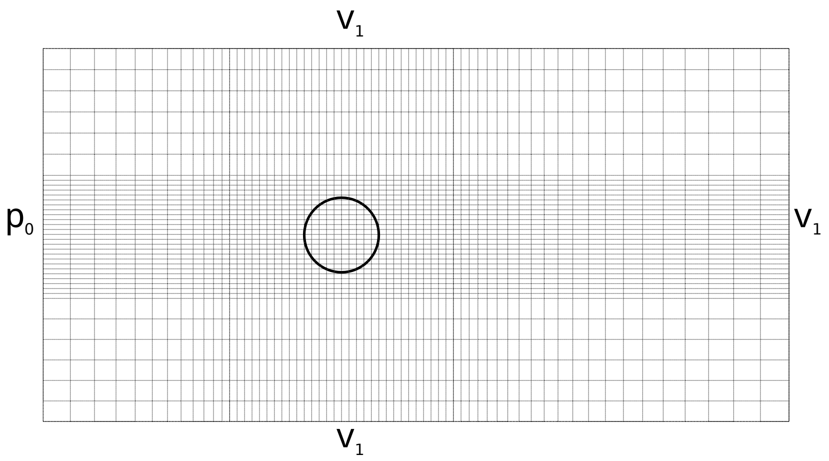

Figure 5.1 – Mesh for flow over a cylinder - case I (2331 elements)

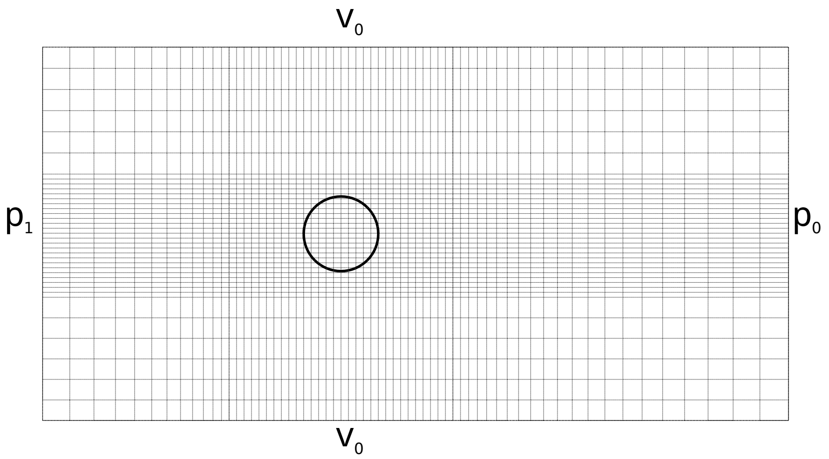

Figure 5.2 – Mesh for flow over a cylinder - case II (2331 elements)

### 5.6.2 Melting cylinder in a channel

The second problem includes the Stefan formulation to allow the cylinder to melt. The problem setup is as follows. A channel, $l = 0.167$ m in length and $h = 0.025$ m in height, contains a solid cylinder of radius 0.005 m. Both phases are initially at the melting temperature $T_m = 273$ K. The cylinder's centre is initially at $(\frac{l}{4}, \frac{h}{2})$. At $t = 0$, a pressure difference $\Delta p = 4$ Pa is applied between the channel's inlet and outlet. The inlet temperature is 274 K. Both top and bottom edges are thermally insulated with a no-slip boundary condition. The pressure difference drives the fluid flow and the buoyancy force was removed from (5.3a). The material properties used are given in table 5.2 and a schematic representation of the problem in figure 5.7. The mesh includes 2904 quadrilateral elements.

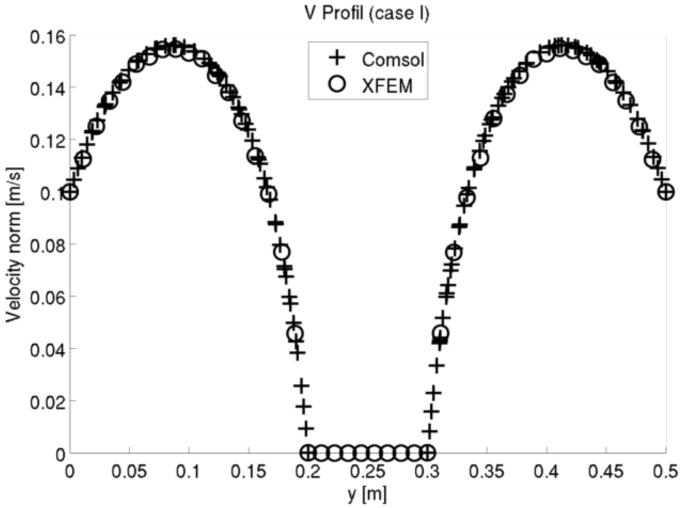

Figure 5.3 – Velocity profil at cylinder center - case I

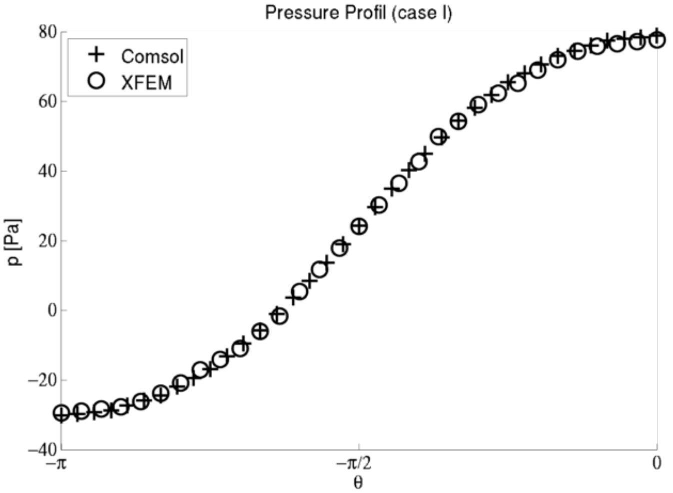

Figure 5.4 – Pressure on cylinder circumference - case I

The presence of fluid flow around the cylinder increases the heat flux on the top and bottom, where the flow is more rapid. The uphill and downhill sides of the cylinder have a slower fluid flow, leading to a lower heat flux. This results in a more oval shaped interface with time.

The time step used is $\Delta t = 1$ s, the tolerance criteria $T_{tol} = 10^8$ and the convergence criteria for the Newton-Raphson algorithm is $10^{-4}$ for the Stokes problem and $10^{-5}$ for the Stefan problem. The penalty parameter for the Stokes problem is $\beta = 10^8$. A linear interpolation for the temperature and Lagrange multiplier fields was used.

Figure 5.8 shows the position of the phase change interface for two different times.

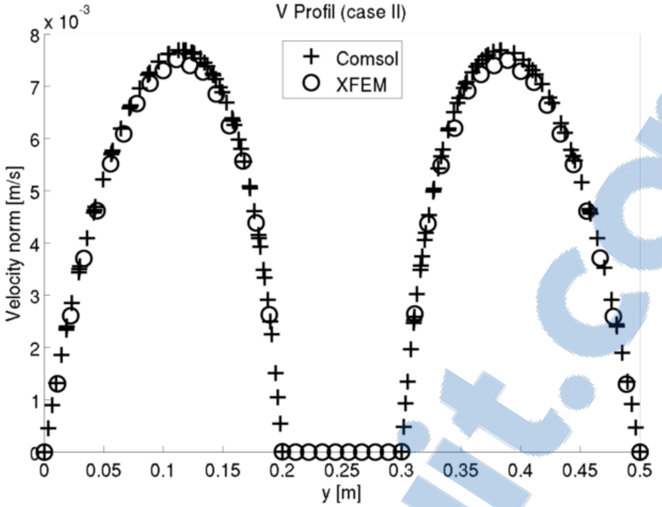

Figure 5.5 – Velocity profile at cylinder center - case II

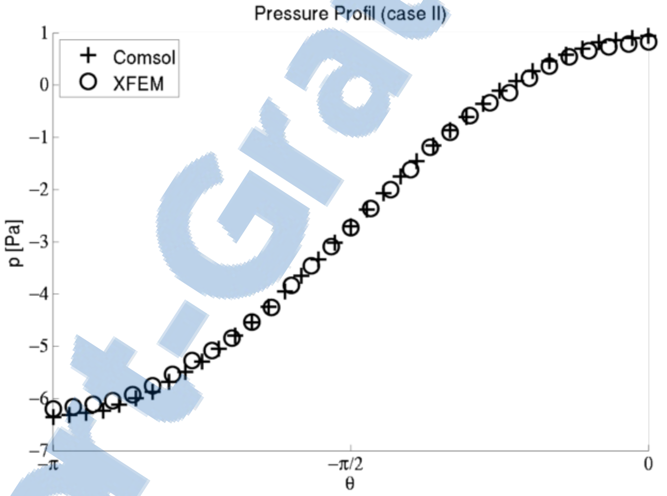

Figure 5.6 – Pressure on cylinder circumference - case II

Figure 5.9 shows the evolution of the temperature with time at two points in the domain (see figure 5.7); one uphill of the cylinder ($\mathbf{x}_1$) and the other downhill ($\mathbf{x}_2$). Figure 5.10 shows the temperature solution in the entire domain at two different times. In all these figures, the Comsol and XFEM models are in excellent agreement. We can observe the change in overall shape of the interface in figure 5.8, as the fluid flow influences the distribution of heat flux around the cylinder. Furthermore, the temperature downhill of the cylinder increases as the cylinder's area decreases and the flow becomes more uniform, as can be seen in figure 5.10.

Figure 5.11 shows the evolution of the velocity with time at points $\mathbf{x}_1$ and $\mathbf{x}_2$ in the domain (see figure 5.7). Figure 5.12 shows the velocity solution in the entire do-

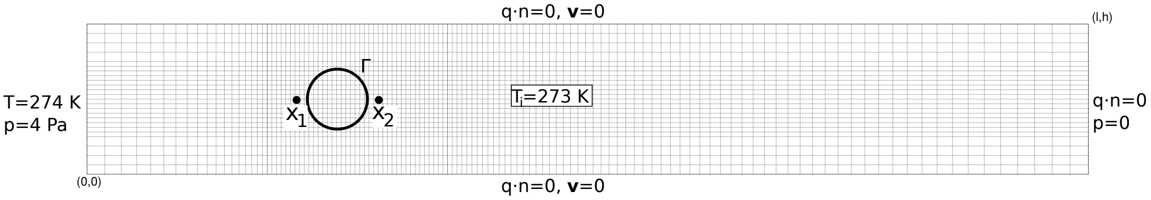

Figure 5.7 – Problem definition for melting cylinder (2904 elements)

Table 5.2 – Material properties for melting cylinder

| Property | Value |
|---|---|
| $\rho$ [kg/m$^3$] | 1000 |
| $T_m$ [K] | 273 |
| $L$ [J/kg] | $1 \times 10^8$ |
| $c_p$ [J/kg] | 1000 |
| $k$ [W/m·K] | 10 |
| $\mu$ [kg/s·m$^2$] | 0.01 |

main at two different times. The figures shows that the XFEM solution is in good agreement with the solution obtained with Comsol. We can observe the increase in velocity with time uphill and downhill of the cylinder in figure 5.12, as the influence of the cylinder on the fluid flow decreases.

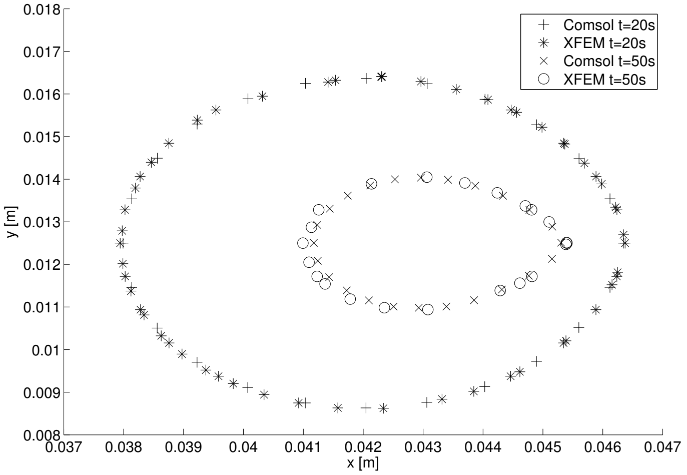

Figure 5.8 – Interface positions for melting cylinder

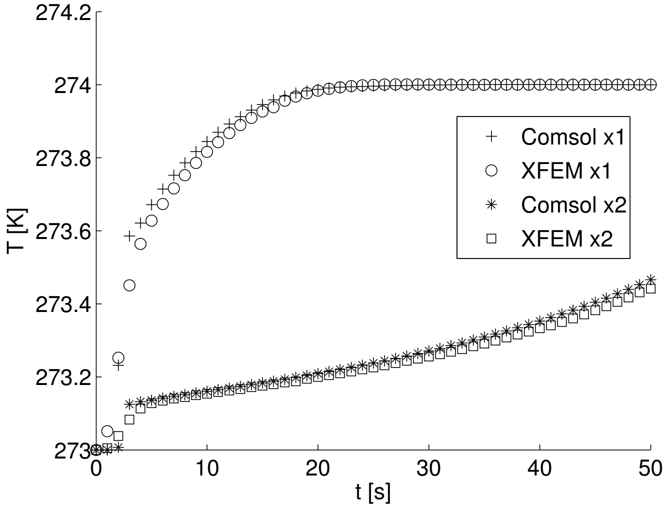

Figure 5.9 – T as function of t at $\mathbf{x}_1$ and $\mathbf{x}_2$ for melting cylinder (see figure 5.7)

### 5.6.3 Melting of pure tin

A final problem, the melting of pure tin, was simulated based on the experimental and numerical data found in [81] and the phase change example model found in Comsol [23]. The same simulation was then run in Comsol using a moving mesh algorithm (ALE) and the solution was compared with the solution obtained using the purely XFEM approach.

The problem setup is as follows. A square cavity, 0.10 m wide and 0.10 m high, is filled with liquid tin on the left and solid tin on the right. Both phases are initially at the melting temperature $T_m = 505K$. The initial interface is vertical at x = 0.02 m. At $t = 0$, the temperature of the left wall is increased to 508 K and the right wall decreased to 503 K, causing the metal to melt. Both top and bottom edges are insulated. The four boundaries are considered walls and a no-slip boundary is applied for the Stokes equations. The no-slip condition on the interface is applied using a penalty term with $\beta = 10^8$. The material properties used are given in table 5.3 and a schematic representation of the problem in figure 5.13.

The presence of natural convection changes the heat flux within the melt by increasing the influx of heat near the top of the enclosure and reducing it near the bottom, resulting in an angled interface.

The time step used is $\Delta t = 3s$, the tolerance criteria $T_{tol} = 10^2$ and the convergence criteria for the Newton-Raphson algorithm is $10^{-6}$ for both Stefan and Stokes prob-

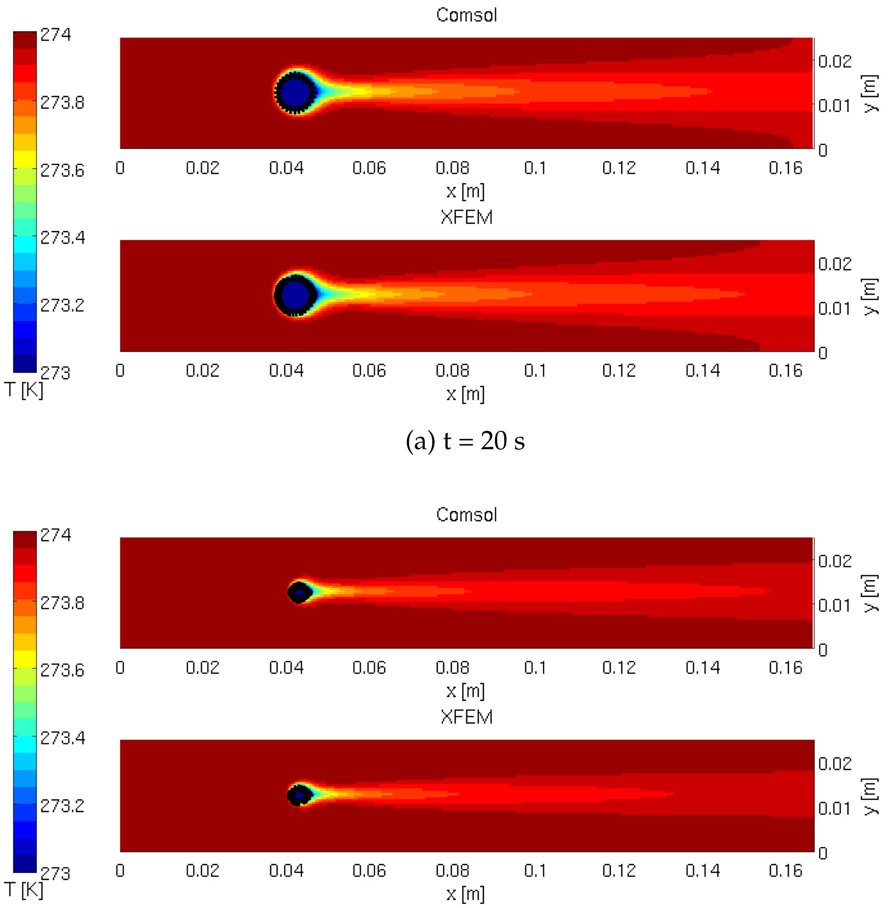

(a) t = 20 s

(b) t = 50 s

Figure 5.10 – Temperature profiles for melting cylinder

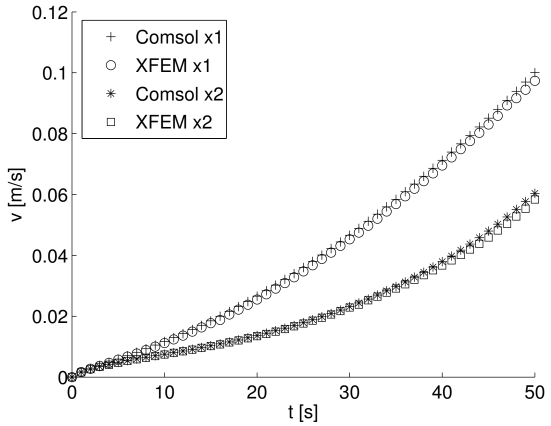

Figure 5.11 – Velocity as function of time at $\mathbf{x}_1$ and $\mathbf{x}_2$ for melting cylinder (see figure 5.7)

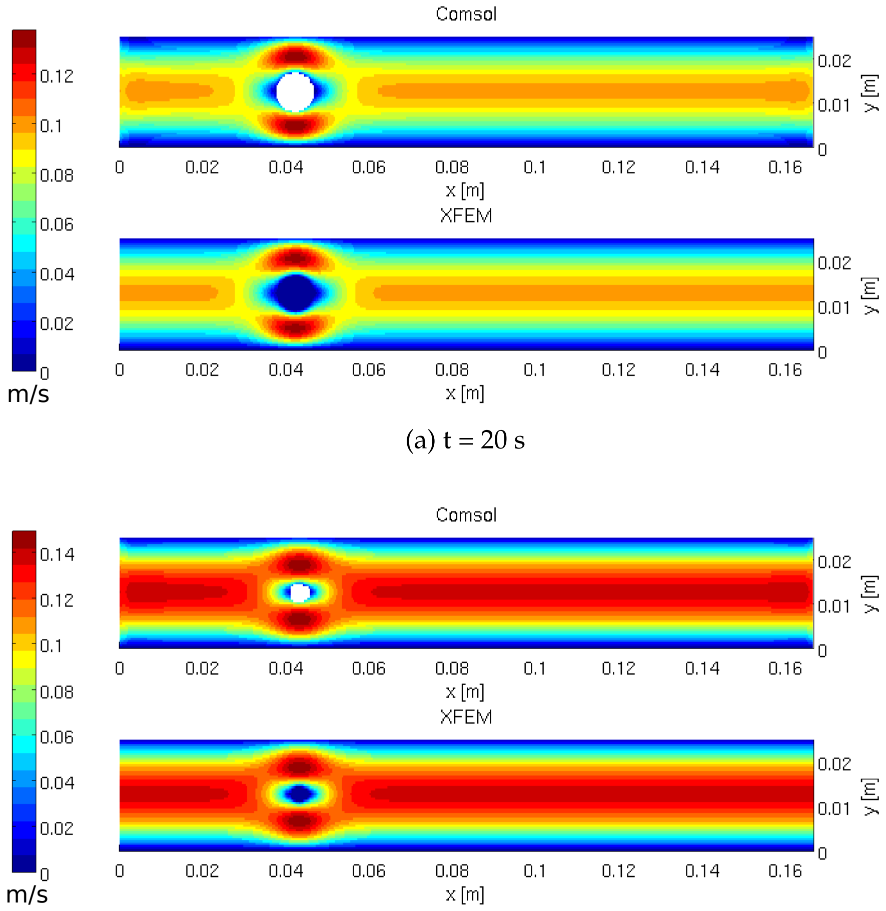

(a) t = 20 s

(b) t = 50 s

Figure 5.12 – Velocity profiles for melting cylinder

lems.

This problem was selected for its simple interface geometry. Our current algorithm does not allow the reinitialization of the level set field. For more uniform interface shapes and displacements, the absence of a reinitialization step has little impact on the model's accuracy [52]. More complex shapes and interface movements would require a reinitialization step and a remeshing step in the Comsol algorithm.

As can be seen in figure 5.14, the interface position obtained with the XFEM formulation is nearly identical to the one produced by Comsol. Furthermore, the temperature profile at various time steps, shown in figure 5.15, are also in excellent agreement.

There is however in figure 5.15a a small "kink" in the interface position for the XFEM

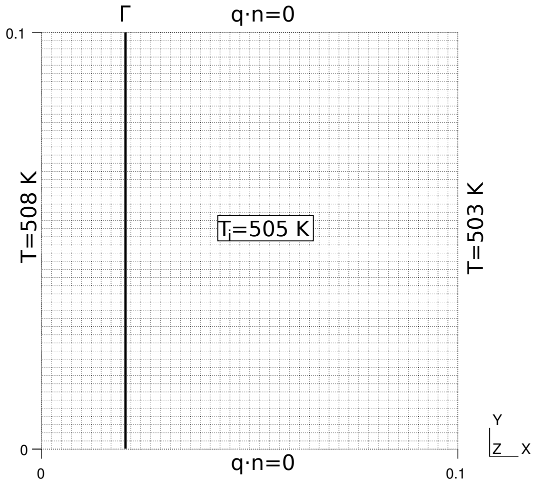

Figure 5.13 – Problem definition for melting of tin (2142 elements)

| Property | Value |
|---|---|
| $\rho$ [kg/m$^3$] | 7500 |
| $T_m$ [K] | 505 |
| $L$ [J/kg] | $6 \times 10^4$ |
| $c_p$ [J/kg] | 200 |
| $k$ [W/m·K] | 60 |
| $\eta$ [1/K] | $2.67 \times 10^{-4}$ |
| $\mu$ [kg/s·m$^2$] | $6 \times 10^{-3}$ |

Table 5.3 – Material properties melting of pure tin [23]

solution. This error is caused by an incorrect evaluation of the interface velocity, due to the use of a constant per element Lagrange multiplier interpolation scheme. As discussed in [52], the use of a linear interpolation scheme is more precise but also more computationally expensive. We tested a linear interpolation and the kink was no longer present, as shown in figure 5.16. Furthermore, it is clear from the other figures that the error produced by the use of a constant interpolation was quickly corrected over the next few time steps.

The velocity profile obtained with the XFEM formulation, shown in figure 5.17, is in good agreement with the solution obtained with Comsol. The areas with a more horizontal flow have the greatest impact on the temperature distribution (interface position) and are nearly identical. The XFEM formulation however, produces an irregular boundary layer on the solid-liquid interface. This error is caused by the removal of inappropriate degrees of freedom with (5.15), mainly due to the low tolerance

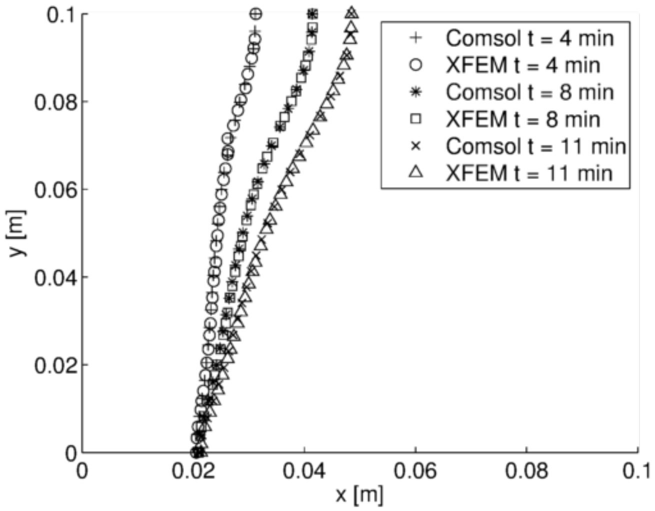

Figure 5.14 – Interface position for three time steps

values used. Higher values of $T_{tol}$ were tried but would lead to a divergent system for certain time steps with critical interface positions. As mentioned previously, the absence of a preconditionner [49] reduced the robustness of the algorithm.

## 5.7 Conclusion

A coupled Stefan and Stokes formulation using the extended finite element method was developed for the resolution of phase change problems involving convection. The Lagrange multiplier technique developed for the diffusive case was successfully applied to the convective-diffusive problem. The temperature and velocity fields obtained using XFEM were compared to the moving mesh algorithm found in Comsol with good results. The XFEM formulation required less degrees of freedom and didn't cause problems with distorted elements. The simple removal of degrees of freedom with a small contribution to the system for the $Q_2$-$Q_1$ Stokes formulation was shown to produce errors in the velocity field for problematic interface configurations. The same observation for a $Q_1$-$Q_1$ formulation was made in [49]. Future work will be done to include the complete Navier-Stokes equations and the application of non-zero velocity boundary conditions on the interface to include density changes between solid and liquid phases.

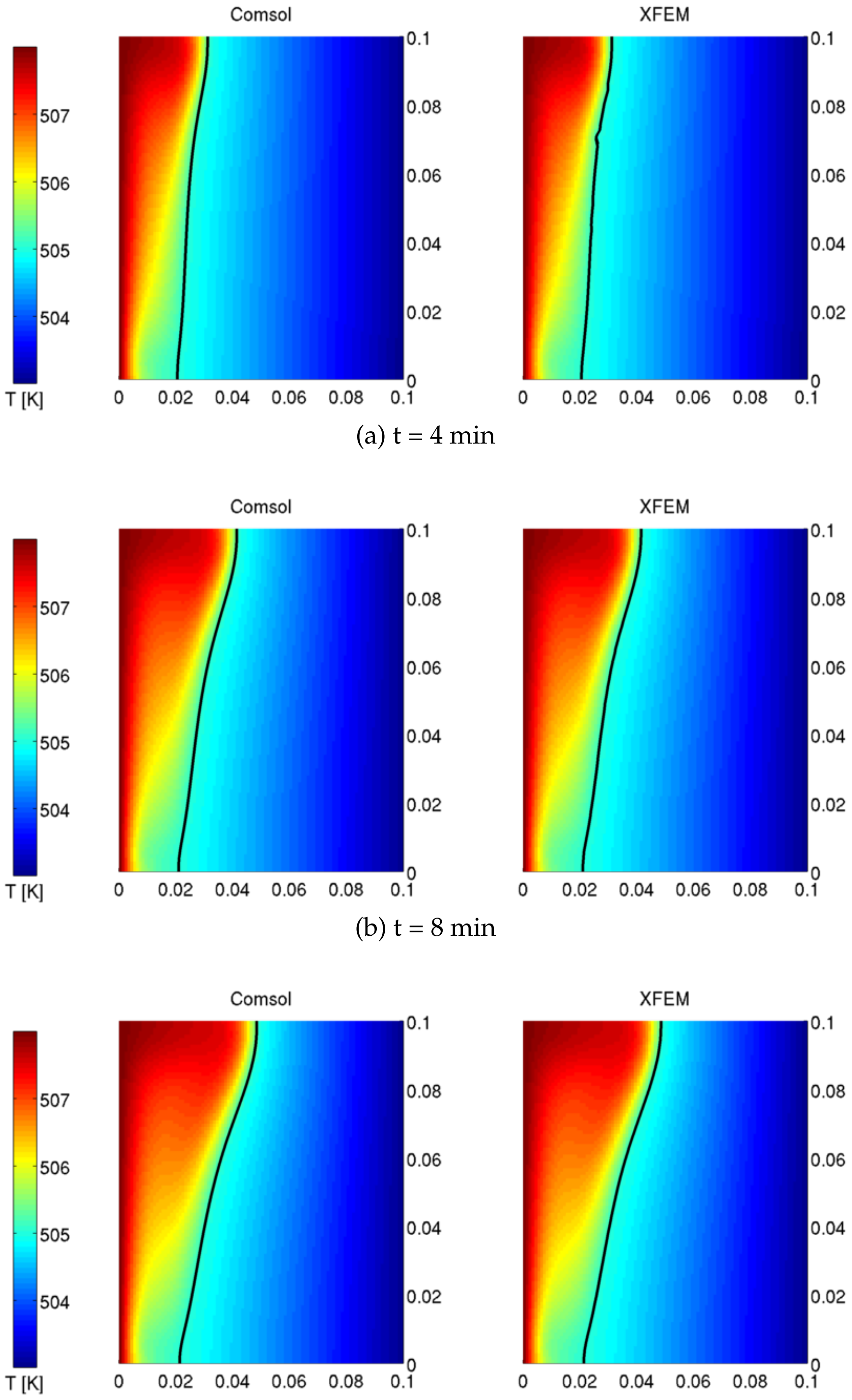

(a) t = 4 min

(b) t = 8 min

(c) t = 11 min

Figure 5.15 – Temperature profile at three time steps

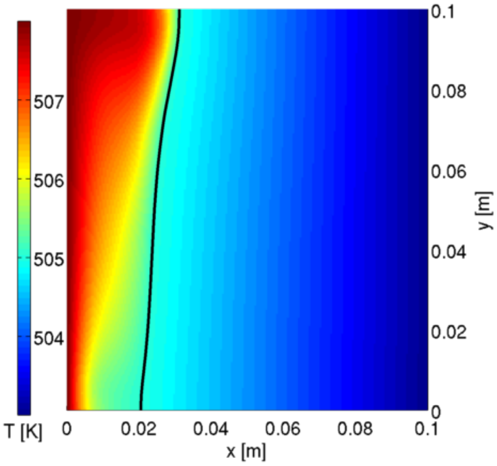

Figure 5.16 – Temperature profile at t = 4 min, using linear **q**

## Acknowledgement

The authors are grateful for the research support of the Natural Sciences and Engineering Research Council of Canada (File IRSCSA 394855 - 07) and Alcoa. A part of the research presented in this paper was financed by the Fonds de recherche du Québec - Nature et Technologies by the intermediary of the Aluminium Research Centre – REGAL. Special thanks to Patrice Goulet for his invaluable assistance with the developpement of the level set algorithm, and advice on the art of code writing.

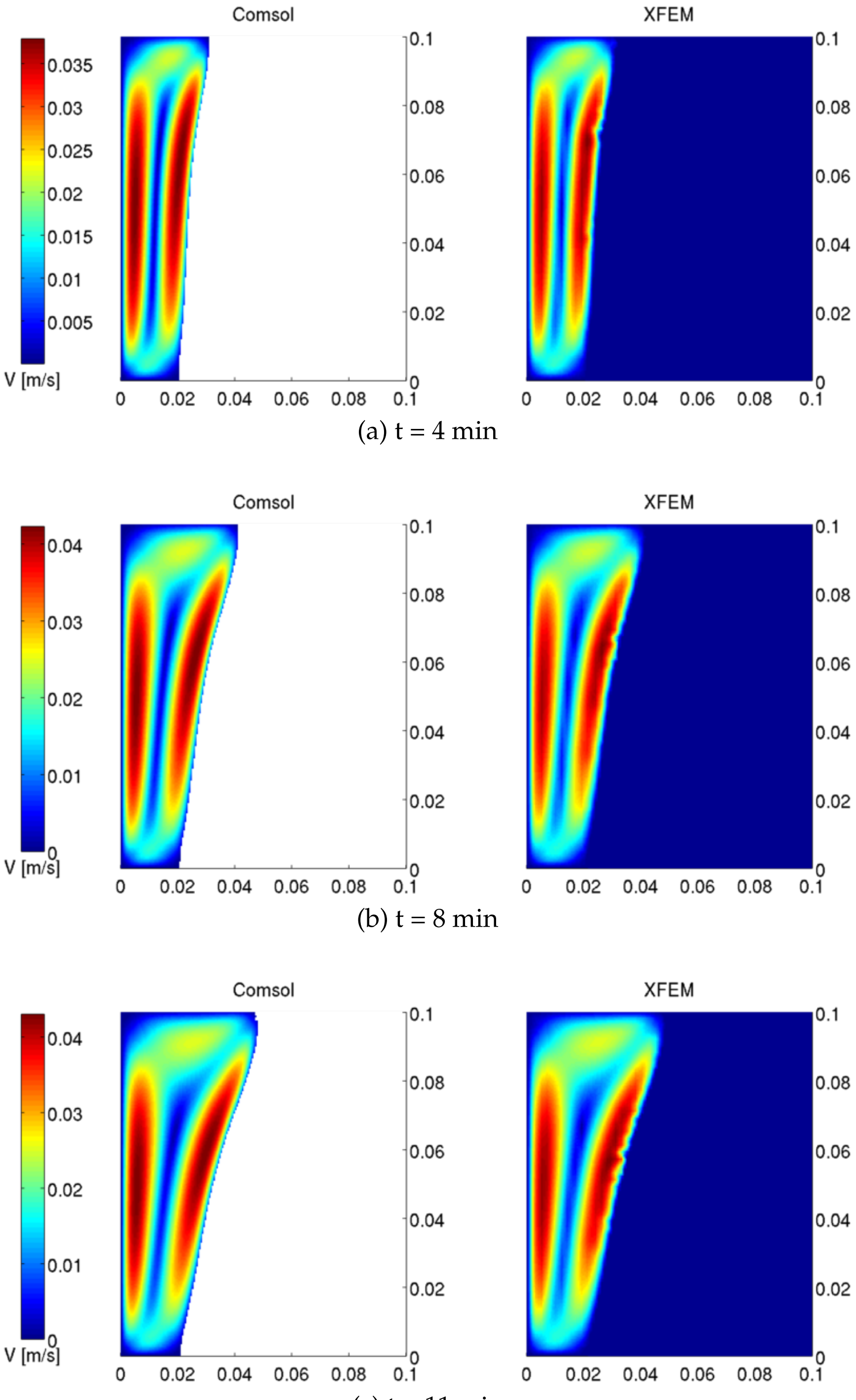

(a) t = 4 min

(b) t = 8 min

(c) t = 11 min

Figure 5.17 – Velocity profile at three time steps

# Chapter 6

# Modelling of Phase Change with Non-Constant Density using XFEM and a Lagrange Multiplier: Article 3

## 6.1 Resumé

Un modèle à deux phases pour des problèmes de solidification bidimensionnelles ayant des densités differentes a été développé en couplant le problème de Stefan avec le problème de Stokes et en applicant une condition aux limites en vitesse sur l'interface de changement de phase pour conserver la masse du système. La méthode des éléments finis étendus (XFEM) a été utilisée pour capturer la forte discontinuité de la vitesse et la pression ainsi que le saut dans le flux de chaleur à l'interface. La température de fusion et la vitesse du fluide à l'interface ont été imposées à l'aide d'un multiplicateur de Lagrange et la méthode par pénalisation, respectivement. Les formulations résultantes ont ensuite été couplées en utilisant un algorithme d'itération par point fixe. Trois exemples ont été étudiés et les résultats ont été comparés aux résultats numériques provenant d'un logiciel commercial utilisant la technique d'ALE pour suivre l'interface liquide/solide. Le modèle a été en mesure de reproduire les simulations de référence tout en conservant une interface nette de changement de phase et la masse total du système.

## 6.2 Abstract

A two phase model for two-dimensional solidification problems with variable densities was developed by coupling the Stefan problem with the Stokes problem and applying a mass conserving velocity condition on the phase change interface. The extended finite element method (XFEM) was used to capture the strong discontinuity of the velocity and pressure as well as the jump in heat flux at the interface. The melting temperature and velocity condition were imposed on the interface using a Lagrange multiplier and the penalization method, respectively. The resulting formulations were then coupled using a fixed point iteration algorithm. Three examples were investigated and the results were compared to numerical results coming from a commercial software using ALE techniques to track the solid/liquid interface. The model was able to reproduce the benchmark simulations while maintaining a sharp phase change interface and conserving mass.

## 6.3 Introduction

Numerous extended finite element models for the solutions of the classical (diffusive) Stefan problem are found in the literature [14, 22, 46, 54]. More complex models involving convection with constant density have also been developed using different numerical techniques [16, 80, 83]. Particularly, a fully XFEM Stefan/Navier-Stokes model was used by [52]. Models including the density variation are more uncommon [82], mainly because assuming the density is constant generally has little impact on the interface position. In certain applications however, the conservation

A straight-forward strategy to include the non-constant material densities is to use a moving-mesh algorithm such as the one found in the commercial code Comsol. This algorithm defines the phase change interface on a set of nodes, allowing the mass conservation boundary condition to be easily applied. However, the moving mesh adds considerable computational costs caused by the increase in degrees of freedom of the overall problem and the remeshing procedure required when the mesh becomes too distorted. These costs may hinder the use of a moving mesh algorithms in large scale multi-physical simulations which often have a large amount of degrees of freedom.

In the work presented here, a new coupled formulation using the extended finite element method for both the Stefan problem and Stokes equations based on [52] is developed for the case of variable phase densities. A fixed point iteration scheme is then used to obtain a converged solution for a given time step. The conservation of mass at the phase change interface is handled by applying a velocity boundary condition.

The paper is divided as follows. The governing equations for the Stefan and Stokes problems are described in section 6.4. The finite element formulation, level set problem and details concerning the interface movement and extended finite element method are described in section 6.5. Benchmark examples are then solved in section 6.6 to validate the algorithm. To this end, the commercial finite element simulation software Comsol was used with a moving mesh algorithm to capture the interface movement. Finally, the paper ends with some concluding remarks.

## 6.4 Governing Equations

### 6.4.1 Stefan Problem Formulation

Consider a domain $\Omega$ with an initial temperature $T(x, t_0)$ and interface $\Gamma$ separating solid ($\Omega_s$) and liquid ($\Omega_l$) phases with different thermal properties and densities. We suppose that the material has an isothermal phase change at some melting temperature $T_m$. Applying the conservation of energy in $\Omega$ results in the following equations [64]:

$$\left(\rho c_p\right)_s \frac{\partial T}{\partial t} - \nabla \cdot (k_s \nabla T) = 0 \qquad \mathbf{x} \in \Omega_s \tag{6.1a}$$

$$\left(\rho c_p\right)_l \left(\frac{\partial T}{\partial t} + \mathbf{v} \cdot \nabla T\right) - \nabla \cdot (k_l \nabla T) = 0 \qquad \mathbf{x} \in \Omega_l \tag{6.1b}$$

$$T - T_m = 0 \qquad \mathbf{x} \in \Gamma \tag{6.1c}$$

$$T = \hat{T} \qquad \mathbf{x} \in \Gamma_D \tag{6.1d}$$

$$-k \nabla T \cdot \mathbf{n} = \hat{q} \qquad \mathbf{x} \in \Gamma_N \tag{6.1e}$$

where $c_p$ is the specific heat, $k$ the thermal conductivity, $\rho$ the density, $\mathbf{v}$ the liquid phase velocity. Subscripts $l$ and $s$ indicate liquid and solid phases, respectively. Additionally, the melting temperature is applied on the solid-liquid interface (6.1c). Dirichlet and Neumann boundary conditions away from the interface are applied on $\partial\Omega = \Gamma_N \cup \Gamma_D$ as usual (6.1d,6.1e).

Conservation of energy at the interface requires that the jump in heat flux normal to the interface (caused by the imposition of the melting temperature) be related to the rate of solidification or melting of the material as described in [64]:

$$[\![-k\nabla T]\!] \cdot \mathbf{n}_\Gamma = (k_l \nabla T_l - k_s \nabla T_s) \cdot \mathbf{n}_\Gamma = \rho_s L v_\Gamma \qquad \mathbf{x} \in \Gamma \tag{6.2}$$

where $L$ is the latent heat and $v_\Gamma$ the normal interface velocity [64]. The normal vector $\mathbf{n}_s$ points from the liquid to solid phase, meaning that the interface velocity is positive for melting and negative for solidification.

### 6.4.2 Stokes Problem formulation

In the present study, the liquid phase velocity $\mathbf{v}$ is governed by the Stokes problem for viscous incompressible fluids:

$$\rho_l \frac{\partial \mathbf{v}}{\partial t} = \nabla \cdot \sigma \qquad \mathbf{x} \in \Omega_l \tag{6.3a}$$

$$\nabla \cdot \mathbf{v} = 0 \qquad \mathbf{x} \in \Omega_l \tag{6.3b}$$

$$\mathbf{v} = \frac{\rho_l - \rho_s}{\rho_l} v_\Gamma \mathbf{n}_\Gamma \qquad \mathbf{x} \in \Gamma \tag{6.3c}$$

$$\mathbf{v} = \hat{\mathbf{v}} \qquad \mathbf{x} \in \Gamma_D \tag{6.3d}$$

$$\sigma \cdot \mathbf{n} = \hat{\sigma} \qquad \mathbf{x} \in \Gamma_N \tag{6.3e}$$

$$\sigma = -p\mathbf{I} + 2\mu D(\mathbf{v}) \tag{6.3f}$$

$$D(\mathbf{v}) = \frac{1}{2}\left(\nabla \mathbf{v} + \nabla \mathbf{v}^T\right) \tag{6.3g}$$

where $p$ is the pressure, $\mu$ the viscosity and $D(\mathbf{v})$ the rate of deformation tensor. The convection term in the complete Navier-Stokes equations was neglected, leading to two linear systems of equations for the heat transfer and fluid flow problems. The only non-linearity is in the coupling terms between the two problems: the convective heat transfer and interface velocity.

The variation in density between the solid and liquid phases creates a mass flux at the interface, which is a function of the interface velocity and specific phase densities (equation (6.3c)). The other physical properties are assumed constant. The initial velocity field $\mathbf{v}(\mathbf{x}, t_0)$ is assumed divergence-free with a given initial pressure field $p(\mathbf{x}, t_0)$. Dirichlet and Neumann boundary conditions away from the interface are applied on $\partial\Omega = \Gamma_N \cup \Gamma_D$ as usual (6.3d, 6.3e).

### 6.4.3 Enriched Interpolation Scheme

The phase change problem is characterized by the jump in the heat flux which is caused by the temperature gradient discontinuity. However, the application of the interface boundary condition (6.1c) implies that the temperature is continuous at the interface. Such a weak discontinuity can be handled using the extended finite element method. This behavior is captured by using approximation (4.3) [22].

In order to capture the jump in the heat flux at the interface, a Lagrange multiplier $\mathbf{q}$ is used [32]. The interpolation scheme for the Lagrange multiplier is given by (4.5) and in matrix form (4.6).

The Navier-Stokes equations are valid (and solved) in the liquid phase only. For this purpose, the fluid-structure interaction approach, proposed in [33], is used. Therefore, the velocity and pressure fields can be interpolated using (5.5)

According to this interpolation scheme, the solid part of the domain is ignored. Also, enriched degrees of freedom are not required because no new information (behavior) is introduced. All velocity and pressure degrees of freedom whose support is completely inside the solid domain are removed from the system of equations.

## 6.5 Numerical Implementation

### 6.5.1 Stefan Problem

The weak form of the energy conservation equations (6.1a,6.1b) is

$$\int_{\Omega} \delta T \rho c_p \frac{\partial T}{\partial t} \, \mathrm{d}\Omega + \int_{\Omega_l} \delta T \rho_l c_p \mathbf{v} \cdot \nabla T \, \mathrm{d}\Omega + \int_{\Omega} \nabla \delta T \, k \nabla T \, \mathrm{d}\Omega - \int_{\Gamma} \delta T \mathbf{q} \cdot \mathbf{n}_{\Gamma} \, \mathrm{d}\Gamma = 0 \tag{6.4a}$$

$$\int_{\Omega} \delta \mathbf{q} \cdot \left( \frac{1}{k} \mathbf{q} + \nabla T \right) \, \mathrm{d}\Omega - \int_{\Gamma} \delta \mathbf{q} \cdot \mathbf{n}_{\Gamma} \left( T - T_m \right) \, \mathrm{d}\Gamma = 0 \tag{6.4b}$$

where $\delta T$ and $\delta \mathbf{q}$ are the test functions. The method used in this work to impose the melting temperature on the interface is the stable Lagrange multiplier used in [52] and originally developed in [6, 34]. The Lagrange multiplier is defined as a vectorial flux and interpolated on the same mesh as the temperature field. The projection of this secondary variable on the interface is then used as a scalar Lagrange multiplier to impose the melting temperature. The Neumann boundary condition has been omitted for the sake of clarity.

Using a backward Euler scheme for the time derivative of T in (6.4) gives [30]:

$$\begin{aligned}\int_\Omega \delta T^{n+1}\frac{(\rho c_p T)^{n+1}-(\rho c_p T)^n}{\Delta t}\,\mathrm{d}\Omega + \int_{\Omega_l}\delta T^{n+1}(\rho c_p)^{n+1}\mathbf{v}^{n+1}\cdot\nabla T^{n+1}\,\mathrm{d}\Omega \\ + \int_\Omega \nabla\delta T^{n+1}k^{n+1}\nabla T^{n+1}\,\mathrm{d}\Omega - \int_\Gamma \delta T^{n+1}\mathbf{q}^{n+1}\cdot\mathbf{n}_\Gamma\,\mathrm{d}\Gamma = 0\end{aligned} \tag{6.5a}$$

$$\int_\Omega \delta\mathbf{q}^{n+1}\cdot\left(\frac{1}{k}\mathbf{q}^{n+1}+\nabla T^{n+1}\right)\,\mathrm{d}\Omega - \int_\Gamma \delta\mathbf{q}^{n+1}\cdot\mathbf{n}_\Gamma\left(T^{n+1}-T_m\right)\,\mathrm{d}\Gamma = 0 \tag{6.5b}$$

where $n$ indicates the previous time step.

After replacing $T$ and $\mathbf{q}$ with their approximations we obtain the system of equations (5.8). In elements which are not cut by the interface, the boundary condition is removed and the system reduces to (5.9).

### 6.5.2 Stokes Problem

The weak form of the Stokes problem (6.3) is given as follows

$$\begin{aligned}&\int_{\Omega_l}\delta\mathbf{v}\cdot\rho_l\frac{\partial\mathbf{v}}{\partial t}\,\mathrm{d}\Omega + \int_{\Omega_l}2\mu\, D(\delta\mathbf{v}):D(\mathbf{v})\,\mathrm{d}\Omega - \int_{\Omega_l}(\nabla\cdot\delta\mathbf{v})p\,\mathrm{d}\Omega = 0\\ &\int_{\Omega_l}\delta p\,\nabla\cdot\mathbf{v}\,\mathrm{d}\Omega = 0\end{aligned} \tag{6.6a}$$

where $\delta\mathbf{v}$ and $\delta p$ are the test functions for the velocity and pressure, respectively. The Neumann boundary condition has been omitted for the sake of clarity. Using a backward Euler scheme for the time derivative of $\mathbf{v}$ in (6.6) gives the system of equations [30]:

$$\begin{aligned}&\int_{\Omega_l}\delta\mathbf{v}^{n+1}\cdot\left(\frac{(\rho_l\mathbf{v})^{n+1}-(\rho_l\mathbf{v})^n}{\Delta t}\right)\,\mathrm{d}\Omega + \int_{\Omega_l}2\mu D(\delta\mathbf{v}^{n+1}):D(\mathbf{v}^{n+1})\,\mathrm{d}\Omega\\ &-\int_{\Omega_l}\nabla\cdot\delta\mathbf{v}^{n+1}p^{n+1}\,\mathrm{d}\Omega = 0\end{aligned} \tag{6.7a}$$

$$\int_{\Omega_l}\delta p^{n+1}\,\nabla\cdot\mathbf{v}^{n+1}\,\mathrm{d}\Omega = 0 \tag{6.7b}$$

Substituting the approximation for the velocity and pressure fields (5.5) into (6.7) leads to the system of equations:

$$\begin{bmatrix} [K] & -[D] \\ [D]^T & 0 \end{bmatrix} \begin{Bmatrix} \{\mathbf{v}\}^{n+1} \\ \{p\}^{n+1} \end{Bmatrix} = \begin{bmatrix} [M]^* & 0 \\ 0 & 0 \end{bmatrix} \begin{Bmatrix} \{\mathbf{v}\}^{n} \\ \{p\}^{n} \end{Bmatrix} \tag{6.8a}$$

$$[K] = [M] + \begin{bmatrix} [A_{11}] & [A_{12}] \\ [A_{12}]^T & [A_{22}] \end{bmatrix} \tag{6.8b}$$

$$[M] = \frac{1}{\Delta t} \sum_e \int_{\Omega^e} ([N_v]^T)^{n+1} \rho_l [N_v]^{n+1} \, \mathrm{d}\Omega \tag{6.8c}$$

$$[M]^* = \frac{1}{\Delta t} \sum_e \int_{\Omega^e} ([N_v]^T)^{n+1} \rho_l [N_v]^{n} \, \mathrm{d}\Omega \tag{6.8d}$$

$$[A_{11}] = \sum_e \int_{\Omega^e} 2\mu \left( \{B_x\}^{n+1} \langle B_x \rangle^{n+1} + \frac{1}{2} \{B_y\}^{n+1} \langle B_y \rangle^{n+1} \right) \, \mathrm{d}\Omega \tag{6.8e}$$

$$[A_{22}] = \sum_e \int_{\Omega^e} 2\mu \left( \frac{1}{2} \{B_x\}^{n+1} \langle B_x \rangle^{n+1} + \{B_y\}^{n+1} \langle B_y \rangle^{n+1} \right) \, \mathrm{d}\Omega \tag{6.8f}$$

$$[A_{12}] = \sum_e \int_{\Omega^e} 2\mu \left( \frac{1}{2} \{B_y\}^{n+1} \langle B_x \rangle^{n+1} \right) \, \mathrm{d}\Omega \tag{6.8g}$$

$$[D] = \sum_e \int_{\Omega^e} \langle \langle B_x \rangle^{n+1} \langle B_y \rangle^{n+1} \rangle^T \langle N_p \rangle^{n+1} \, \mathrm{d}\Omega \tag{6.8h}$$

$$\tag{6.8i}$$

The mass flux interface boundary condition is imposed using the penalty method [14, 22]. This technique multiplies the residual form of equation (6.3c) by a very large penalization parameter $\beta$ and introduces it in the finite element formulation of the momentum equation. This method is simple to implement and has proven to be robust for a variety of problems. The formulation for elements intersected by the interface becomes:

$$\begin{bmatrix} [K'] & -[D] \\ [D]^T & 0 \end{bmatrix} \begin{Bmatrix} \{\mathbf{v}\}^{n+1} \\ \{p\}^{n+1} \end{Bmatrix} = \begin{bmatrix} [M]^* & 0 \\ 0 & 0 \end{bmatrix} \begin{Bmatrix} \{\mathbf{v}\}^{n} \\ \{p\}^{n} \end{Bmatrix} + \begin{Bmatrix} \{\mathbf{f}_p^{n+1}\} \\ 0 \end{Bmatrix} \tag{6.9a}$$

$$[K'] = [K] + [P] \tag{6.9b}$$

$$[P] = \sum_e \int_{\Gamma^e} ([N_v]^T)^{n+1} \beta [N_v]^{n+1} \, \mathrm{d}\Gamma \tag{6.9c}$$

$$\{\mathbf{f}_p^{n+1}\} = \sum_e \int_{\Gamma^e} ([N_v]^T)^{n+1} \beta \left( \frac{\rho_l - \rho_s}{\rho_l} v_\Gamma \mathbf{n}_\Gamma \right) \, \mathrm{d}\Gamma \tag{6.9d}$$

To solve the system of equations (6.8)-(6.9) the interpolation functions for the velocity and pressure fields must satisfy the LBB condition [3, 17]. In this work, a pair of stable $Q_2$-$Q_1$ quadrilateral elements was used for the velocity and pressure fields, respectively.

The validation problems presented in the results section are compared with the solution obtained through the commercial finite element code Comsol where the phase change problem was solved using a moving mesh algorithm (ALE) to capture the interface movement.

The interpolation scheme (5.4) is known to cause problems when the physical domain (liquid phase) covers a very small area of the node's support [49]. The small contribution of the concerned degree of freedom causes a significant increase in the condition number of the global system [49], leading to divergent solutions. An efficient solution was developed in [49]. When a degree of freedom's contribution to the system is too small, it is removed from the system. The criteria for removing a degree of freedom used here is (5.15) [49]

The systems of equations (5.8) and (6.8) are coupled through the convection and mass flux boundary terms, respectively. To obtain a converged solution for both systems, a fixed point iteration scheme is used.

### 6.5.3 Interface velocity calculation

The proper evaluation of the interface velocity is crucial in obtaining a precise and robust model [52]. For this particular problem, the interface velocity is determined by the jump in heat flux at the interface as described in equation (6.2). The use of a Lagrange multiplier to impose the melting temperature allows the evaluation of the jump in heat flux directly from the Lagrange field $\mathbf{q}$, given by

$$v_\Gamma = \frac{[\![\mathbf{q}]\!] \cdot \mathbf{n}_s}{\rho_s L} = \frac{(\mathbf{q}_l - \mathbf{q}_s) \cdot \mathbf{n}_s}{\rho_s L} \tag{6.10}$$

where $\mathbf{q}_s$ and $\mathbf{q}_l$ are the heat flux at the interface approaching from the solid and liquid phases, respectively.

The final algorithm can be described as follows. Assuming that a given time $t^n$, solution ($T^n$, $\mathbf{v}^n$, $p^n$, $\phi^n$) are known, the strategy to solve for ($T^{n+1}$, $\mathbf{v}^{n+1}$, $p^{n+1}$, $\phi^{n+1}$) consists in the following steps:

1. Compute the interface velocity $\mathbf{v}_\Gamma^n$ using (6.10)

2. Construct F on the level set domain by solving (3.28)
3. Solve for $\phi^{n+1}$ using (3.26)
4. Solve the coupled Stefan-Stokes problem:
   4.1. Solve for $T^{n+1}_{i+1}$ using (5.8) and $\mathbf{v}^{n+1}_{i}$
   4.2. Solve for $\mathbf{v}^{n+1}_{i+1}$ and $p^{n+1}_{i+1}$ using (6.8) and $T^{n+1}_{i+1}$
5. Evaluate (5.8) and (6.8). If both residuals are below the tolerance criteria ($1 \times 10^{-5}$ L2 norm), go to step 6. If not, $i = i + 1$ and go to step 4
6. Set $t^{n+1} = t^{n}$ and go to step 1.

## 6.6 Results

The Lagrange multiplier formulation used in this work to solve the Stefan problem (5.1) has been previously validated. For details on the specific simulations used and its performance compared to a finite difference approximation of equation (6.2), the interested reader is referred to [52].

To validate the coupled model three benchmark problems were simulated. The first and second are based on the one- and two-dimensional analytical phase change problems [54, 65]. The third benchmark problem involves more realistic boundary conditions, using the material properties of cryolite, known for its important change in density (≈ 25%).

In all cases, the simulations were also run in Comsol, using a moving mesh algorithm (ALE) to account for the displacement of the interface using triangle elements. The Stokes formulation uses a $P_2 - P_1$ formulation, the temperature field is linear and the Lagrange multiplier is constant per element [52]. In Comsol, the mesh geometry is quadratic. The results were then compared to the solution obtained using the purely XFEM approach. The Comsol simulations did not include a remeshing step during the simulation. An appropriate element size was used to maintain a low enough Peclet number to avoid oscillations in the Stefan problem.

These problems were selected for their relatively simple interface geometry and no reinitialization procedure was applied to the level set field during the simulation. For smooth interface shapes and relatively uniform displacements, the absence of a reinitialization step had little impact on the model's accuracy [52]. More complex shapes and interface movements would require a reinitialization step as well as a remeshing step in the Comsol algorithm.

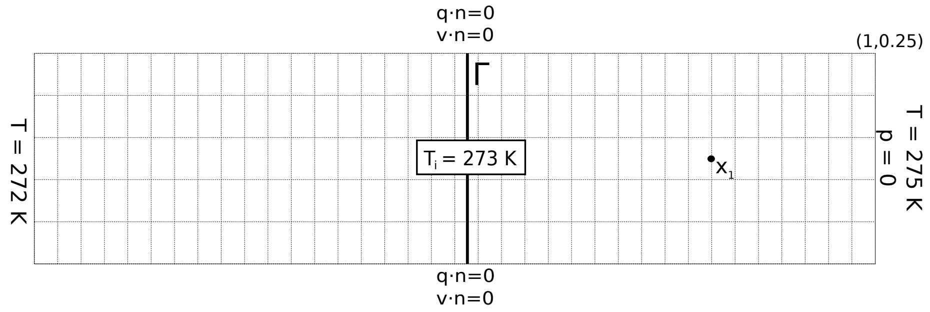

Figure 6.1 – 1D problem definition

| Properties | Solid | Liquid | Interface |
|---|---|---|---|
| $\rho$ [kg/m$^3$] | 1.0 | 0.75 | - |
| $c_p$ [J/kg K] | 50 | 50 | - |
| $k$ [W/m K] | 0.1 | 0.1 | - |
| $\rho_s L$ [J/m$^3$] | - | - | 2.5 |
| $T_m$ [K] | - | - | 273.0 |
| $\mu$ [kg/s·m] | - | 10 | - |

Table 6.1 – Material properties for 1D and 2D problems

### 6.6.1 One Dimensional Phase Change Problem

The first benchmark problem is inspired by the one dimensional two phase analytical solution of the Stefan problem in a semi-infinite domain ($x > 0$), taken from [54]. The thermal properties are constant except for the density and are given in table 6.1. These properties were chosen so that the convection term would affect the position of the interface with respect to the same problem without convection. The domain is 1m long and 0.25 m wide and the initial interface is at x = 0.515 m with the liquid phase on the right and solid phase on the left, as shown in figure 6.1. The initial temperature is $T_m$ (see table 6.1). The top and bottom edges are insulated. At $t = 0$, the temperature on the left edge is lowered to 272 K and the right edge is increased to 275 K. For the Navier-Stokes equations, the right boundary is open (no stress) while for the top and bottom edges the following boundary condition is applied: $\mathbf{v} \cdot \mathbf{n} = 0$. The time step is 0.05 sec, $\beta$ =$1 \times 10^8$, $T_{tol}$ =$1 \times 10^8$ and the convergence criteria for the Newton-Raphson algorithm is $10^{-6}$ for both problem. The mesh contains 180 quadrilateral elements in XFEM and 196 in Comsol.

The interface position as a function of time for both Comsol and XFEM algorithms is shown in figure 6.2. The temperature at point $\mathbf{x}_1$ over time is given in figure 6.3

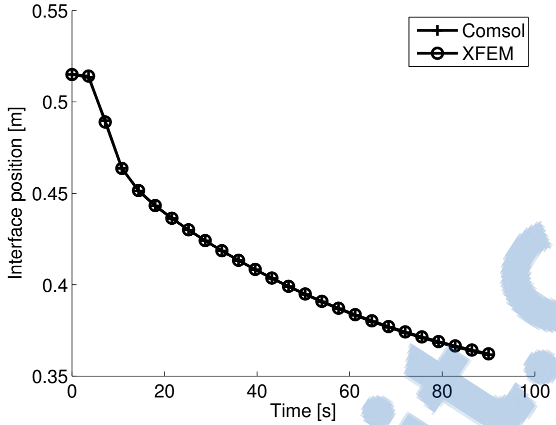

Figure 6.2 – Interface position vs time, 1D problem

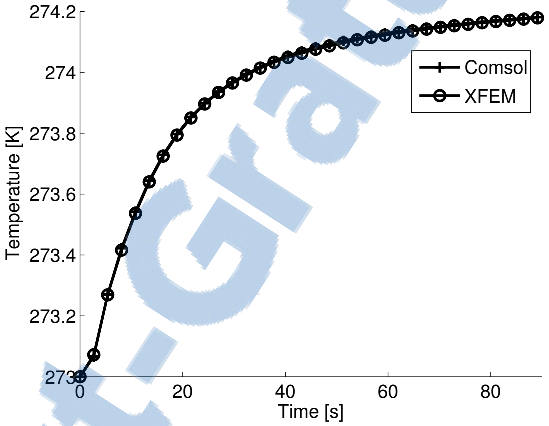

Figure 6.3 – Temperature at point $\mathbf{x}_1$, 1D problem (see figure 6.1)

for Comsol and XFEM algorithms. The convection velocity (constant in the liquid domain) is shown in figure 6.4 for both algorithms. These results show that the XFEM method reproduces the solution obtained through the standard finite element method (Comsol) using the moving mesh algorithm.

### 6.6.2 Two Dimensional Phase Change Problem

The second benchmark problem is two dimensional and based on the analytical solution of melting (or freezing) in a corner first solved in [65]. The thermal properties are constant except for the density and are identical to the first example, given in table 6.1. The domain is 1 m long and 1 m wide with the initial interface is at x = 0.1 m from the left and bottom boundaries, with the liquid phase on the lower left and solid phase on the top right, as shown in figure 6.5. The initial temperature is

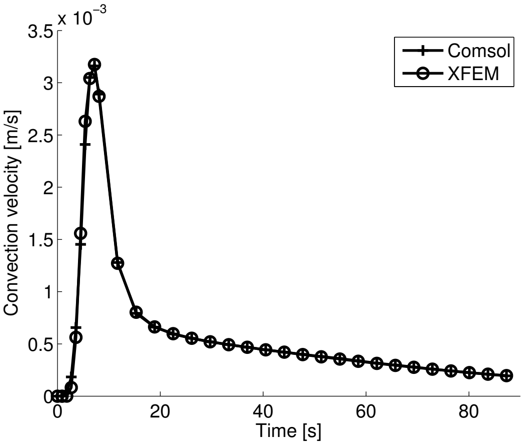

Figure 6.4 – Convection velocity in liquid phase, 1D problem

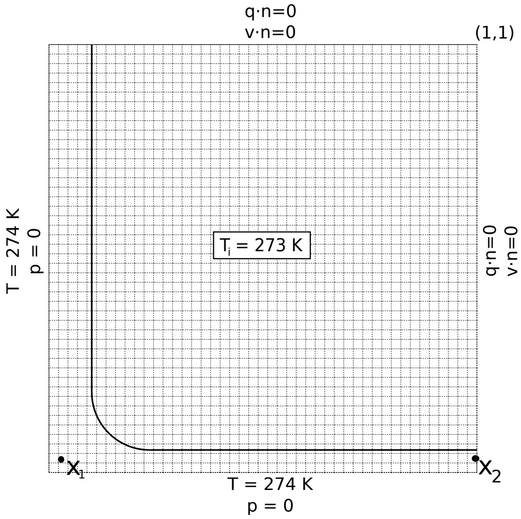

Figure 6.5 – 2D problem definition.

$T_m$ (table 6.1). The top and right edges are thermally insulated. At $t = 0$, the temperature on the left and bottom boundaries is increased to 274 K. For the Navier-Stokes equations, the left and bottom boundaries are open (no stress). For the top and right boundaries the boundary condition $\mathbf{v} \cdot \mathbf{n} = 0$ is applied. The time step is 0.05 sec, $\beta = 1 \times 10^4$, $T_{tol} = 1 \times 10^2$ and the convergence criteria for the Newton-Raphson algorithm is $10^{-5}$ for the Stokes problem and $10^{-4}$ for the Stefan problem. The mesh contains 3025 quadrilateral elements in XFEM and 6590 triangle elements in Comsol.

The interface position for two different time steps for both Comsol and XFEM algorithms is shown in figure 6.6. The figure shows that the Comsol and XFEM algorthims give identical interface positions.

The temperature profile at the end of the simulation is shown in figure 6.7. Figure 6.8 shows the temperature at two points $\mathbf{x}_1$ and $\mathbf{x}_2$ over time (see figure 6.5). In both cases, the Comsol and XFEM algorithms are in excellent agreement.

The convection velocity at the final time step for both algorithms is shown in figure 6.9. The velocity is in good agreement in both cases. Figure 6.10 shows the fluid velocity at points $\mathbf{x}_1$ and $\mathbf{x}_2$ over time, showing good agreement between the two algorithms, although fluctuations are present in the XFEM solution.

Two distinct causes contribute to these fluctuations. First, the interface geometry in XFEM (the level set field) is stored using a linear interpolation. Consequently, the curved interface is approximated by line segments which reduces the accuracy of the solution. Comsol uses a quadratic interpolation for its moving mesh solution, allowing it to reproduce the interface curvature precisely. To validate this hypothesis, a solution was obtained using Comsol and a linear geometry. Using a mesh size similar to figure 6.5, Comsol is unable to produce a converge solution. To obtain a converged solution, over 24 000 triangle elements had to be used and the velocity solution showed small errors, similar to the XFEM solution in figure 6.10. Furthermore, refining the XFEM mesh, thus reducing the error caused by the linear geometry, reduces the error in the solution as can be seen in figure 6.11, where the error norm is defined as $||v_C - v_X||_2$, $v_C$ is the Comsol velocity and $v_X$ the XFEM velocity over time at point $\mathbf{x}_2$.

To eliminate this error, a quadratic interface geometry (level set solution) can be used for significantly curved interfaces. Note that this does not require the use of a quadratic interpolation of the *mesh*, (as in Comsol) but the level set field only, limiting the number of additional degrees of freedom required. However, the geometric calculations done using the level set solution (element intersections, normals) becomes more complex to implement and the algorithms supposing a linear interpolation must be rewritten. Note that the use of a linear interface may reduce precision but still leads to converged solutions, whereas Comsol struggles to produce converged solutions using a linear mesh interpolation. These findings suggest that the use of the extended finite element method combined with the level set method allows for a significant reduction in the number of degrees of freedom required to reach a converged solution, as opposed to Comsol's moving mesh algorithm.

The second factor is the absence of a preconditioning matrix [49] for the Stokes problem, which meant that lower $T_{tol}$ values had to be used to obtain a converged solu-

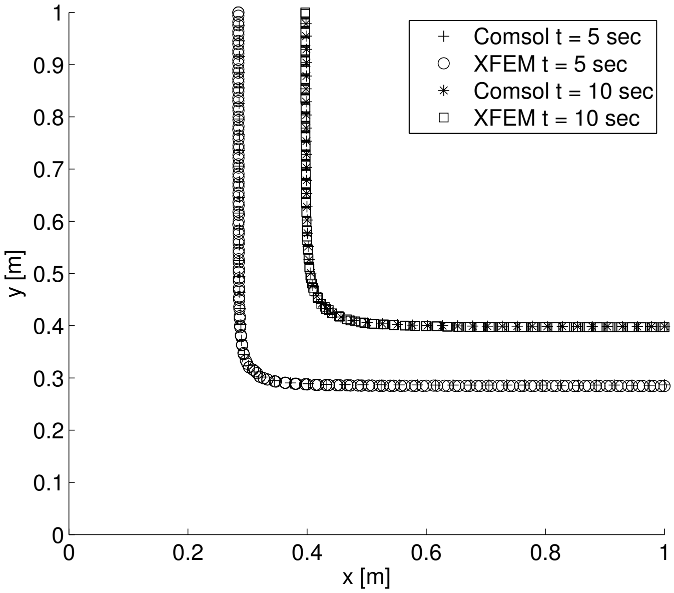

Figure 6.6 – Interface Comsol and XFEM, 2D problem

tion. This low $T_{tol}$ value causes important local errors in the velocity near the interface for problematic time steps; the more significant jumps in 6.10 are caused by this. To evaluate the sensitivity of the solution with respect to $T_{tol}$, the problem was solved using three different values for $T_{tol}$: $1 \times 10^0$, $1 \times 10^2$ and $1 \times 10^4$. The velocity norm at point $\mathbf{x}_1$ for all three $T_{tol}$ values compared to the Comsol solution is given in figure 6.12. As can be seen in the figure, at $T_{tol}$ $=1 \times 10^4$, certain critical degrees of freedom are not removed and the error becomes quite significant at 3.5 seconds. This error distorts the level set solution and leads to a divergent solution a few time steps later. At $T_{tol}$ $=1 \times 10^0$ too many degrees of freedom are removed and the system is unable to reproduce the solution at any time step. Between these two values, at $T_{tol}$=$1 \times 10^2$, the solution shows much smaller errors at critical time steps and reproduces the correct solution. These results indicate that without a preconditionner, the solution can be quite sensitive to a change in $T_{tol}$.

This source of error can be resolved by adding the preconditioning matrix defined in [49] to the Stokes problem. Although this error impacted only certain time steps, even at the quite low $T_{tol}$, more general applications involving other sources of fluid flow may not be so stable [52].

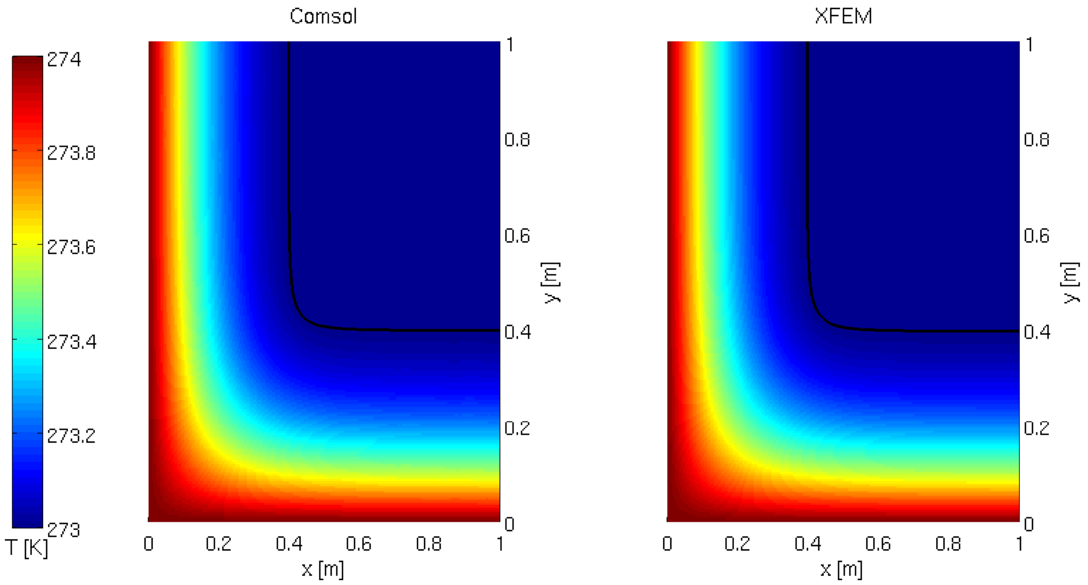

Figure 6.7 – Temperature at final time step, 2D problem

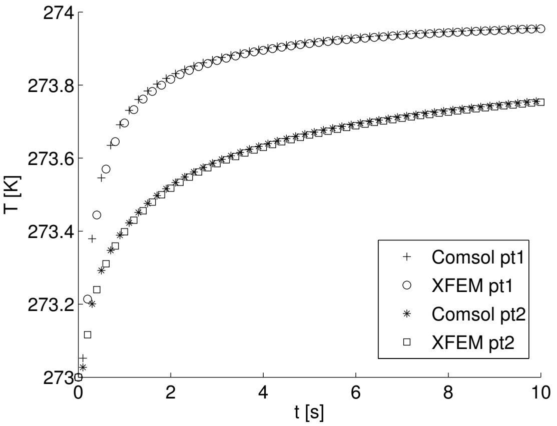

Figure 6.8 – Temperature as function of time at $\mathbf{x}_1$ and $\mathbf{x}_2$, 2D problem (see figure 6.5)

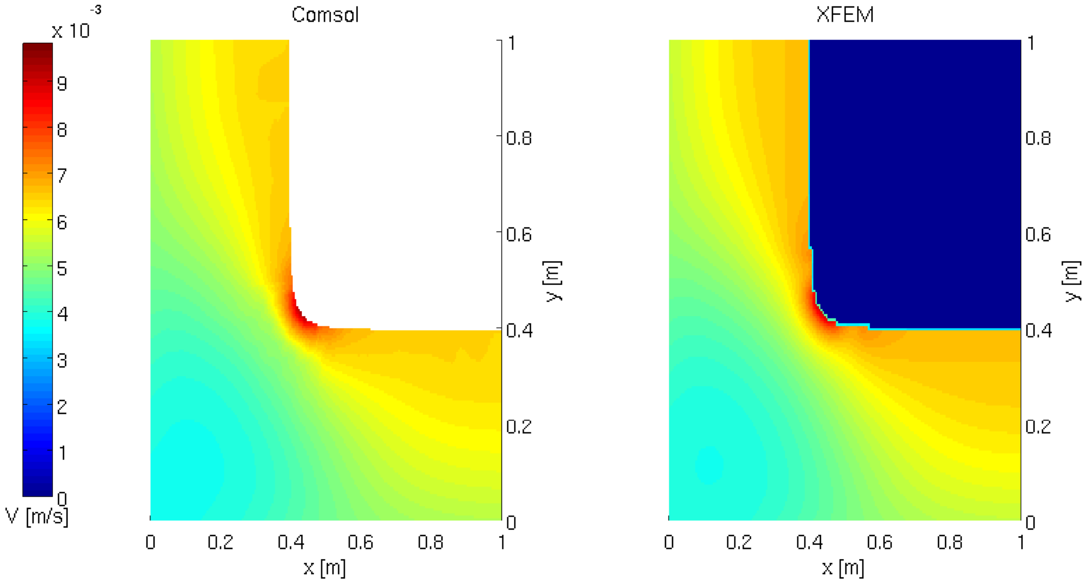

Figure 6.9 – Velocity at final time step, 2D problem

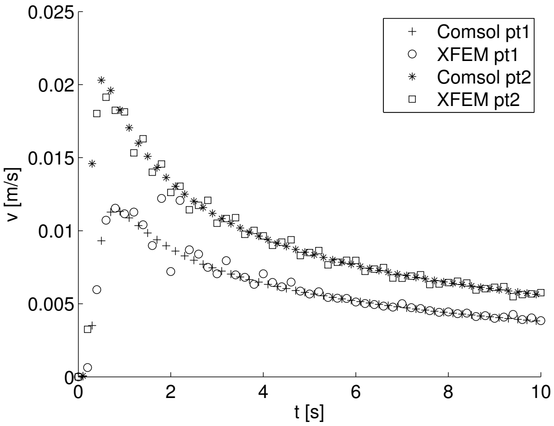

Figure 6.10 – Velocity as function of time at $\mathbf{x}_1$ and $\mathbf{x}_2$, 2D problem (see figure 6.5)

### 6.6.3 Melting of Cryolite Problem

The last benchmark problem is the melting of cryolite inside a rectangular cavity. The material properties are taken from the FactSage software [7] and assumed constant except for the density (see table 6.2). Note that natural convection was not included. The initial interface is at x = 0.05 m with the liquid phase on the left and solid phase on the right, as shown in figure 6.13. The initial temperature is $T_m$ (table 6.2). The top and bottom edges are thermally insulated. The temperature on the left and right boundaries are functions of y and given in figure 6.13. For the Navier-Stokes equations, all boundaries are no-slip walls ($\mathbf{v} = 0$) except for an open boundary ($p = 0$)

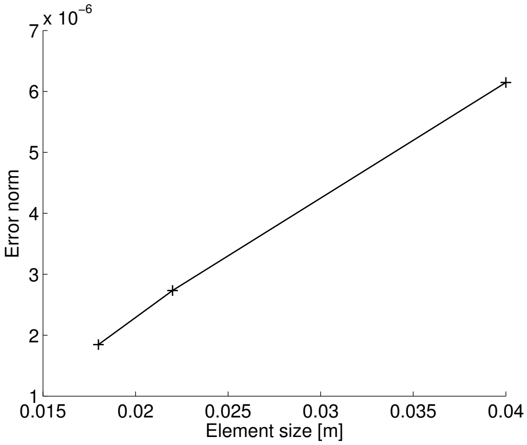

Figure 6.11 – Error norm of velocity over time of XFEM compared to Comsol for different mesh sizes

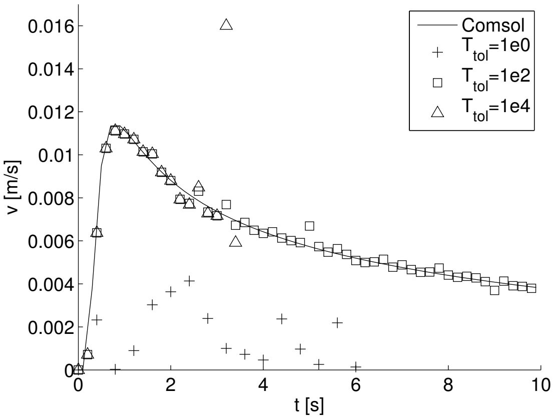

Figure 6.12 – Velocity at $\mathbf{x}_1$ for different $T_{tol}$ values

on the top left side of width 0.01 m (see figure 6.13). The time step used is $2 \times 10^3$ sec, $\beta = 1 \times 10^4$, $T_{tol} = 1 \times 10^1$ and the convergence criteria for the Newton-Raphson algorithm is $10^{-6}$ for the Stokes problem and $10^{-5}$ for the Stefan problem. The mesh contains 1350 quadrilateral elements in XFEM and 2799 triangle elements in Comsol.

The varying temperature profile along the left and right boundaries will create a variation in heat flux along the interface, causing it to curve. As the solid phase melts, excess mass is released in the liquid phase and leaves the domain through the open boundary in order to fulfill the mass conservation principal.

The interface position for three different time steps for both Comsol and XFEM algorithms are shown in figure 6.14 and are in excellent agreement. The temperature

| Properties | Solid | Liquid | Interface |
|---|---|---|---|
| $\rho$ [kg/m$^3$] | 2900 | 2050 | - |
| $c_p$ [J/kg K] | 1650 | 1650 | - |
| $k$ [W/m K] | 0.4 | 0.4 | - |
| $\rho_s L$ [J/m$^3$] | - | - | $2.81 \times 10^9$ |
| $T_m$ [K] | - | - | 1000 |
| $\mu$ [kg/s·m] | - | $2.4 \times 10^{-3}$ | - |

Table 6.2 – Material properties of cryolite, taken from FactSage [7]

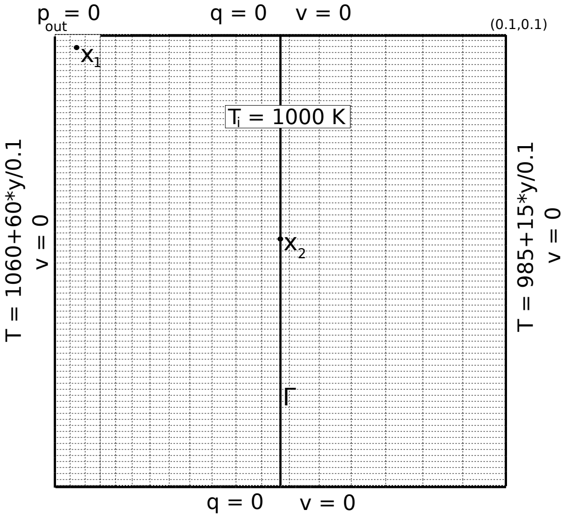

Figure 6.13 – Cryolite problem definition

profile at the end of the simulation is shown in figure 6.15 whereas figure 6.16 shows the temperature over time at two points $\mathbf{x}_1$ and $\mathbf{x}_2$ (see figure 6.13). In both cases, the Comsol and XFEM algorithms are in excellent agreement.

The velocity profile at the end of the simulation is shown in figure 6.17. Figure 6.18 shows the fluid velocity at point $\mathbf{x}_1$ over time. Finally, figure 6.19 shows the mass flux across the open boundary over time. The graphs clearly indicate that the XFEM algorithm correctly solves the interface, temperature and velocity variables. A mismatch between the Comsol and XFEM algorithms can be seen at earlier time steps, when the interface velocity varies rapidly. This is caused by the use of an explcit time stepping scheme for the level set field, requiring the use of the previous time step's temperature values to calculte the interface velocity (equation 6.2).

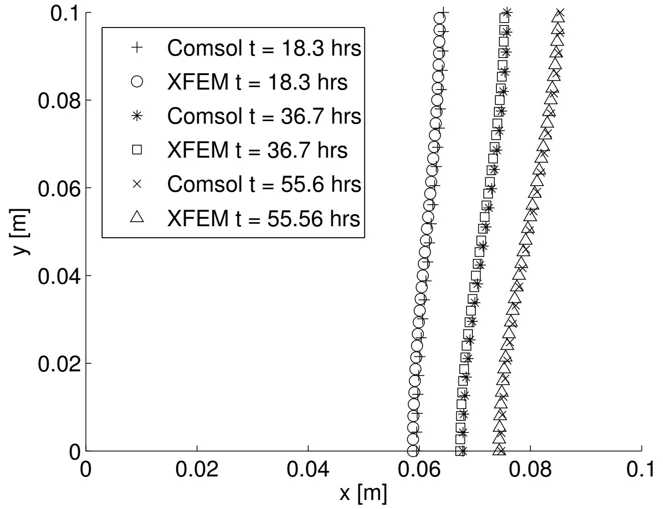

Figure 6.14 – Interface position for cryolite problem

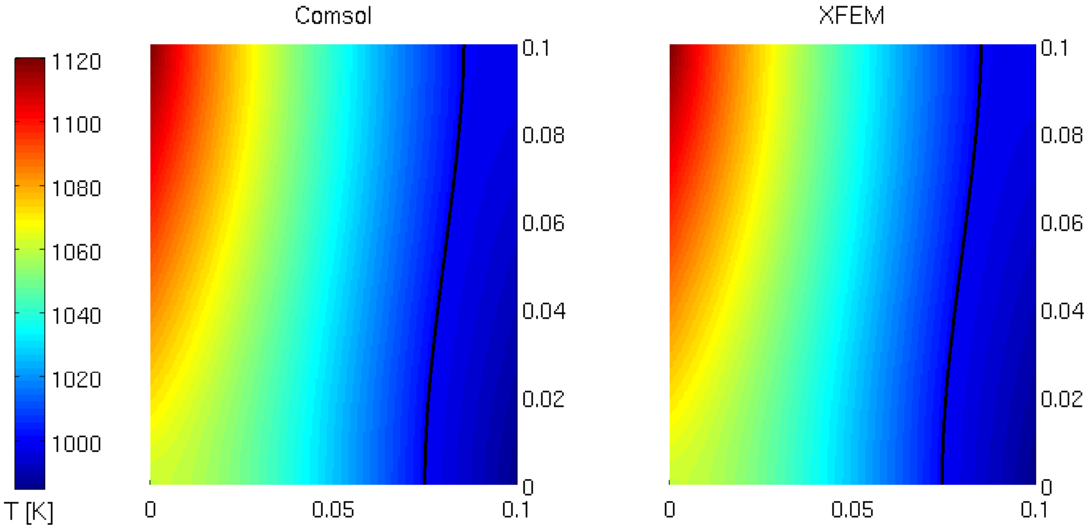

Figure 6.15 – Temperature profile at the final time step for cryolite problem

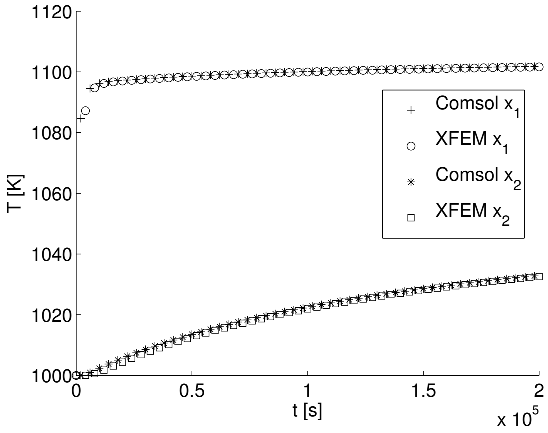

Figure 6.16 – Temperature as function of time at $\mathbf{x}_1$ and $\mathbf{x}_2$ for cryolite problem (see figure 6.13)

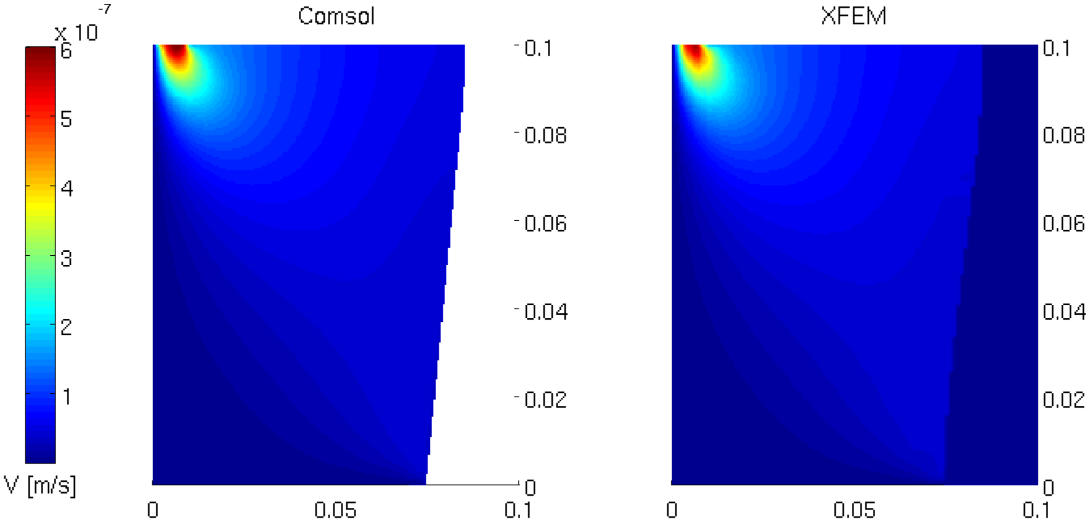

Figure 6.17 – Velocity profile at the final time step for cryolite problem

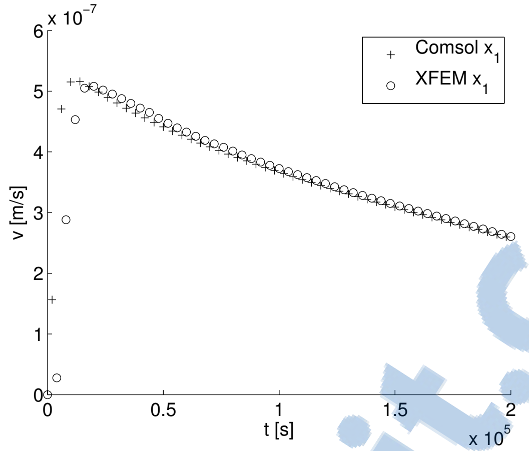

Figure 6.18 – Velocity as function of time at $\mathbf{x}_1$ and $\mathbf{x}_2$ for cryolite problem (see figure 6.13)

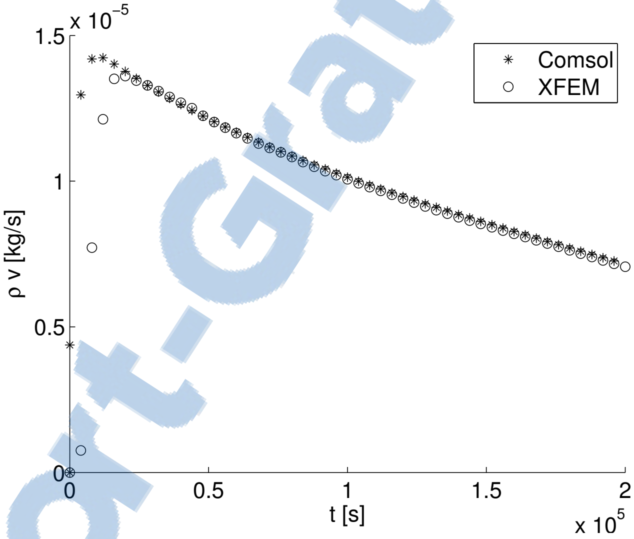

Figure 6.19 – Mass flux at outflow boundary, cryolite problem

## 6.7 Conclusion

Coupled Stefan and Stokes formulations using the extended finite element method were developed for the resolution of phase change problems involving variable densities. The density jump at the interface was used to apply a velocity boundary condition and conserve the global mass of the system, using the penalty method. The temperature and velocity fields obtained using XFEM were compared to the moving mesh algorithm in Comsol and are in good agreement. The use of a linear interpolation for the level set solution lead to errors in the mass flux velocity at the interface compared to the quadratic interpolation used by Comsol but required fewer degrees of freedom. When a linear interpolation was used in Comsol, the number of degrees of freedom required to obtain a converged solution was much greater than in XFEM. The simple removal of degrees of freedom with a small contribution to the system for the $Q_2$-$Q_1$ Stokes formulation was shown to produce errors in the velocity field for problematic interface configurations. The same observation for a $Q_1$-$Q_1$ formulation was made in [49]. The resolution of a more physically realistic benchmark problem using cryolite showed the XFEM algorithm to be quite effective at evaluating the mass flux caused by the density change. Future work will be done to include the complete Navier-Stokes equations and a stabilized $Q_1$-$Q_1$ formulation to implement the preconditionner scheme.

# Chapter 7

# Conclusion

## 7.1 Conclusion

As described in chapter 1, the main goal of this thesis was to develop a numerical model to predict the behaviour of the cryolite bath inside the electrolytic cell which could include the jump in density between the liquid and solid phases of the cryolite. The presence of multiple phases leads to various discontinuities in the solution which the model had to include. The model also had to scale easily and efficiently with an increase in degrees of freedom either through mesh size (or an increase in element density), the inclusion of additional physics (electromagnetism, chemistry) or the extension to three dimensions.

As discussed in chapter 2, the restrictions imposed on the model made current modelling techniques rather difficult to implement and costly in computing power. Diffused interface models considerably increase the mesh density required to obtain precise results and can make the application of boundary conditions on the interface difficult, particularly for the Navier-Stokes problem. Moving mesh algorithms offer excellent convergence rates and simple enforcement of boundary conditions. However, these advantages come at the cost of additional degrees of freedom for each spatial dimension and remeshing operations, causing interpolation errors in the solution.

To overcome theses challenges, the extended finite element method was selected as a modelling framework. The main aspects of this method: the enrichment strategies, numerical integration and level set formulation, are described in detail in chapter 3. However, the models using the extended finite element method found in the literature did not suit the needs of the present thesis. Consequently, a novel application of the extended finite element method was specifically designed for use in modelling the cryolite bath.

This new model involves three main contributions to the improvement of modelling techniques using XFEM. In chapter 4, a new Lagrange formulation to apply the melting temperature in the Stefan problem was introduced. This formulation was shown to reproduce the analytical solution in one and two dimensions. This technique was also shown to be efficient, robust and more precise than the penalization technique commonly used in the literature to impose Dirichlet boundary conditions. Furthermore, the elimination of user-defined numerical parameters ($\beta$, $\delta x$) simplified the use of this method in an industrial context.

Chapter 5 detailed the addition of convective heat transfer using a XFEM formulation for the Stokes equations, improving the model's ability to reproduce real-life scenarios. The coupled formulation was shown to converge to the correct solution using benchmark examples and the moving mesh algorithm found in Comsol. This approach allows a single extended finite element algorithm to be applied to both heat transfer and fluid flow problems, lowering the programming over-head of the model. It also introduces a solid mathematical basis to implement non-constant density materials as an explicitly described interface is present.

In chapter 6, the non-constant density model for the cryolite bath was successfully developed. The resulting velocity boundary condition on the interface was easily implemented thanks to the extended finite element framework of the Stokes equations described in chapter 5. This boundary condition being directly dependent on the interface velocity, the use of the Lagrange multiplier described in chapter 4 improved the precision of the fluid velocity at interface and consequently the global mass conservation. The model was validated with benchmark examples, using Comsol's moving mesh algorithm, including one using the properties of cryolite.

In the designing of the model, certain known weakness of the extended finite element method were set aside. Mainly, the reinitialization step of the level set field, important in models with rather complex geometries and longer time spans, should be added before the model is put to practical use. Although this additional step will increase the computational costs of the model, its impact is small because the level set solution can (and should) be defined on a relatively small band of elements surrounding the interface, drastically lowering the number of degrees of freedom involved [22].

Two major assumptions are inherent to the Stefan problem. First, that the melting point of the material is constant (isothermal). For materials including multiples species such as croylite this assumption is rarely valid. The phase change actually happens over a temperature interval, creating three distinct phases: solid, liquid and a "mushy" zone. Furthermore, the melting point varies considerably with chemical composition, a property which changes during aluminum production. The second assumption is the initial presence of an interface. Currently, the model does not include a mechanism to trigger the appearance of a second phase if no interface is present at $t = 0$. This assumption limits the application of the model to later phases of an electrolytic cell's life-cycle, when the cryolite ledge has already formed.

Finally, the non-linear convection term in the Navier-Stokes equations (as well as the accompanying stabilization) must be added to the Stokes formulation used here to ensure that the inertial component of the fluid flow be properly accounted for. This addition does not affect the performance of the extended finite element formulation of the Navier-Stokes equations, as shown in [32]. The robustness of the model can also be improved by implementing the precondionner suggested in [49].

## 7.2 Future Work

An important step in the development of a more powerful model is the extension of the algorithm to three dimensions. The use of the extended finite element method has already eliminated a part of the difficulty, as there is no need to handle node movement. The level set formulation is also easily applied to three dimensions, though the geometric calculations (interface intersections with elements) will require some modifications. Concerning the extended finite element formulation for the Stefan and Stokes problems, the only hurdle is the integration of cut elements, requiring the three dimensional elements to be cut in tetrahedron without intersecting the interface. Libraries, similar to the one used in 2D here, are readily available [70].

To properly take into account the presence of the "mushy" zone, future research should be done to develop new enrichment strategies which could reproduce the complete material behaviour. More specifically, an alternative could be to add a second level set field, with its own set of enriched degrees of freedom, to create three distinct sub-domains (phases) and handle each phase transition (solid to mushy and mushy to liquid) separately. An interesting challenge in this context is the implementation of non-constant density materials, as the boundary mass flux is now applied in a small area (volume) instead of a line (area).

Adding a species transport formulation to the global resolution scheme would also be beneficial. It would allow the cryolite's melting point to vary with its local composition. Furthermore, the presence of a mushy zone during the phase change implies that not all the species in the cryolite change phase at the same temperature. This results in an interface mass flux that may have a different composition than either phases, increasing the complexity and non-linearity of the system.

The inclusion of electromagnetism is also an important part of the electrolytic cell's behaviour as it is coupled with the other physics: heat transfer (Joule effect), fluid flow (Lorentz force) and chemistry (conservation of charge). The discontinuities discussed in the thesis, caused by the presence of multiple phases with different properties, will also affect the electromagnetic formulation. The extended finite element method, already used in the other aspects of the model, would once again be an excellent choice to take into account these discontinuities.

Although the removal of problematic degrees of freedom in the Stokes (or Navier-Stokes) formulation together with the application of the preconditionner described in [49] lead to precise solutions, a user-defined numerical parameter is still required. The results in [49] suggest that the performance of the method is not highly dependent on a particular choice of the threshold value but a bad choice can still lead to errors in the solution and some trial and error may be required before an acceptable value is found for a particular set of modelling conditions. Consequently, a better approach to selecting this threshold value (or its complete removal) would lead to more robust and easy-to-use formulation.

The Heaviside enrichment of the Lagrange multiplier could also cause problems in certain situations because of its similarity with the void enrichment used for the velocity (or pressure) field. Like the void enrichment, small areas of one phase in a particular element can lead to near zero contributions to the element matrix. The consequences were not as important, as the Stefan problem did not have problems converging, but local errors in the interface velocity could appear. Perhaps the removal of enriched degrees of freedom or the application of a preconditionner could eliminate theses local errors.

It is important to note, as in [32], that a rigorous mathematical demonstration of the stability of the Lagrange multiplier formulation used in this thesis has yet to be published. Currently, only numerical experience, in this thesis and elsewhere in the literature, give confidence that stabilization of the formulation is not needed. As of the writing of this thesis, the Lagrange multiplier has been used with a void enrichment scheme, as in [32], and a weak enrichment, using the absolute value of the level set field. Future applications could test the formulation using a Heaviside enrichment scheme for the solution variable. This enrichment strategy can reproduce strong [50] and weak [36] discontinuities, allowing for a wider range of applications.

# Bibliography

[1] S. Abbas, A. Alizada, and T.-P. Fries. The XFEM for high-gradient solutions in convection-dominated problems. *International Journal for Numerical Methods in Engineering*, 82:1044–1072, 2010.

[2] A. Aysoufi and T. Keith. Application of the conservation element and solution element method in numerical model. *International Journal of Numerical Methods for Heat & Fluid Flow*, 13:448–472, 2003.

[3] I. Babuska. Error-bounds for finite element method. *Numerische Mathematik*, 16:322–333, 1969.

[4] I. Babuska. Finite element method with lagrangian multipliers. *Numerische Mathematik*, 20(3):179–192, 1973.

[5] I. Babuska and J. Melenk. The partition of unity method. *International Journal for Numerical Methods in Engineering*, 40(4):727–758, Feb 1997.

[6] J. Baiges, R. Codina, F. Henke, S. Shahmiri, and W. A. Wall. A symmetric method for weakly imposing Dirichlet boundary conditions in embedded finite element meshes. *International Journal for Numerical Methods in Engineering*, 90:636–658, 2012.

[7] C. W. Bale, E. Bélisle, P. Chartrand, S. A. Decterov, K. H. G. Eriksson, I. H. Jung, Y. B. Kang, A. D. P. J. Melançon, C. Robelin, and S. Petersen. Factsage thermochemical software and databases - recent developments. *Calphad*, 33:295–331, 2009.

[8] E. Béchet, N. Moes, and B. Wohlmuth. A stable Lagrange multiplier space for stiff interface conditions within the extended finite element method. *International Journal for Numerical Methods in Engineering*, 78:931–954, 2009.

[9] C. Beckermann, H. Diepers, I. Steinbach, A. Karma, and X. Tong. Modeling melt convection in phase-field simulations of solidification. *Journal of Computational Physics*, 154(2):468–496, SEPT 1999.

[10] Y. Belhamadia. *Modélisation Mathématique et Simulation Numérique de Problèmes de Changement de Phase avec Applications à la Cryochirurgie*. PhD thesis, Université Laval, 2004.

[11] M. Bellet and V. D. Fachinotti. Ale method for solidification modelling. *Computer Methods in Applied Mechanics and Engineering*, 193(39-41):4355 – 4381, 2004. <ce:title>The Arbitrary Lagrangian-Eulerian Formulation</ce:title>.

[12] T. Belytschko, R. Gracie, and G. Ventura. A review of extended/generalized finite element methods for material modeling. *Modelling and Simulation in Materials Science and Engineering*, 17, 2009.

[13] T. Belytschko, N. Moes, S. Usui, and C. Parimi. Arbitrary discontinuities in finite elements. *International Journal for Numerical Methods in Engineering*, 50:993–1013, FEB 2001.

[14] M. Bernauer and R. Herzog. Implementation of an XFEM solver for the classical two-phase Stefan problem. *Journal of Scientific Computing*, 52:271–293, 2011.

[15] H. Braess and P. Wriggers. Arbitrary lagrangian eulerian finite element analysis of free surface flow. *Computer Methods in Applied Mechanics and Engineering*, 190(1-2):95 – 109, 2000.

[16] A. Brent, V. Voller, and K. Reid. Enthalpy-porosity technique for modeling convection-diffusion phase change: Application to the melting of a pure metal. *Numerical Heat Transfer: An International Journal of Compuation and Methodology*, 13:3:297–318, 1988.

[17] F. Brezzi. On the existence, uniqueness and approximation of saddle-point problems arising from lagrangian multipliers. *Revue française d'automatique, informatique, recherche opérationelle. Analyse numérique*, 8:129–151, 1974.

[18] A. Brooks and T. Hughes. Streamline upwind Petrov-Galerkin formulations for convection dominated flows with particular emphasis on the incompressible navier-stokes equations. *Computer methods in applied mechanics and engineering*, 32(1-3):199–259, 1982.

[19] S. Chen, B. Merriman, S. Osher, and P. Smereka. A simple level set method for solving Stefan problems. *Journal of Computational Physics*, 135(1):8–29, JUL 1997.

[20] K. W. Cheng and T.-P. Fries. Higher-order XFEM for curved strong and weak discontinuities. *International Journal for Numerical Methods in Engineering*, 82:564–590, 2010.

[21] J. Chessa and T. Belytschko. An extended finite element method for two-phase fluids. *Journal of Applied Mechanics*, 70:10, 2003.

[22] J. Chessa, P. Smolinski, and T. Belytschko. The extended finite element method (XFEM) for solidification problems. *International Journal for Numerical Methods in Engineering*, 53(8):1959–1977, MAR 2002.

[23] Comsol. http://www.comsol.com/model/tin-melting-front-6234.

[24] J. Dolbow, N. Moës, and T. Belytschko. Discontinuous enrichment in finite elements with a partition of unity method. *Finite Elements in Analysis and Design*, 36(3–4):235 – 260, 2000. Robert J. Melosh Medal Competition, Duke University, Durham NC, USA, March 1999.

[25] K. Dréau, N. Chevaugeon, and N. Moes. Studied X-FEM enrichment to handle material interfaces with higher order finite element. *Computer Methods in Applied Mechanics and Engineering*, 199:1922–1936, 2010.

[26] P. Díez, R. Cottereau, and S. Zlotnik. A stable extended FEM formulation for multi-phase problems enforcing the accuracy of the fluxes through lagrange multipliers. *International Journal for Numerical Methods in Engineering*, 96(5):303–322, 2013.

[27] H. Fortin, N. Kandev, and M. Fafard. FEM analysis of voltage drop in the anode connector induced by steel stub diameter reduction. *Finite Elements in Analysis and Design*, 52:71–82, 2011.

[28] T.-P. Fries. A corrected XFEM approximation without problems in blending elements. *International Journal for Numerical Methods in Engineering*, 75(5):503–532, JUL 2008.

[29] T. P. Fries. The intrinsic XFEM for two-fluid flows. *International Journal for Numerical Methods in Fluids*, 60(4):437–471, JUN 2009.

[30] T.-P. Fries and A. Zilian. On time integration in the XFEM. *International Journal for Numerical Methods in Engineering*, 79(1):69–93, JUL 2009.

[31] T. Gelhard, G. Lube, M. A. Olshanskii, and J.-H. Starcke. Stabilized finite element schemes with LBB-stable elements for incompressible flows. *Journal of Computational and Applied Mathematics*, 177(2):243 – 267, 2005.

[32] A. Gerstenberger. *An XFEM Based Fixed-grid Approach to Fluid-Structure Interaction*. PhD thesis, Technical University of Munich, 2010.

[33] A. Gerstenberger and W. A. Wall. An extended finite element method/lagrange multiplier based approach for fluid-structure interaction. *Computer Methods in Applied Mechanics and Engineering*, 197(19-20):1699–1714, 2008.

[34] A. Gerstenberger and W. A. Wall. An embedded Dirichlet formulation for 3D continua. *International Journal for Numerical Methods in Engineering*, 82(5):537–563, APR 2010.

[35] P. Goulet. *Modélisation du Comportement Thermo-électro-mécanique des Interfaces de Contact d'une Cuve de Hall-Héroult*. PhD thesis, Université Laval, 2004.

[36] A. Hansbo and P. Hansbo. A finite element method for the simulation of strong and weak discontinuities in solid mechanics. *Computer Methods in Applied Mechanics and Engineering*, 193:3523–3540, 2004.

[37] B. Helenbrook. A two-fluid spectral-element method. *Computer Methods in Applied Mechanics and Engineering*, 191(3-5):273 – 294, 2001.

[38] B. Helenbrook, L. Martinelli, and C. Law. A numerical method for solving incompressible flow problems with a surface of discontinuity. *Journal of Computational Physics*, 148(2):366 – 396, 1999.

[39] B. T. Helenbrook. High-order adaptive arbitrary-Lagrangian-Eulerian (ALE) calculations of solidification. In *Proc. of the ASME FEDSM*, volume 1C, 2013.

[40] C. Hirt and B. Nichols. Volume of fluid (VOF) method for the dynamics of free boundaries. *Journal of Computational Physics*, 39(1):201 – 225, 1981.

[41] T. J. Hughes, L. P. Franca, and G. M. Hulbert. A new finite element formulation for computational fluid dynamics: Viii. the Galerkin/least-squares method for advective-diffusive equations. *Computer Methods in Applied Mechanics and Engineering*, 73(2):173 – 189, 1989.

[42] T. J. R. Hughes and al. *Encyclopedia of Computational Mech.* Multiscale and Stabilized Methods. John Wiley & Sons, Ltd., 2004.

[43] N. S. J. Kapusta, P. Mackey, editor. *The Canadian Metallurgical & Materials Landscape 1960 to 2011*. The Candian Institute of Mining, Metallurgy and Petroleum, 2011.

[44] M. Jaeger and M. Carin. The front-tracking ale method: Application to a model of the freezing of cell suspensions. *Journal of Computational Physics*, 179(2):704 – 735, 2002.

[45] A. H. Jean Donea. *Finite Element Methods for Flow Problems*. Wiley, 2003.

[46] H. Ji, D. Chopp, and J. Dolbow. A hybrid extended finite element/level set method for modeling phase transformations. *International Journal for Numerical Methods in Engineering*, 54(8):1209–1233, JUL 2002.

[47] H. Ji and J. E. Dolbow. On strategies for enforcing interfacial constraints and evaluating jump conditions with the extended finite element method. *International Journal for Numerical Methods in Engineering*, 61:2508 2535, 2004.

[48] R. Khurram and A. Masud. A multiscale/stabilized formulation of the incompressible Navier-Stokes equations for moving boundary flows and fluid-structure interaction. *Computational Mechanics*, 38:403–416, 2006.

[49] C. Lang, D. Makhija, A. Doostan, and K. Maute. A simple and efficient preconditioning scheme for heaviside enriched XFEM. *Computational Mechanics*, 54:1357–1374, Nov. 2014.

[50] A. Laouati. *Modélisation de Problèmes Thermoélectriques Non Linéaires dans un Milieu Fissurė par XFEM*. PhD thesis, Université Laval, 2013.

[51] E. Lefrançois and J.-P. Boufflet. An introduction to fluid-structure interaction: Application to the piston problem. *SIAM Review: SIAM Rev.*, 52(4):747–767, 2010.

[52] D. Martin. *Multiphase Modelling of Melting/Solidification with High Density Variations using XFEM*. PhD thesis, Université Laval, 2016.

[53] J. Melenk and I. Babuska. The partition of unity finite element method: Basic theory and applications. *Computer Methods in Applied Mechanics and Engineering*, 139:289–314, 1996.

[54] R. Merle and J. Dolbow. Solving thermal and phase change problems with the extended finite element method. *Computational Mechanics*, 28:339–350, 2002. 10.1007/s00466-002-0298-y.

[55] N. Moes, E. Bechet, and M. Tourbier. Imposing Dirichlet boundary conditions in the extended finite element method. *International Journal for Numerical Methods in Engineering*, 67(12):1641–1669, SEP 2006.

[56] N. Moes, J. Dolbow, and T. Belytschko. A finite element method for crack growth without remeshing. *International Journal for Numerical Methods in Engineering*, 46:131–150, 1999.

[57] S. Mousavi and N. Sukumar. Generalized Gaussian quadrature rules for disconitnuities and crack singularities in the extended finite element method. *Computer Methods in Applied Mechanics and Engineering*, 199:3237–3249, 2010.

[58] S. Mousavi and N. Sukumar. Numerical integration of polynomials and discontinuous functions on irregular convex polygons and polyhedrons. *Computational Mechanics*, 47:535–554, May 2011.

[59] N. Moës, M. Cloirec, P. Cartraud, and J.-F. Remacle. A computational approach to handle complex microstructure geometries. *Computer Methods in Applied Mechanics and Engineering*, 192(28–30):3163 – 3177, 2003. Multiscale Computational Mechanics for Materials and Structures.

[60] B. Nedjar. An enthalpy-based finite element method for nonlinear heat problems involving phase change. *Computers & Structures*, 80(1):9 – 21, 2002.

[61] S. Osher and R. Fedkiw. Level set methods: An overview and some recent results. *Journal of Compuational Physics*, 169(2):463–502, MAY 2001.

[62] S. Osher and R. Fedkiw. *Level Set Methods and Dynamic Implicit Surfaces*. Springer-Verlag, 2003.

[63] S. Osher and J. A. Sethian. Fronts propagating with curvature-dependent speed: Algorithms based on Hamilton-Jacobi formulations. *Journal of Computational Physics*, 79(1):12 – 49, 1988.

[64] M. N. Özişik. *Heat Conduction*. John Wiley & Sons, Inc., 1993.

[65] K. Rathjen and L. Jiji. Heat conduction with melting or freezing in a corner. *Journal of Heat Transfer, ASME*, 93:101–109, 1971.

[66] J. Reddy. *An Introduction to the Finite Element Method*. McGraw-Hill, third edition, 2006.

[67] D. Samanta and N. Zabaras. Modelling convection in solidification processes using stabilized finite element techniques. *International Journal for Numerical Methods in Engineering*, 64(13):1769–1799, DEC 2005.

[68] J. R. Shewchuk. Triangle: Engineering a 2d quality mesh generator and delaunay triangulator. In M. C. Lin and D. Manocha, editors, *Applied Computational Geometry: Towards Geometric Engineering*, volume 1148 of *Lecture Notes in Computer Science*, pages 203–222. Springer-Verlag, May 1996. From the First ACM Workshop on Applied Computational Geometry.

[69] K. Shibanuma and T. Utsunomiya. Reformulation of XFEM based on PUFEM for solving problem caused by blending elements. *Finite Elements in Analysis and Design*, 45(11):806–816, SEP 2009.

[70] H. Si. Tetgen, a delaunay-based quality tetrahedral mesh generator. *ACM Transactions on Mathematical Software*, 41, 2015.

[71] F. L. Stazi, E. Budyn, J. Chessa, and T. Belytschko. An extended finite element method with higher-order elements for curved cracks. *Computational Mechanics*, 31(1-2):38–48, 2003.

[72] N. Sukumar, D. Chopp, N. Moes, and T. Belytschko. Modeling holes and inclusions by level sets in the extended finite-element method. *Computer m*, 190:6183–6200, 2001.

[73] M. Sussman, P. Smereka, and S. Osher. A level set approach for computing solutions to incompressible 2-phase flow. *Journal of Compuational Physics*, 114(1):146–159, SEP 1994.

[74] C. Swaminathan and V. Voller. A general enthalpy method for modeling solidification processes. *Metallurgical transactions B-process metallurgy*, 23(5):651–664, OCT 1992.

[75] L. Tan and N. Zabaras. A level set simulation of dendritic solidification with combined features of front-tracking and fixed-domain methods. *Journal of Compuational Physics*, 211(1):36–63, JAN 2006.

[76] H. Thomas and Z. Zhou. Minimum time-step size for diffusion problem in fem analysis. *International Journal for Numerical Methods in Engineering*, 40:3865–3880, 1997.

[77] G. Ventura. On the elimination of quadrature subcells for discontinuous functions in the extended finite-element method. *International Journal for Numerical Methods in Engineering*, 66(5):761–795, 2006.

[78] G. Ventura, R. Gracie, and T. Belytschko. Fast integration and weight function blending in the extended finite element method. *International Journal for Numerical Methods in Engineering*, 77(1):1 – 29, JAN 2009.

[79] V. Voller and C. Swaminathan. Fixed grid techniques for phase change problems: A review. *International Journal for Numerical Methods in Engineering*, 30:875–898, 1990.

[80] M. Vynnycky and S. Kimura. An analytical and numerical study of coupled transient natural convection and solidification in a rectangular enclosure. *International Journal of Heat and Mass Transfer*, 50:5204–5214, 2007.

[81] F. Wolff and R. Viskanta. Soldification of a pure metal at a vertical wall in the presence of liquid superheat. *International Journal of Heat and Mass Transfer*, 31:1735–1744, 1988.

[82] H. Yoo and R. S. Tack. Melting process with solid-liquid density change and natural convection in a rectangular cavity. *International Journal of Heat and Fluid Flow*, 12(4):365 – 374, 1991.

[83] N. Zabaras, B. Ganapathysubramanian, and L. Tan. Modelling dendritic solidification with melt convection using the extended finite element method. *Journal of Computational Physics*, 218(1):200–227, OCT 2006.

[84] A. Zilian and T. P. Fries. A localized mixed-hybrid method for imposing interfacial constraints in the extended finite element method (XFEM). *International Journal for Numerical Methods in Engineering*, 79:733–752, 2009.